Fracture Mechanics Analysis of Multiple Edge Cracks

Muhamad Saifuldin ABDUL MANAN

Submitted for the Degree of
Doctor of Philosophy

Department of Mechanical Engineering
University College London

February 2008

ProQuest LLC
789 East Eisenhower Parkway
P.O. Box 1346
Ann Arbor, MI 48106-1346

Declaration

I declare that:

This submission is entirely my own work. Any uses made within it of the works of other authors in any form, wherever published, unpublished, printed, electronic or other information sources have been used as a contribution or component of this work, these are explicitly, clearly and individually acknowledged by appropriate use of quotation marks, citations, references and statements in text. A full list of the references employed is included.

SIGNATURE:..... .....

DATE: ..... 22 MARCH 2008 .....

Abstract

This thesis is concerned with the evaluation of crack propagation in the presence of other cracks within the same two-dimensional body. The parameter known as the Stress Intensity Factor (SIF) is used within Linear Elastic Fracture Mechanics (LEFM) to predict crack propagation rate knowing the appropriate material properties. Unfortunately the number of SIF solutions for multiple cracks is very small especially for real engineering cases. This thesis investigates the use of the SIF weight function for the efficient evaluation of SIFs for two one-dimensional cracks in close proximity to each other. The SIF weight function has proved to be a powerful tool for the evaluation of single cracks however, has not before been used to solve multiple crack problems. The main objective of the thesis is to investigate the mechanics of multiple cracks through an experimental and numerical analysis programme and to develop engineering solutions for prediction of multiple crack behaviour in steels and materials that exhibit LEFM characteristics.

A Finite Element (FE) approach was employed to model multiple crack interaction. In addition, the FE model was used to study the non-uniform stress distribution caused by the interaction effect between cracks. Over one hundred FE models were analysed for this study. A major experimental programme was conducted to study the interaction effect between two edge cracks. A total of seven specimens with different crack geometries were completed under fatigue loading in tension. The purpose of this experimental work was to better understand the mechanisms of crack interaction and to provide information for validation of the numerical anlayses. The experimental results show that cracks in close proximity to each other interact to varying degrees depending on relative crack lengths, crack separation and plate width. A novel weight function method was developed in order to predict SIFs of two edge cracks under uniform tension. The crack interaction effect was established using the idea of non-uniform stress distributions along the potential crack plane due to the presence of an additional edge crack. Generally the novel weight function approach shows good results compared to finite element analysis.

Finally, further work to explore the wide range of SIFs for multiple cracks using the weight function method is identified and proposed.

Acknowledgements

I wish to acknowledge the excellent supervision and constant support offered by Professor Feargal Brennan throughout this PhD research study. I am grateful to him for giving the opportunity to pursue this study.

I would like to thank my wife for her support and patience throughout my study.

I would also like to thank my colleagues at the NDE centre especially Andy, Song, Amir, Tanya and Bello for their technical support and advice.

Table of Contents

List of Tables

List of Figures

Nomenclature

a	Crack length
a1	Crack 1 of length a1
a2	Crack 2 of length a2
a_{cr}	Critical crack size
a_f	Final crack length
a_i	Initial crack length
A	Area
B	Plate thickness
c	Empirical material constant in Paris Equation
COD	Crack opening displacement
CT	Compact Tension
d	Distance between two cracks
da/dN	Fatigue crack growth rate
E	Young's Modulus of material
FE	Finite Element
FEA	Finite Element Analysis
G	Energy release rate
K	Stress intensity factor (SIF)
K_I	SIF mode I
K_{II}	SIF mode II
K_{Ic}	Fracture toughness
K_{a1}	SIF for crack 1
K_{a2}	SIF for crack 2
LEFM	Linear elastic fracture mechanics
m(a,x)	SIF weight function
m	Empirical material constant in Paris Equation
M	Bending moment
MRS	Multiple Reference State
N	Number of fatigue cycles in linear elastic fracture mechanics

N_f	Crack propagation life to failure
P	Axial load
r	Radius
SIF	Stress intensity factor
T	Plate width
t	Plate thickness
U.T.S	Ultimate tensile strength
u(a,x)	Crack opening displacement
W	Strip length
x	Distance along potential crack plane
Y	Normalised SIF
Y_{a1}	Normalised SIF of crack 1
Y_{a2}	Normalised SIF of crack 2
ν	Poisson ratio
γ_S	Surface energy of material
σ	Stress
σ_f	Fracture stress
σ_y	Yield strength
σ_0	Remotely applied stress
$\sigma(x)$	Stress distribution along uncracked plane
$\sigma 1(x)$	Stress distribution along potential crack 1
$\sigma 2(x)$	Stress distribution along potential crack 2
τ	Shear stress
θ, α	Angle
ΔK	Stress intensity factor range
ΔK_{max}	Maximum stress intensity factor range
ΔK_{th}	Threshold stress intensity factor range

Chapter 1: Introduction and Background

1.0 Introduction

The cause of structural failure can be due to negligence during design, construction or manufacturing. Poor workmanship, unsuitable materials and errors in stress analysis are examples that contribute to failure. Another cause of failure is due to application of a new design or material, which produces an undesirable result. This type of failure is more difficult to prevent. Introduction of new design or materials not only offer advantages but may also give potential problems. One of the most famous failures due to the introduction of a new design is the brittle fracture of the World War II Liberty ships. The Liberty ships were the first ships to have an all-welded hull. Even though they could be fabricated faster and cheaper than earlier riveted designs, the ships sustained serious fractures as a result of the design change. Now almost all steel ships are welded but sufficient knowledge was gained from the failures to avoid similar problems.

Traditional failure criteria cannot adequately explain many structural failures that occur at stress levels lower than the ultimate strength of the material. Examples of engineering structures that have this problem are offshore platforms, railway track, ships, aeroplanes and bridges. A fracture mechanics theory is therefore introduced as opposed to the use of the traditional fracture criteria. Fracture research began in the early 1920s by Griffith. He applied the first law of thermodynamics to formulate a fracture theory based on a simple energy balance. According to the theory, a flaw becomes unstable and thus fracture occurs when the strain energy change that results from an increment of crack growth is sufficient to overcome the surface energy of the material. The theory originally only applied to brittle materials and modification of the theory for application to more ductile materials only began in 1948.

Design by fracture mechanics requires knowledge of a critical crack size and a parameter which characterizes the tendency of a crack to grow. Such a parameter should be able to

relate analysis results or laboratory test results to structural performance. Thus the response of a structure with cracks can be predicted from analysis or laboratory test data. This parameter is known as the stress intensity factor (SIF) and is determined in terms of crack size, structural geometry and loading conditions. On the other hand, the critical value of this parameter known as fracture toughness which is a property of the material is determined from laboratory tests. By equating this parameter to its critical value a relation between applied load, crack size and structure geometry can be obtained. Fracture toughness can be defined as the ability of the material to resist fracture in the presence of cracks. It is similar to yield strength of material which measures the resistance of the material to yield.

Many engineering structures such as aircraft, boilers, pressure vessels and pipes contain multiple cracks. The study of multiple cracks has become increasingly important in the design of these structures. Structural failure usually happens as a result of interaction of these cracks. A crack can be enhanced or shielded due to crack interaction. More understanding of the interaction between cracks may provide engineers with the quantitative tools to asses multiple cracks problem. Current design codes apply certain rules and conditions for example characterising multiple cracks as a single larger crack and the fracture assessment is considered as a single crack. The characterisation of multiple cracks can be unrealistic and may lead to unreliable predictions of the service life of multiple cracked components. Only individual cracks can provide actual SIF values.

There is a strong need for an easy method that can be used to determine the SIFs of multiple cracks. It is important to isolate and consider a potential crack that can cause failure to components rather than characterising multiple cracks as a single larger crack in order to obtain true fracture analysis. Few researchers have studied multiple cracks especially in finite bodies. It is difficult to obtain an exact solution of multiple cracks in finite bodies by using analytical methods due to the complexity of the analysis. One of the methods to determine SIF that can be further developed for multiple cracks is the weight function method. The weight function is a unique property that represents the

influence of crack and component geometry independent of externally applied loading. It can be isolated, combined and composed to allow evaluation of SIFs for real engineering application. Currently the weight function method can only be applied to solve SIFs of a single crack. It is necessary to improve the versatilities of weight function method beyond a single crack as multiple cracks are also common flaws found in engineering applications.

1.1 Linear Elastic Fracture Mechanics

The study of fracture mechanics begins in early 1920 when Griffith [1.1] first proposed an energy-based theory of brittle fracture. The approach applies only for materials that obey Hooke's law. Griffith's theory for elastic materials was modified by Orowan [1.2] to accommodate plasticity effects that are encountered during metal fracture. Irwin [1.3] also adapted Griffith's theory to metals by including the energy dissipated by local plastic flow. In 1956, Irwin [1.4] developed the energy release rate concept, making Griffith's theory a more useful tool for engineering applications. Based on analysis of stresses and displacements ahead of a sharp crack by Westergaard [1.5], Irwin [1.6] showed that the stresses and displacements near the crack tip could be incorporated in a single parameter related to the energy release rate. This parameter, characterizing the stress field ahead of the crack tip, is the stress intensity factor (SIF). Since 1960, fracture mechanics theories have been developed to include various types of nonlinear material behaviour.

Linear Elastic Fracture Mechanics (LEFM) describes the fracture behaviour of materials and components that respond elastically under loading. LEFM theories are used to define the stress distribution and magnitude near to a crack tip in terms of parameters such as load, crack geometry and material properties. The SIF is the most common fracture parameter that characterizes the stress field ahead of a crack. LEFM assumes that linear elastic theory can be applied to bodies containing cracks even though a singularity field exists at the crack tip. At this singularity field, a plastic zone will form near the crack tip, which is plastically deformed beyond the yield stress. However, LEFM remains valid on

the condition that the plastic zone is comparatively smaller than the crack length or the remaining ligament of uncracked material.

Fracture mechanics often plays a role in life prediction of components that are subject to time-dependent crack growth mechanisms such as fatigue or stress corrosion cracking. The rate of cracking can be correlated with fracture mechanics parameters such as the SIF. Consider a body that undergoes crack propagation with crack length *a* under constant amplitude stress with *N* cycles. The fatigue crack growth rate in metals can be described by the following empirical relationship [1.7]:

$$\frac{da}{dN} = c(\Delta K)^m \qquad (1.1)$$

where ΔK is the SIF range, and *c* and *m* are material constants. A typical plot of log da/dN versus log ΔK, a sigmoidal curve, is shown in Figure 1.1. The curve can be divided into three regions. Most of the current application of LEFM concepts to describe crack growth behaviour is associated with Region II where the slope of the log da/dn versus log ΔK curve is approximately linear.

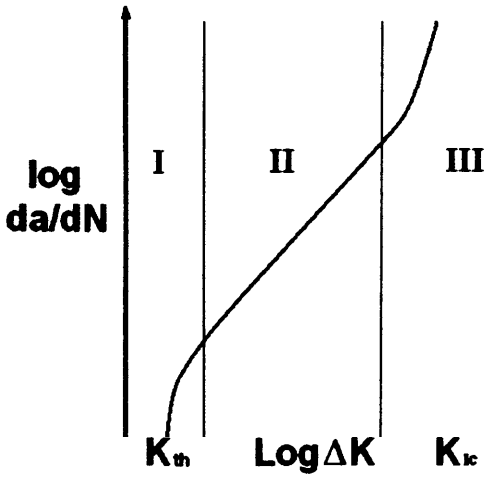

Figure 1.1: Typical fatigue crack propagation behaviour in metals.
Figure 1.1: Typical fatigue crack propagation behaviour in metals.

From Eqn.(1.1) the crack propagation life to failure, N_f can be integrated as:

$$N_f = \int_{a_i}^{a_f} \frac{1}{c(\Delta K)^m} \cdot da \tag{1.2}$$

where subscript *i* and *f* refer to initial and final crack length respectively.

If the increase of crack tip stress field equals or exceeds resistance to crack extension, total fracture would occur at a critical SIF, K_{Ic}. This K_{Ic} value, which is a measure of fracture toughness, is a material constant that is independent of the size and geometry of the cracked body. By defining K as $Y\sigma_0\sqrt{\pi a}$, where Y is a geometric factor, the critical crack size a_{cr} can be expressed as:

$$a_{cr} = \frac{K_{Ic}^{\ 2}}{Y^2\sigma_0^{\ 2}\pi} \tag{1.3}$$

It is clear that the fracture mechanics design approach that uses time dependent crack growth and critical crack size for failure depends on the knowledge of SIF. Therefore, a comprehensive knowledge of the SIF concept is a prerequisite to a fracture design or control plan.

1.1.1 Energy Principle

According to the First Law of Thermodynamics, when a system goes from a non equilibrium state to equilibrium, there will be a net decrease in energy. Griffith [1.1] applied this idea to the formation of a crack. The Griffith fracture criterion stated that initial fracture in an ideally brittle material occurs when the elastic energy supplied at the crack tip during an incremental increase in crack length is equal to or greater than the elastic energy at the crack tip during crack growth.

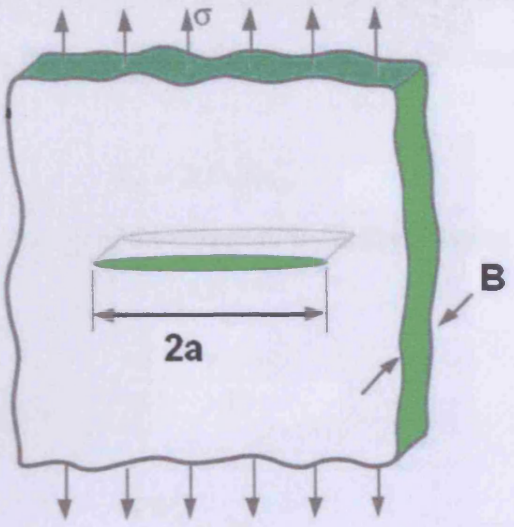

Figure 1.2: A through-thickness crack in an infinitely wide plate subjected to a remote tensile stress.

Consider an infinite plate under plane stress with thickness, B subjected to a constant stress, σ, which contains a crack 2a long as shown in Figure 1.2. The Griffith energy balance for an incremental increase in the crack area, dA, under equilibrium conditions can be expressed as:

$$\frac{dU}{dA} = \frac{d\Pi}{dA} + \frac{dW_s}{dA} = 0 \tag{1.4}$$

or

$$-\frac{d\Pi}{dA} = \frac{dW_s}{dA} \tag{1.5}$$

where U is the total energy, Π is the potential energy and W_s is the work required to create new surfaces. For the cracked plate shown in Figure 1.2, Griffith used the stress analysis of Inglis [1.8] to show that:

$$\Pi = \Pi_0 - \frac{\pi\sigma^2 a^2 B}{E} \tag{1.6}$$

where Π_0 is the potential energy of an uncracked plate and B is the plate thickness. E is Young's modulus. Since the formation of a crack requires the creation of two surfaces, W_S is given by:

$$W_S = 2(2aB)\gamma_S \tag{1.7}$$

where γ_S is the surface energy of the material. By differentiating Eqn.(1.6) and (1.7) with respect to A gives:

$$-\frac{d\Pi}{dA} = \frac{\pi\sigma^2 a}{E} \tag{1.8}$$

and

$$\frac{dW_S}{dA} = 2\gamma_S \tag{1.9}$$

By substituting Eqn.(1.8) and (1.9) into Eqn.(1.5), the fracture stress, σ_f can be expressed as:

$$\sigma_f = \sqrt{\frac{2E\gamma_S}{\pi a}} \tag{1.10}$$

The equation of fracture stress is valid only for ideally brittle solids. Orowan [1.2] and Irwin [1.3] independently modified the Griffith expression to account for materials that are capable of plastic flow. The revised expression of fracture stress is given by:

$$\sigma_f = \sqrt{\frac{2E(\gamma_S + \gamma_P)}{\pi a}} \tag{1.11}$$

1.1.1.1 Energy Release Rate

Irwin [1.4] proposed an energy approach in a form that is more convenient for solving engineering problems. Energy release rate, G is defined as the rate of change in potential energy with crack area for a linear elastic material. It can be expressed as:

$$G = -\frac{d\Pi}{dA} \tag{1.12}$$

The energy release rate for an infinite plate in plane stress with a crack length $2a$ is given by:

$$G = \frac{\pi\sigma^2 a}{E} \tag{1.13}$$

where E is Young's modulus, σ is the remotely applied stress and a is the half crack length. At fracture, G is equal to G_c where it is a measure of the fracture toughness of the material. It can be expressed as:

$$G_c = \frac{\pi\sigma_f^2 a_{cr}}{E} \tag{1.14}$$

where σ_f is the fracture stress and a_{cr} is the critical crack size. The energy release rate, G can be treated as the driving force for fracture while G_c is the material's resistance to fracture.

1.1.2 Stress Intensity Factor

Assuming that the material is homogenous and isotropic, the closed form expressions for the stresses in the body can be derived for certain cracked configurations subjected to external forces. If we define a polar coordinate axis with the origin at the crack tip as shown in Figure 1.3, it can be shown that the stress field in any linear elastic cracked body is given by:

$$\sigma_{ij} = \frac{K_{I,II,III}}{\sqrt{2\pi r}} f_{ij}^{(I,II,III)}(\theta) + \text{other terms} \tag{1.15}$$

where σ_{ij} are the stresses acting on a material element at a distance r from the crack tip and at an angle θ from the crack plane and $f_{ij}(\theta)$ are known trigonometric functions of θ depending on modes I, II or III. As r approaches zero, the leading term approaches infinity but the other terms remain constant or approach zero. The stress near the crack tip varies with $1/\sqrt{r}$, regardless of the configuration of the cracked body. Eqn.(1.15) describes a stress singularity, since stress is asymptotic to r equal to zero.

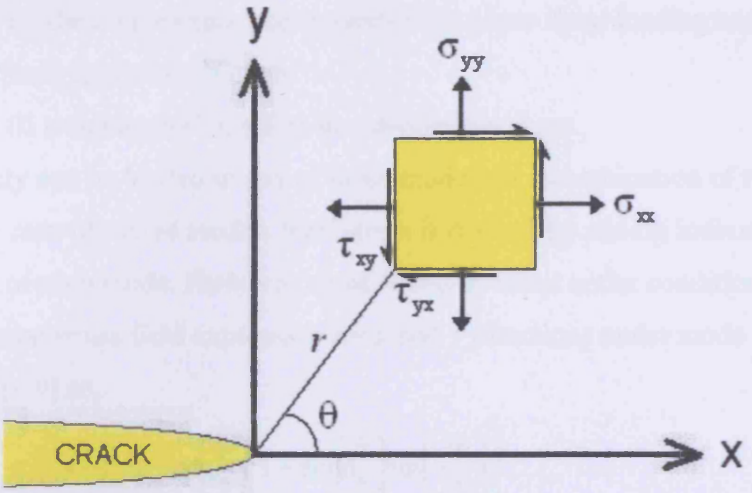

Figure 1.3: Definition of the coordinate system and stress component ahead of crack tip.

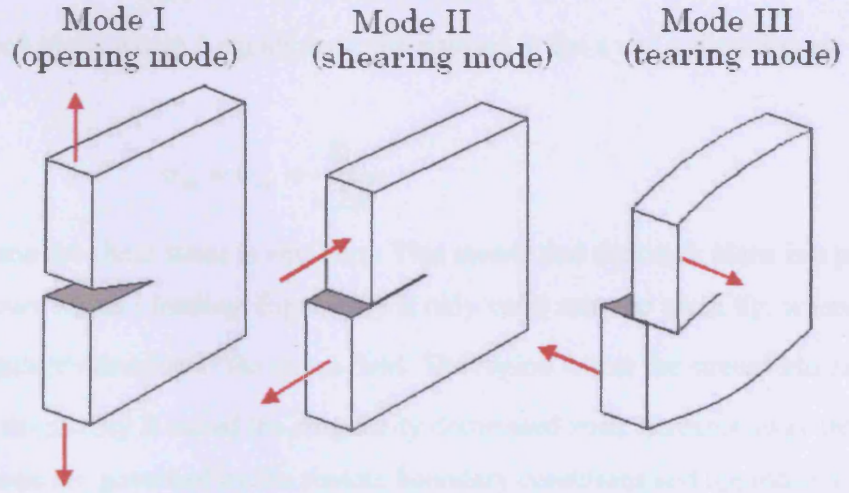

Figure 1.4: The three modes of loading that can be applied to a crack.

There are three types of loading that a crack can experience. The three types are as shown in Figure 1.4 and can be categorized as follows:

1. Mode I (opening mode), where the principal load is applied normal to the crack plane tends to open the crack.

2. Mode II (shearing mode), corresponds to in-plane shear loading and tends to slide crack faces against each other.
3. Mode III (tearing mode), refers to out-of-plane shear.

A cracked body can be loaded in any of these modes, or a combination of two or three modes. In the case of mixed modes, total stress is defined by adding individual contributions of each mode. However, most fractures occur under conditions of mode I loading. Singular stress field expression for x and y directions under mode I loading can be expressed [1.9] as:

$$\sigma_{xx} = \frac{K_I}{\sqrt{2\pi r}}\cos\left(\frac{\theta}{2}\right)\left[1-\sin\left(\frac{\theta}{2}\right)\sin\left(\frac{3\theta}{2}\right)\right] \tag{1.16}$$

$$\sigma_{yy} = \frac{K_I}{\sqrt{2\pi r}}\cos\left(\frac{\theta}{2}\right)\left[1+\sin\left(\frac{\theta}{2}\right)\sin\left(\frac{3\theta}{2}\right)\right] \tag{1.17}$$

$$\tau_{xy} = \frac{K_I}{\sqrt{2\pi r}}\cos\left(\frac{\theta}{2}\right)\sin\left(\frac{\theta}{2}\right)\cos\left(\frac{3\theta}{2}\right) \tag{1.18}$$

On the crack plane where θ equals zero, the stresses in the x and y direction are equal. Thus:

$$\sigma_{xx} = \sigma_{yy} = \frac{K_I}{\sqrt{2\pi r}} \tag{1.19}$$

On this plane the shear stress is also zero. This means that the crack plane is a principal plane for pure Mode I loading. Eqn.(1.19) is only valid near the crack tip, where the $1/\sqrt{r}$ singularity dominates the stress field. The region where the stress field exhibits the $1/\sqrt{r}$ singularity is called the singularity dominated zone. Stresses away from the crack tip zone are governed by the remote boundary conditions and approach a constant value, σ^{∞}.

Figure 1.5 shows a plot of σ_{yy}, the stress normal to the crack plane versus distance from the crack tip. The SIF defines the amplitude of the crack tip singularity because the stresses near the crack tip increase in proportion to K. The SIF also defines the crack tip conditions because with the K value it is possible to solve for all components of stress, strain and displacement. This single parameter description of crack tip conditions turns

out to be one of the most important concepts in fracture mechanics. Detailed expressions for displacement at a crack tip as a function of r and θ can be found in Ref. [1.9].

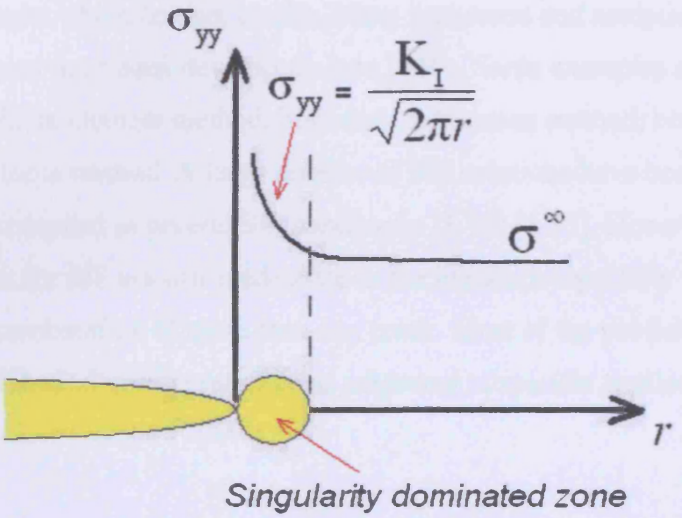

Figure 1.5: Stress normal to the crack plane in Mode I when $\theta = 0$.

1.1.2.1 Geometry Correction Factor Y

In general, K is a function of the loading condition, crack size and shape, and other geometrical parameters. Eqn.(1.15) shows that K is linearly related to stress and characteristic crack dimension. Normally K is defined as:

$$K = Y \cdot \sigma_0 \sqrt{\pi a} \qquad (1.20)$$

where σ_0 is the remotely applied stress, a is the crack length and Y is the geometric factor which is a dimensionless constant that depends on crack geometry and mode of loading. The geometry correction factor, Y usually referred to as non-dimensional SIF, is the most common form of representation for SIF solutions, as documented in a number of SIF handbooks [1.10]-[1.13].

1.2 SIF Determination Method in LEFM

The stress intensity factor K is a very important parameter in fracture mechanics. For example, it is needed to calculate critical crack length and remaining strength or life for structural components which contain cracks. Many numerical and analytical methods of obtaining K solutions have been developed since 1950s. Some examples are the weight function method, finite element method, boundary collocation method, boundary element method and body force method. A large number of SIF solutions have been published in the literature and compiled in several SIF handbooks [1.10]-[1.13]. However the published solutions for SIF are still inadequate in the literature especially for complex geometries and a combination of more than one crack. Most of the published solutions are for simple geometrical configurations and subjected to specific applied stress systems.

1.2.1 Finite Element Analysis (FEA)

FEA has great capability to analyze complicated engineering geometries whether in two-dimensions or three-dimensions. FEA also permits the use of elastic-plastic elements to include crack tip plasticity. A finite element (FE) model is a discrete representation of the continuous physical body under analysis. This discrete representation is created using nodes and elements. Nodes are connected together to form elements. The grid of connecting elements at common nodes comprises the mesh. When adjacent elements share nodes, the displacement field is continuous across the shared element boundary and loads can be transferred between the elements.

The stiffness finite element method [1.14] is usually applied to stress analysis. Local and global coordinates for a two-dimensional isoparametric element are shown in Figure 1.6. Local coordinates or parametric coordinates vary from -1 to +1 over the element area. Consider a point on the element at (ξ,η), the global coordinates of this point are given by

$$x = \sum_{i=1}^{n} N_i(\xi,\eta)x_i \qquad (1.21)$$

$$y = \sum_{i=1}^{n} N_i(\xi,\eta) y_i$$

where n is the number of nodes in the element and N_i are the shape functions corresponding to the node i, whose coordinates are (x_i, y_i) in the global system and (ξ_i,η_i) in the parametric system. The shape functions are polynomials that interpolate field quantities within the element. The degree of the polynomial depends on the number of nodes. An isoparametric four-sided, 8-node element shown in Figure 1.6 requires a quadratic interpolation.

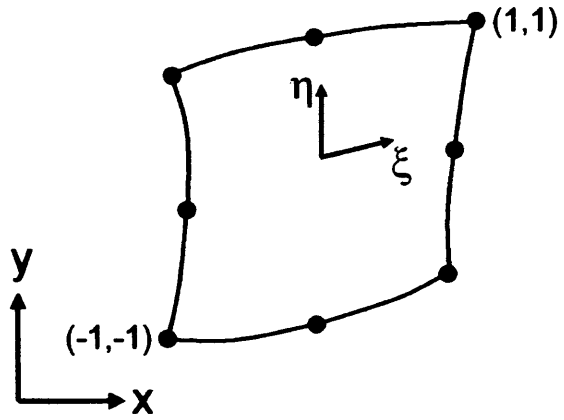

Figure 1.6: Local and global coordinates for a two-dimensional isoparametric element.

The displacements within an element are interpolated as follows:

$$u = \sum_{i=1}^{n} N_i(\xi,\eta) u_i \qquad (1.22)$$

$$v = \sum_{i=1}^{n} N_i(\xi,\eta) v_i$$

where (u_i, v_i) are nodal displacements in the x and y directions, respectively. The stress and strain distribution throughout the body can be inferred from nodal displacements and the stress-strain constitutive law. The displacements at the nodes depend on the element stiffness and the nodal forces. The elemental stiffness matrices are assembled to give the

global stiffness matrix [K] that relates a generalised nodal force vector [F] and the vector of the global nodal displacements [u] as:

$$[K][u] = [F] \tag{1.23}$$

FE models can only provide stresses, displacement, strains and strain energy. From these parameters, SIF can be obtained by few methods such as the energy domain integral method. Many commercial numerical analysis codes like ABAQUS [1.15] have incorporated fracture mechanics routines and implemented efficient numerical domain integral algorithms to enable rapid and accurate evaluation of J and K solutions.

1.2.1.1 Special Crack Tip Elements

The study of fracture mechanics normally needs to focus on the singularity point at the crack tip. At this point quantities such as stress become mathematically infinite but not physically infinite. For this reason a number of modifications have been made to include special functions within an element which exhibit $1/\sqrt{r}$ singularity in the strain variation. Henshell *et al.* [1.16] and Barsoum [1.17] have shown that the desired $1/\sqrt{r}$ singularity in strain variation can be achieved by moving the mid-side node of an 8-node quadrilateral element to a quarter point position. Barsoum [1.18] further enhanced numerical accuracy by collapsing the quadrilateral element into a triangular element by coalescing nodes along one side to occupy the same geometric location at the crack tip as shown in Figure 1.7. This quarter point 6-node collapsed triangular element which exhibits the desired strain singularity has since been widely applied in standard FEM codes. In the case of three-dimensional problems one face of a brick element is collapsed into prism or wedge element.

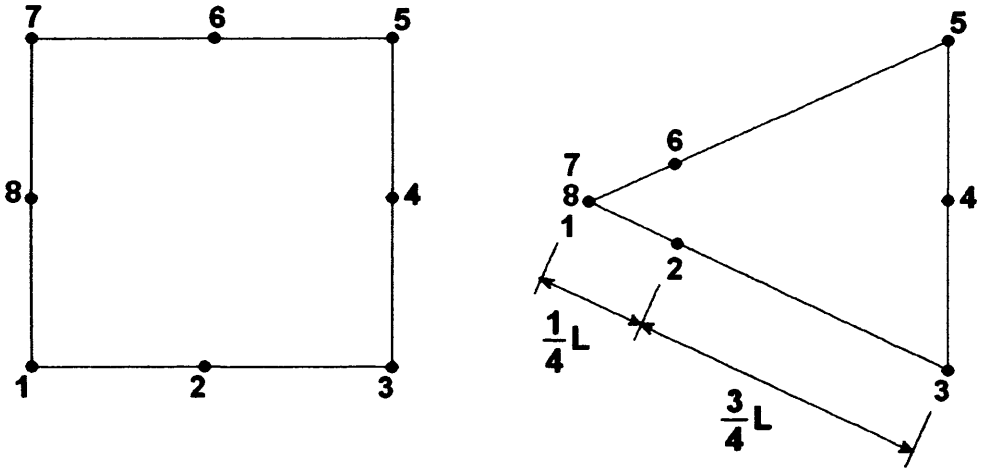

Figure 1.7: Generation of quadrilateral element to 6-node triangular element with mid-side nodes at the quarter point position.

1.2.1.2 FEA Using ABAQUS

FE packages such as ABAQUS [1.15] have implemented a highly efficient domain integral method based on Parks [1.19] and Shih *et al.* [1.20] to enable rapid and accurate evaluation of J-integral and hence K values at the crack tip. J-integral in two-dimensions is defined as:

$$J = \lim_{\Gamma \to 0} \int n \cdot H \cdot q d\Gamma \quad (N/m) \tag{1.24}$$

where Γ is a contour beginning on the bottom crack surface and ending on the top surface; q is a unit vector in the virtual crack extension direction; and n is the outward normal to Γ. H is given by:

$$H = WI - \sigma \cdot \frac{\partial u}{\partial x} \tag{1.25}$$

where W is the elastic strain energy. Based on Shih *et al.* [1.20], Eqn.(1.24) was rewritten by ABAQUS [1.15] as:

$$J = -\int_{C_+ + \Gamma + C_-} m.H.\bar{q}\, d\Gamma - \int_{C_+ + C_-} t \cdot \frac{\partial u}{\partial x} \cdot \bar{q}\, d\Gamma \quad (N/m) \tag{1.26}$$

where $\bar{q}$ is a sufficiently smooth weighting function within the region enclosed by the closed contour $C+C_{+}+\Gamma+C_{-}$; m is the outward normal to the domain enclosed by the closed contour, as shown in Figure 1.8 ; m=-n on Γ; and t is the surface traction on the crack surfaces C_{+} and C_{-}.

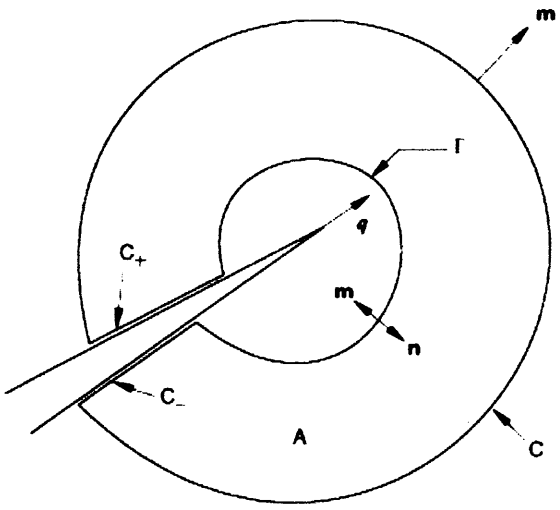

Figure 1.8: Closed contour $C+C_{+}+\Gamma+C_{-}$ encloses a domain A that includes the crack-tip region as $\Gamma\rightarrow 0$ (Diagram from Ref. [1.15]).

Abaqus [1.15] converted closed contour integral (equation 1.26) into domain integral as:

$$J=-\int_{A}\left[H:\frac{\partial\bar{q}}{\partial x}+\left(f\cdot\frac{\partial u}{\partial x}-\sigma:\frac{\partial\varepsilon^{th}}{\partial x}\right)\cdot\bar{q}\right]d\Gamma-\int_{C_{+}+C_{-}}t\cdot\frac{\partial u}{\partial x}\cdot\bar{q}\,d\Gamma \quad \text{(N/m)} \qquad (1.27)$$

where A is the domain enclosed by the closed contour $C+C_{+}+\Gamma+C_{-}$, f is the body force per unit volume and ε^{th} is the thermal strain. Symbol ':' means scalar product of two matrices.

To evaluate these integrals, ABAQUS [1.15] defines the domain in terms of rings of elements surrounding the crack tip. Different contours (domains) are created. The first contour consists of those elements directly connected to crack-tip nodes. The next

contour consists of the ring of elements that share nodes with the elements in the first contour as well as the elements in first contour. Each subsequent contour is defined by adding the next ring of elements that share nodes with the elements in the previous contour as shown in Figure 1.9.

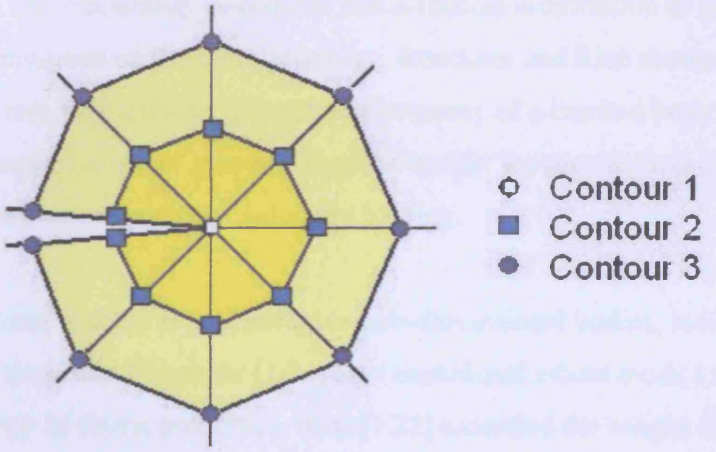

Figure 1.9: Contours are defined by ring of elements surrounding the crack tip.

The number of possible J-integral evaluations corresponds to the number of such rings of elements defined in the FE model. J-integral estimates from different contours may vary due to numerical approximations. Strong variations in these J-integral estimations indicate a need for mesh refinement. As mentioned in ABAQUS [1.15] at least two contours are needed because the estimate from the first ring of elements closest to the crack tip does not provide a very accurate result. Stress intensity factor K is related to the energy release rate (the J-integral) through:

$$J = \frac{1}{E'}\left(K^2\right) \quad \text{(N/m)} \tag{1.28}$$

where, $E' = E$ for plane stress

and $E' = E/(1+\nu^2)$ for plane strain.

1.2.2 Weight Function

When analysis is performed to determine SIF for a cracked body, the K value that is calculated applies only to one set of boundary conditions that are used during the calculation. Different loading conditions produce different K values for the same geometry. However, Bueckner [1.21] and Rice [1.22] showed that the SIF solution subjected to one set of boundary conditions has sufficient information to obtain SIFs for any boundary conditions on the same geometry. Bueckner and Rice showed that the weight function m(a,x) is a unique geometrical property of a cracked body for any given geometry independent of stress system. Once the weight function m(a,x) is determined, it can be used for the same geometry under any loading.

The weight function concept is not limited to two-dimensional bodies, mode I loading or isotropic elastic materials. Bueckner [1.21] also considered mixed mode I and II and allowed anisotropy in elastic properties. Rice [1.22] extended the weight function to three-dimensional cracks and also modelled anisotropy in elastic properties.

1.2.2.1 SIF Weight Function

The SIF weight function m(a,x) is a function of geometry of the crack, component geometry and loading. The SIF of an isotropic elastic cracked body under mode I loading can be obtained by integrating the product of the stress distribution along the potential crack plane $\sigma(x)$ and the weight function m(a,x) along the crack length a with respect to distance x from the crack mouth as follows [1.22]:

$$K = \int_0^a \sigma(x)m(a,x)dx \quad (MN/m^{3/2}) \tag{1.29}$$

Consider two arbitrary loading conditions on an isotropic elastic cracked body. Both loadings are symmetric with respect to the crack plane so that the cracked body experiences pure mode I loading for each loading condition. Rice [1.22] showed that SIF

values for loading condition one, $K^{(1)}$ and loading condition two, $K^{(2)}$ are related as follows:

$$K^{(2)} = \frac{H}{2K^{(1)}}\left[\int_{\Gamma} T_i \frac{\partial u_i^{(1)}}{\partial a} d\Gamma + \int_{A} F_i \frac{\partial u_i^{(1)}}{\partial a} dA\right] \tag{1.30}$$

where H=E for plane stress and H=E/(1-ν^2) for plane strain; T_i and F_i are traction and body forces acting on the perimeter Γ and area A of the body respectively; u_i are the displacements in the x and y directions. Since both loading systems are arbitrary, it follows that $K^{(2)}$ cannot depend on $K^{(1)}$ and $u_i^{(1)}$. Therefore, the function:

$$m(a,x) = \frac{H}{2K_r}\frac{\partial u_r(a,x)}{\partial a} \quad \left(1/\sqrt{m}\right) \tag{1.31}$$

which is referred to as a weight function must be independent of the nature of any loading that provides the reference SIF, K_r and reference crack opening displacement field (COD), $u_r(a,x)$.

The weight function identifies a geometric singularity in a cracked elastic domain as a function of stress intensity at the crack tip, independent of externally impressed forces. The weight function method is a very versatile approach to determine stress intensity factors with remarkable computational efficiency without compromising accuracy. Accuracy in the weight function method depends on accurate determination of the weight function itself.

The significance of the weight function method was not widely appreciated due to the difficulty in defining COD, $u_r(a,x)$ until it was proposed by Petroski and Achenbach [1.23] when dealing with edge crack problems under mode I loading. The assumed COD is as below:

$$u(a,x) = \frac{\sigma_0}{H\sqrt{2}}\left[4F\left(\frac{a}{t}\right)\sqrt{a(a-x)} + \frac{G\left(\frac{a}{t}\right)(a-x)^{\frac{3}{2}}}{\sqrt{a}}\right] \tag{1.32}$$

where $$F\left(\frac{a}{t}\right) = \frac{K}{\sigma_0\sqrt{\pi a}} \tag{1.33}$$

$$G\left(\frac{a}{t}\right)=\frac{\left[\frac{\sqrt{2}}{\sigma_0}I_1-4F\left(\frac{a}{t}\right)a^{\frac{1}{2}}I_2\right]a^{\frac{1}{2}}}{I_3} \tag{1.34}$$

$$I_1=\int_0^a[K(a)]^2da \tag{1.35}$$

$$I_2=\int_0^a\sigma(x)(a-x)^{\frac{1}{2}}dx \tag{1.36}$$

$$I_3=\int_0^a\sigma(x)(a-x)^{\frac{3}{2}}dx \tag{1.37}$$

SIF weight function results computed by applying this COD into the weight function agree well with those for edge cracks, radial cracks from circular holes and radially cracked rings. In addition, it was proven that the assumed COD expression could be used successfully to describe the SIF for a three-dimensional semi-elliptical surface crack [1.24]-[1.27].

1.2.2.1.1 Multiple Reference State (MRS) Weight Function

The previous method to define weight function is by assuming a crack opening displacement (COD) field. The assumed COD needs to be differentiated before it can be substituted into the weight function equation. This requires computational effort and numerical differentiation of the assumed COD field and also may reduce the accuracy of SIF results. Ojdrovic and Petroski [1.28] proposed the use of COD derivative instead of the COD field. This reduces computational effort significantly and avoids inaccuracy caused by numerical differentiation. The COD derivative can be expressed as an arithmetic series:

$$\frac{\partial u(a,x)}{\partial a}=\frac{4\sigma_0}{H}\sqrt{2}\sum_{j=0}^{m}C_j\left(1-\frac{x}{a}\right)^{j-\frac{1}{2}} \tag{1.38}$$

where $C_0 = \frac{1}{2}F_1\left(\frac{a}{t}\right) = \frac{1}{2}\frac{K_1}{\sigma_0\sqrt{\pi a}}$ with the subscript 1 referring to the first reference load case; C_j are the unknown coefficients: the number of terms is m+1; where m is the number of symmetrical loading systems, i.e. (K_1, K_2, K_3,..., K_m; m≥1).

For every known K_i, Eqn.(1.29) and Eqn.(1.31) can be written as:

$$\int_0^a \frac{H}{2}\sigma_i(x)\frac{\partial u(a,x)}{\partial a}dx = K_i(a)K_1(a) \tag{1.39}$$

where $K_1(a)$ is the first reference stress intensity factor and subscript *i* is the *i*th load case. Substituting Eqn.(1.38) into Eqn.(1.39) gives:

$$2\sqrt{2}\sigma_0\int_0^a \sigma_i(x)\sum_{j=0}^{m} C_j\left(1-\frac{x}{a}\right)^{j-\frac{1}{2}}dx = K_i(a)K_1(a) \tag{1.40}$$

Letting

$$W_{ij} = \int_0^a \sigma_i(x)\left(1-\frac{x}{a}\right)^{j-\frac{1}{2}}dx \tag{1.41}$$

gives

$$\sum_{j=0}^{m} W_{ij}C_j = K_i(a)\frac{F_1\left(\frac{a}{t}\right)}{2}\sqrt{\frac{\pi a}{2}} \tag{1.42}$$

Knowing C_0, Eqn.(1.42) can be written as:

$$\sum_{j=1}^{m} W_{ij}C_j = \frac{F_1\left(\frac{a}{t}\right)}{2}\left[K_i(a)\sqrt{\frac{\pi a}{2}} - W_{i0}\right] \tag{1.43}$$

Let the right side of Eqn.(1.43) equal to q_i, then the unknown coefficients C_j can be solved by a system of *m* simultaneous linear equations with *m* unknowns.

For a problem where two reference cases are available,

$$\left\{\begin{matrix} W_{11}C_1 + W_{12}C_2 = q_1 \\ W_{21}C_1 + W_{22}C_2 = q_2 \end{matrix}\right\} \tag{1.44}$$

gives

$$C_1 = \frac{q_1 W_{22} - q_2 W_{12}}{W_{11} W_{22} - W_{21} W_{12}} \tag{1.45}$$

and

$$C_2 = \frac{q_2 W_{11} - q_1 W_{21}}{W_{11} W_{22} - W_{21} W_{12}} \tag{1.46}$$

Knowing the coefficients C_j, the weight function is determined as:

$$m(a,x) = 2\sqrt{2}\frac{\sigma_0}{K_1(a)}\sum_{j=0}^{m} C_j \left(1 - \frac{x}{a}\right)^{j-\frac{1}{2}} \tag{1.47}$$

This approach which is called the multiple reference state (MRS) weight function approach effectively eliminates differentiation and reduces the number of integrations as compared with other methods to obtain the weight function. Brennan [1.29] proved that the approach is less computationally involved to form the required weight function and more accurate than the traditional method which used an assumed COD. Errors in the SIF weight function solutions using this method come only from the reference SIF solutions, the associated stress fields and the integration procedures.

1.3 Structural Failures Due to Multiple Cracks

Structural failure due to multiple cracks can bee seen in engineering structures such as aging aircraft. In April 1988 [1.30], multiple cracks caused Aloha Airlines Boeing 737 aircraft to lose part of its upper fuselage. The accident which happened at Hawaii is generally considered to be the event that began the US Federal Aviation Administration (FAA) focus on aging aircraft. In addition to ageing fuselages multiple cracks also can cause failure in other aircraft components. In May 2005, part of the landing gear of a Boeing 747 aircraft as shown in Figure 1.10 was found to be fractured during push back from its gate at Sydney International Airport for a scheduled passenger flight to Japan. A report [1.31] by the Australian Transport Safety Bureau concluded that the fatigue cracks had initiated from multiple origins to form a single large crack before fracture occurred. A photo of the initiation location of the cracks is shown in Figure1.11.

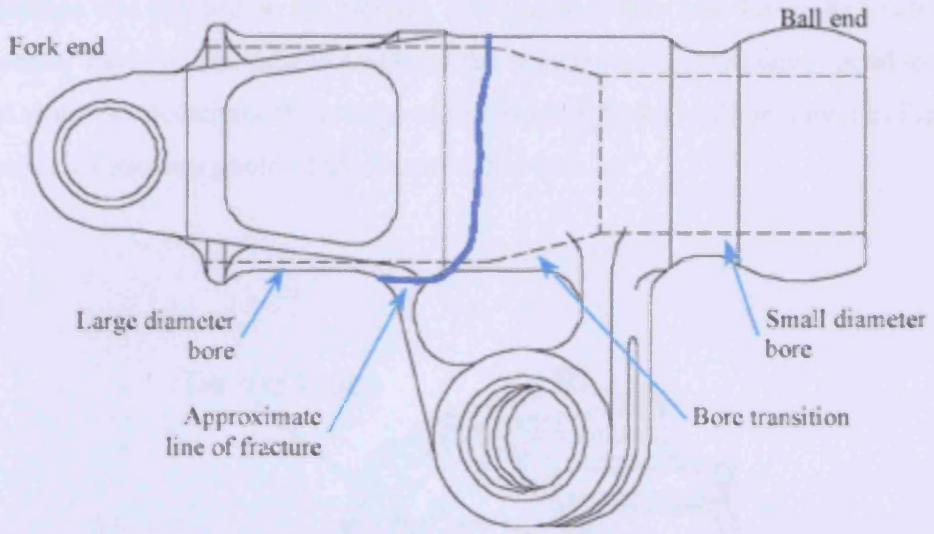

Figure 1.10: A diagram from Ref. [1.31] showing the fracture location in the landing gear (trunnion) of a Boeing 747 aircraft.

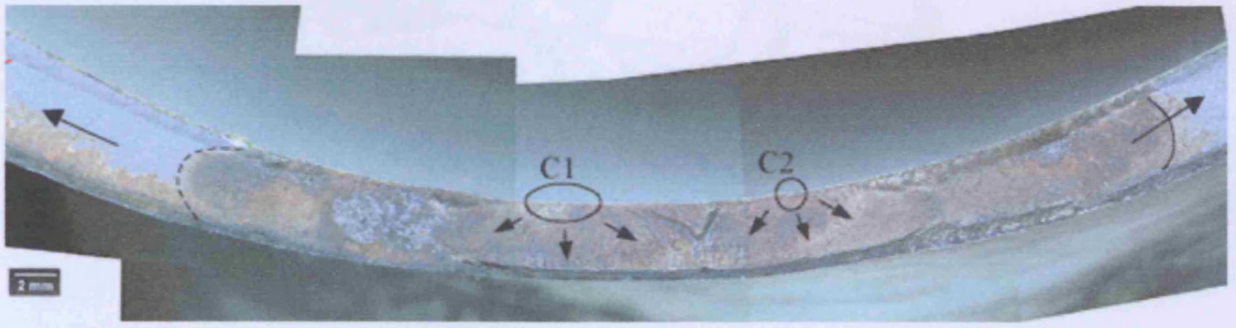

Figure 1.11: A photo [1.31] showing two locations of cracks initiation labelled C1 and C2.

In July 1996 a McDonnell Douglas MD-88 aircraft, experienced an engine failure during the takeoff at Pensacola Regional Airport in Pensacola, Florida. The takeoff was aborted, and the airplane was stopped on the runway. The engine failure was due to the fracture of the compressor fan hub. The fatigue cracks of the compressor fan hub were found to have originated at the two locations of the edge of the 'tie-rod' hole [1.32] as shown in Figure 1.12. Figure 1.13 shows a photo of the fractured fan hub.

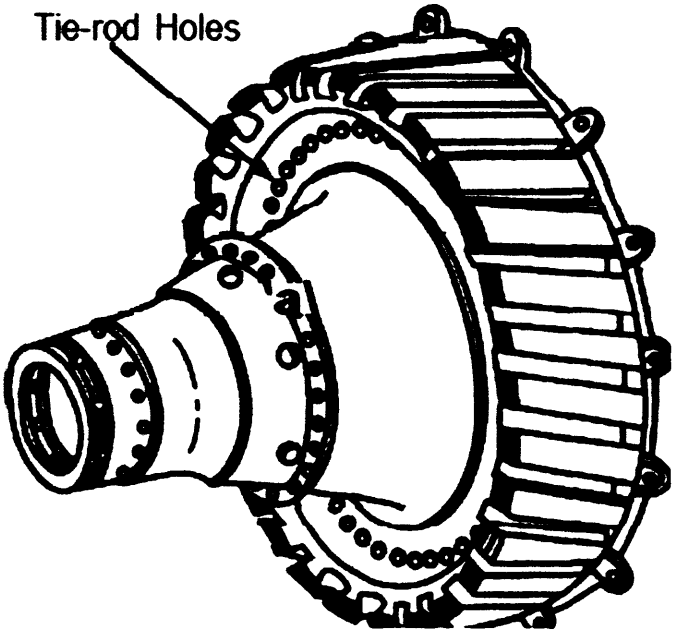

Figure 1.12: A diagram [1.32] showing tie-rod holes of the engine fan hub.

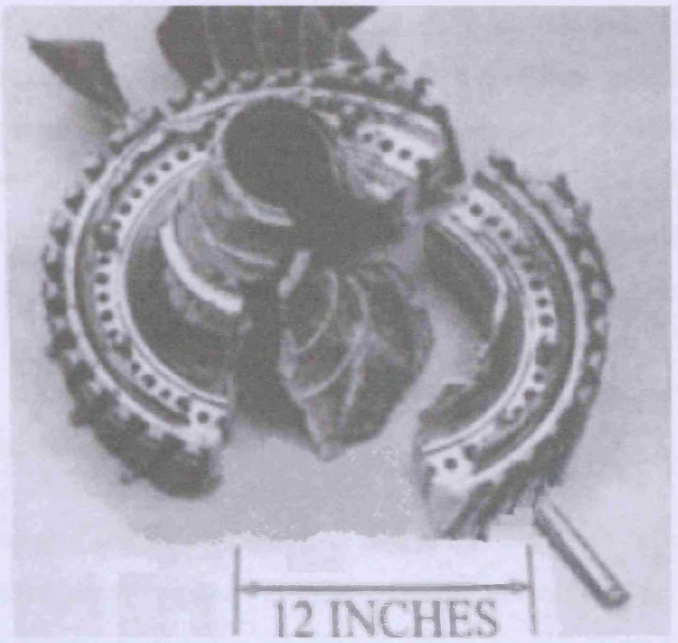

Figure 1.13: A photo [1.32] showing a fractured fan hub.

Multiple cracks also can cause fracture to rail tracks. In October 2000, a train travelling from London to Leeds derailed at Hatfield, Hertfordshire due to rail fractures. Based on the report by the Office of Rail Regulation (ORR) the fractured rail was due to the presence of multiple and pre-existing fatigue cracks in the rail [1.33]. The maintenance contractor failed to manage effectively the inspection and maintenance of the rail at the site of the accident. The fatigue cracks grew to a critical size and fracture occurred when the damaged rail could no longer support the applied fatigue load.

Fracture in pipes can also be due to multiple cracks. A fracture of an oil pipe in Alberta, Canada in January 2001 caused a release of 3,800 cubic metres of crude oil. The failed joint pipe was sent to the laboratory for analysis. A report published by the Transportation Safety Board of Canada [1.34] concluded that multiple cracks had initiated on the outer pipe surface along the corner formed between the pipe body and the edge of the weld. Multiple cracks had coalesced to form one single crack and had continued to grow by fatigue until the pipe could no longer support the normal internal operating pressure of the pipeline. In July 2002, a pipe fracture in Minnesota, U.S. had

caused a release of approximately 6,000 barrels of crude oil. Analysis [1.35] shows that the fracture surfaces of the fatigue crack contained multiple crack initiation sites at seam welds. The cracks were initiated during transport before installation. The failed component travelled approximately 1,000 miles by rail from manufacturing source to the site. After the pipe was installed, the fatigue crack grew with pressure cycle stresses until the crack reached a critical size and the fracture occurred.

1.4 Background Studies of Multiple Cracks

In general the number of studies of multiple cracks is few especially cracks in finite bodies. It is difficult to obtain an exact solution of multiple cracks by an analytical method. Normally numerical methods are used to obtain the SIF of multiple cracks. Studies of multiple cracks require understanding of the crack interaction effect. The crack interaction may increase or reduce the crack tip SIF depending on the crack separation, the applied stress and the crack geometry. Therefore, to obtain the true fracture analysis of multiple cracks an accurate analysis of their interaction is essential. Generally the approach used for multiple crack analysis is based on the approach used for a single crack.

Chen [1.36] proposed the Fredholm integral equation to solve the multiple crack problems in an infinite strip. The proposed approach can be stated as follows. In the situation that a pair of normal and tangential forces is applied at some point on the crack boundary, the solution is defined as the elementary solution of the multiple crack problems. The elementary solution is composed of two parts and satisfies the conditions (a) the first part corresponds to a pair of normal and tangential concentrated forces acting at a prescribed point on both edges of a single crack, and (b) the second part corresponds to a particular solution of the infinite strip without a crack. The second part of the elementary solution is obtained by the use of a numerical technique. Using the obtained elementary solution and the principle of superposition, the interaction effect between the cracks is evaluated and the Fredholm integral equation for the multiple crack problems in

an infinite plate can be formulated. Chen [1.37] modified the elementary solution for use in a finite strip. The modification is to include the interaction effect between the interior cracks and the boundaries of the region.

Other researchers [1.38]-[1.41] used finite element approaches and from the FEA results, derived empirical SIF formulae. Chen and Chang [1.42] used a finite element alternating method in their analysis of two-dimensional mixed-mode fracture problems with multiple cracks under mixed boundary conditions. Their finite element alternating method involved iterative superposition of a finite element solution of an uncracked structure and analytical solution of an unbounded crack body subjected to arbitrary normal and shear loadings on crack surfaces. To satisfy the prescribed mixed boundary conditions, based on the analytical solution derived, the resultant residual nodal displacements and resultant residual equivalent nodal forces are repeatedly computed during the iterative solution process until the variation of stress intensity factors and resultant residual stresses on each crack converge to a small value. Tsang *et al.* [1.43] developed a fractal-like finite element method to evaluate SIFs of multiple cracks. Their method separated a cracked elastic body into a singular and regular region. The regular region was modelled using conventional finite elements but within the singular region, an extremely large number of layers of conventional finite elements were generated layer by layer in a self-similar manner to model the crack tip singular behaviour.

The boundary element technique was used by Chen [1.44] to compute SIFs of multiple cracks in a two-dimensional finite body and by Lo *et al.* [1.45] in a three-dimensional infinite body. The attraction [1.46] of the boundary element method can be largely attributed to the reduction in the dimensionality of the problem; for two-dimensional analysis only the line boundary of the domain needs to be discretized into elements and for three-dimensional problems only the surface of the domain needs to be discretized. Based on this advantage, Chen [1.44] derived a displacement integral equation for the outer boundary and the traction integral equation is established on only one of the crack surfaces of the finite cracked body. A virtual boundary is connected to one of the crack surfaces to construct a closed integral path. It is then employed for evaluating the

hypersingular integral. The constant and quadratic isoparametric elements are taken to discretize the closed integral paths and outer boundary, respectively.

Another method to compute SIFs of multiple cracks is by using an experimental method. Soboyojo *et al.* [1.47] used an experimental method to investigate the interaction and coalescence of two equal sizes of coplanar semi-elliptical cracks in a plate under bending. Recently Cali *et al.* [1.48] used an experimental method to obtain SIFs for a combination of four cracks; three from holes and one from an edge in a plate under tension. An experimental method was also used by Jiang *et al.* [1.49] to study the behaviour of crack growth of two similar cracks sizes in a plate under tension. With fatigue crack growth data collected during fatigue testing and together with appropriate LEFM equations the SIFs of the crack can be computed. This method is not really simple especially for different cracks sizes. It is difficult to prepare a specimen with different crack sizes at a desired crack separation.

Most of the studies in finite bodies are restricted to simple multiple crack configurations and loading conditions. So far there are no studies of multiple cracks found in literature that use the weight function method. One of the advantages of the weight function approach is, once it is determined, it can be applied for the same geometry under any loading condition. It can be isolated, combined and composed to allow evaluation of SIFs for real engineering applications. Brennan and Teh [1.50] proved the versatility of the weight function approach by the developing composition weight function model that uses available weight functions from simple geometries in order to obtain SIFs of complex geometries in finite bodies. Their composition can be established because of the unique property of the weight function that represents the influence of the crack and component geometry independent of externally applied loading. Therefore it is important to further improve the versatility of the weight function method for use in multiple crack problems. It has great potential to solve multiple crack problems for more complex geometries especially in finite bodies.

1.5 Conclusion and Scope of Thesis

This chapter introduced the fundamentals of linear elastic fracture mechanics (LEFM) and the difficulty in modelling multiple crack problems. This discussion will help to understand and appreciate the work in this thesis where the primary objective is to better model multiple cracks and to further expand the capability of the weight function method for use in multiple cracks. The SIF is the most important parameter in LEFM and its methods of determination were briefly discussed.

Currently the weight function method can only be applied for single crack problems. The work of Brennan and Teh [1.50] proved the versatility of the weight function approach that allows more complex geometries to be solved. So far no work to improve the weight function method for multiple crack problems has been published. The scope of the thesis is to study the crack interaction effect between two edge cracks under tension loading and to establish weight function approach in order to predict the SIFs of these two cracks.

Chapter 2 reports the technique and procedure in FE modelling. FE modelling was used to study the non-uniform stress distribution caused by the interaction effects between cracks. The FE model that was used to determine SIFs of two edge cracks in a strip under uniform tension is also discussed.

There is a shortage of studies of multiple cracks in the published literature including limited experimental work. This is not surprising considering the difficult nature of any experimentation involving multiple cracks. Chapter 3 describes the experimental work conducted in this PhD study to examine the interaction between cracks. A total of seven specimens which contain two edge cracks were fatigue tested under tension. Chapter 3 also demonstrates the difficulties associated with preparing cracked specimens with two different crack lengths. The work illustrates the difficulties in carrying out such tests and also to assists in understanding the real crack growth mechanisms of multiple cracks.

Chapter 4 addresses the modification made to the weight function method in order to predict the SIFs of two edge cracks in a strip under uniform tension. The crack interaction effect was established using the idea of non-uniform stress distributions along the potential crack plane due to the presence of an additional edge crack. Results using the modified weight function method were compared with FEA results to examine their validity.

Chapter 5 draws conclusions based on the research work and propose work in order to further explore the wide range of multiple cracks that can be modelled using the SIF weight function method.

1.6 References

1.1 Griffith A.A., The phenomenon of rupture and flow in solids. Philosophical Transactions of the Royal Society, London, 1921, A221, pp.163-197.

1.2 Orowan E., Fracture and strength of solids. In report on Progress in Physics, 1948, XII, pp.185-232.

1.3 Irwin, G.R., Fracture dynamics. Fracturing of Metals, American Society for Metals, Cleveland, 1948, pp.147-166.

1.4 Irwin, G.R.,Onset of fast crack propagation in high strength steel and aluminium alloys. Sagamore Research Conference Proceedings, 1956, 2, pp.289-305.

1.5 Westergaard, H.M., Bearing pressures and cracks. Journal of Applied Mechanics, 1939, 6, pp.49-53.

1.6 Irwin, G.R., Analysis of stresses and strains near the end of a crack traversing a plate. Journal of Applied Mechanics, 1957, 24, pp.361-364.

1.7 Paris, P.C. and Erdogan, F., A critical analysis of crack propagation laws. Journal of Basic Engineering, 1963, 85, pp.528-534.

1.8 Inglis, C.E., Stress in a plate due to the presence of cracks and sharp corners. Transactions of the Institute of Naval Architects, 1913, 55, pp.219-241.

1.9 Anderson, T.L., Fracture Mechanics. CRC Press, 2nd Edition, New York, 1995.

1.10 Murakami, Y. Stress Intensity Factors Handbook, Vol. I-II, Pergamon Press, Oxford, 1987.

1.11 Murakami, Y. Stress Intensity Factors Handbook, Vol. III, Pergamon Press, Oxford, 1991.

1.12 Sih, G.C., Handbook of Stress Intensity Factors, Institute of Fracture and Solid Mechanics, Lehigh University, Bethlehem, Pennsylvania, 1973.

1.13 Rooke, D.P. and Cartwright, D.J., Compendium of Stress Intensity Factors, Her Majesty's Stationery Office, London, 1976.

1.14 Zienkiewicz, O.C. and Taylor, R.L., The Finite Element Method. McGraw-Hill, 4th Edition, London, 1989.

1.15 ABAQUS, version 6.4. Hibbitt, Karlsson & Sorensen, Inc.

1.16 Henshell, R.D. and Shaw, K.G., Crack tip finite elements are unnecessary. International Journal for Numerical Methods in Engineering, 1975, 9, pp.495-507.

1.17 Barsoum, R.S., Further application of quadratic isoparametric finite elements to linear fracture mechanics of plate bending and general shells. International Journal of Fracture, 1975, 11, pp.167-169.

1.18 Barsoum, R.S., On the use of isoparametric finite elements in linear fracture mechanics. International Journal for Numerical Methods in Engineering, 1976, 10, pp.25-37.

1.19 Parks, D.M., The virtual crack extension method for nonlinear material behaviour. Computer Methods in Applied Mechanics and Engineering, 1977, 12, pp.353-364.

1.20 Shih, C.F., Moran, B. and Nakamura, T., Energy release rate along a three-dimensional crack front in a thermally stressed body. International Journal of Fracture, 1986, 30, pp.79-102.

1.21 Bueckner, H.F., A novel principle for the computation of the stress intensity factors. Zeitschrift für Angewandte Mathematik und Mechanik, 1970, 50, No.9, pp.529-546.

1.22 Rice, J.R., Some remarks on elastic crack-tip stress fields. International Journal of Solids and Structures, 1972, 8, pp.751-758.

1.23 Petroski, H.J. and Achenbach, J.D., Computation of the weight function from a stress intensity factor. Engineering Fracture Mechanics, 1978, 10, pp.257-266.

1.24 Niu, X. and Glinka, G., Stress intensity factors for semi-elliptical surface cracks in welded joints. International Journal of Fracture, 1989, 40, pp.255-270.

1.25 Mattheck, C., Munz, D. and Stamm, H., Stress intensity factor for semi-elliptical surface cracks loaded by stress gradients. Engineering Fracture Mechanics, 1983, 18, pp.633-641.

1.26 Niu, X. and Glinka, G., Weight function for edge and surface semi-elliptical cracks in flat plates and plates with corners. Engineering Fracture Mechanics, 1990, 36, pp.459-476.

1.27 Niu, X. and Glinka, G., Theoretical and experimental analyses of surface fatigue cracks in weldments. In Surface Crack Growth: Models, Experiments and Structures. Editors: Reuter, W.G., Underwood, J.H. and Newman, J.C., ASTM STP 1060, 1990, pp.390-413.

1.28 Ojdrovic, R.P. and Petroski, H.J., Weight functions from multiple reference states and crack profile derivatives. Engineering Fracture Mechanics, 1991, 39, pp.105-111.

1.29 Brennan, F.P., Evaluation of stress intensity factors by multiple reference state

weight function approach. Theoretical and Applied Fracture Mechanics, 1994, 20, pp.249-256.

1.30 Schmidt, H.J., Schmidt Brandecker, G. and Tober, G., Design of modern aircraft structure and the role of NDI. The Online Journal of Non-destructive Testing, http://www.ndt.net/abstract/ecndt98/aero.htm, June 1999.

1.31 Aviation Safety Investigation Report - Fractured trunnion, Boeing B747-300 aircraft, JA 8184 at Sydney Aero. Australian Transport Safety Bureau, June 2006.

1.32 Aircraft Accident Report, Uncontained engine failure Delta Airlines Flight 1288 McDonnell Douglas MD-88. National Transportation Safety Board, Washington D.C., Jan. 1998.

1.33 A final report by the Independent Investigation Board, Train derailment at Hatfield. Office of Rail Regulation, July 2006.

1.34 Pipeline Investigation Report P01H0004, Crude oil pipeline rupture – Enbridge Pipelines Inc. near Hardisty, Alberta. Transportation Safety Board of Canada. 2001.

1.35 Pipeline Accident Report, Rupture of Enbridge Pipeline and release of crude oil near Cohasset, Minnesota. National Transportation Safety Board, Washington D.C., July 2002.

1.36 Chen, Y.Z., A Fredholm integral equation approach for multiple crack problem in an infinite plate. Engineering Fracture Mechanics, 1984, 20, pp.767-776.

1.37 Chen, Y.Z., Multiple crack problems for finite plate with arbitrary contour configuration. Engineering Fracture Mechanics, 1988, 31, pp.289-295.

1.38 Jiang, Z.D., Zeghloul, A., Bezine, G. and Petit, J., Stress intensity factors of parallel

cracks in a finite width sheet. Engineering Fracture Mechanics, 1990, 35, pp.1073-1079.

1.39 Jiang, Z.D., Petit, J. and Bezine, G., An investigation of stress intensity factors for two unequal parallel cracks in a finite width plate. Engineering Fracture Mechanics, 1992, 42, pp. 129-138.

1.40 Jiang, Z.D., Petit, J. and Bezine, G., Stress intensity factors of two parallel 3D surface cracks. Engineering Fracture Mechanics, 1991, 40, pp.345-354.

1.41 Shu, H.M., Petit, J. and Bezine, G., Stress intensity factors for several groups of equal and parallel cracks in finite plates. Engineering Fracture Mechanics, 1994, 49, pp.933-941.

1.42 Chen, W.H. and Chang, C.S., Analysis of two dimensional fracture problems with multiple cracks under mixed boundary conditions. Engineering Fracture Mechanics, 1989, 34, pp.921-934.

1.43 Tsang, D.K.L., Oyadiji, S.O. and Leung, A.Y.T., Multiple penny-shaped cracks interaction in a finite body and their effect on stress intensity factor. Engineering Fracture Mechanics, 2003, 70, pp.2199-2214.

1.44 Chen, W.H. and Chen, T.C., An efficient dual boundary element technique for a two-dimensional fracture problem with multiple cracks. International Journal For Numerical Methods In Engineering, 1995, 38, pp.1739-1756.

1.45 Lo, S.H., Dong, C.Y. and Cheung, Y.K., Integral equation approach for 3D multiple-crack problems. Engineering Fracture Mechanics, 2005, 72, pp.1830-1840.

1.46 Yan, X., Numerical analysis of a few complex crack problems with a boundary element method. Engineering Failure Analysis, 2006, 13, pp.805-825.

1.47 Soboyejo, W.O., Kishimoto, K., Smith, R.A., Knott, J.F., A study of the interaction and coalescence of two coplanar fatigue cracks in bending. Fatigue and Fracture of Engineering Materials and Structures, 1989, 12, pp.167-174.

1.48 Cali, C., Citarella, R. and Perrella, M., Three-Dimensional Crack Growth: Numerical Evaluations And Experimental Tests. BEASY, 2006.

1.49 Jiang, Z.D., Petit, J. and Bezine, G., Fatigue propagation of two parallel cracks. Engineering Fracture Mechanics, 1990, 37, pp. 1139-1144.

1.50 Brennan, F.P. and Teh, L.S., Determination of crack-tip stress intensity factors in complex geometries by the composition of constituent weight function solutions. Fatigue and Fracture of Engineering Materials and Structures, 2004, 27, pp.1-7.

Chapter 2: Finite Element Modelling

2.0 Introduction

Finite element analysis (FEA) is widely used in fracture mechanics to solve problems of complex crack geometries since relatively few closed-form analytical solutions are available in the literature. FEA is one such numerical method that can be applied through the use of commercial software packages. Many commercial finite element software packages include fracture mechanics capabilities allowing the user to analyze the stress analysis of cracked bodies.

Two-dimensional FE models were constructed to calculate SIFs of two parallel edge cracks situated in a sheet under uniform tension. These were used for comparison with experimental results in Chapter 3 and weight function results in Chapter 4. FE models containing an edge crack of varying lengths were also constructed to study the non-uniform stress distributions along the potential neighbouring crack. This is to examine the relationship between the non-uniform stress distribution and the crack interaction effects. As discussed in Chapter 4 the results of this study will be used to establish a general form of interaction effect between two cracks.

The results of FEA SIFs were compared with available published solutions. The comparison demonstrates the versatility and accuracy of FEA to obtain SIFs of two edge cracks under uniform tension. More than one hundred FE models were constructed for SIF determination and study of non-uniform stress distribution.

2.1 Finite Element Modelling Techniques

The use of FEA to determine the SIF is briefly discussed in Chapter 1. The FE software package that was used for FEA in this thesis is the ABAQUS software [2.1] which

comprises of a collection of engineering simulation programs based on the finite element method. A typical analysis of a finite element problem comprises the three stages of pre-processing, simulation and post-processing. The pre-processing stage involves modelling of the physical problem to create an input file. This file contains all information such as that relating to definition of crack tip, nodal coordinates, elements, mesh, boundary conditions and applied load. During the simulation stage, the analysis module in ABAQUS software uses this input file to solve the numerical problem. The analysis module produces a number of output files ready for post processing. The post processing stage offers a graphical representation of the model and its solution such as results in the form of graphs, colour contour plots and deformed meshes.

There are two types of FE model constructed for the analysis. One was used to determine the SIF of two edge cracks under tension and another was used for the non-uniform stress distribution study. The two models are similar except the FE model constructed for SIF determination contain two edge cracks while the FE model used for the non-uniform stress distribution study contained only an edge crack in order to investigate the stress distributions ahead of a potential neighbouring crack. Only stress in the longitudinal direction was measured as the SIF solutions evaluated in this work are for crack opening mode (mode I). A full FE model was constructed to model a finite strip with length 10 times longer than its width. To model uniform tension, nodes at the end of the strip were constrained and nodes at the opposite end were applied with a point load.

2.1.1 Mesh Generation Technique

The ABAQUS software provides a graphical tool to create, view or modify input files in the pre-processing stage. The nature of the thesis work involves numerous finite element models with a succession of crack geometries to obtain the SIF solutions. Therefore it is not really practical to repeatedly use this graphical tool for modelling numerous finite element models in order to obtain their SIF solutions. To avoid this repetition, the FE models were prepared using a mesh generating program coded in the Visual Fortran [2.2].

The program produced FE models pre-processing information in a format compatible with an input file required at the simulation stage for solving the numerical problem.

The mesh generator programs for two cracks were modified from the work of Love [2.3] which was used to generate a mesh for a single crack in various geometries. Teh *et al.* [2.4] employed same modelling technique to conduct extensive validation of SIFs for a single edge crack by comparison with published solutions. The mesh generator program only requires geometric parameters as inputs. FE models were partitioned into a number of quadrilateral areas for meshing. Two-dimensional isoparametric continuum elements were used throughout the mesh. The elements used were plane stress elements having eight nodes. They are termed bi-quadratic or second order elements and are denoted by CPS8R. The elements surrounding the crack tip were formed from the same bi-quadratic elements used throughout the model but are collapsed into a triangular element.

As discussed in Chapter 1, ABAQUS employs a domain integral method to evaluate the J-integral by defining the domain in terms of rings of elements surrounding the crack tip. For each crack tip, a total of six rings of elements as shown in Figure 2.1 were used in the mesh generator program allowing six values of J-integral to be evaluated. Typically the innermost J-integral evaluation shows strong variation due to the domain or contour dependence. However, stability is achieved in subsequent J-integrals evaluated further from the crack tip. Most of the evaluations show similar values from the third to sixth J-integral which demonstrate that the use of six rings of elements is judged sufficient to obtain steady value of J-integral. The convergence study [2.3] shows that the number of elements surrounding the crack tip equal to 16 was found to yield the most accurate solutions. Figure 2.2 shows an example of an FE mesh containing two edge cracks generated using the mesh generator program.

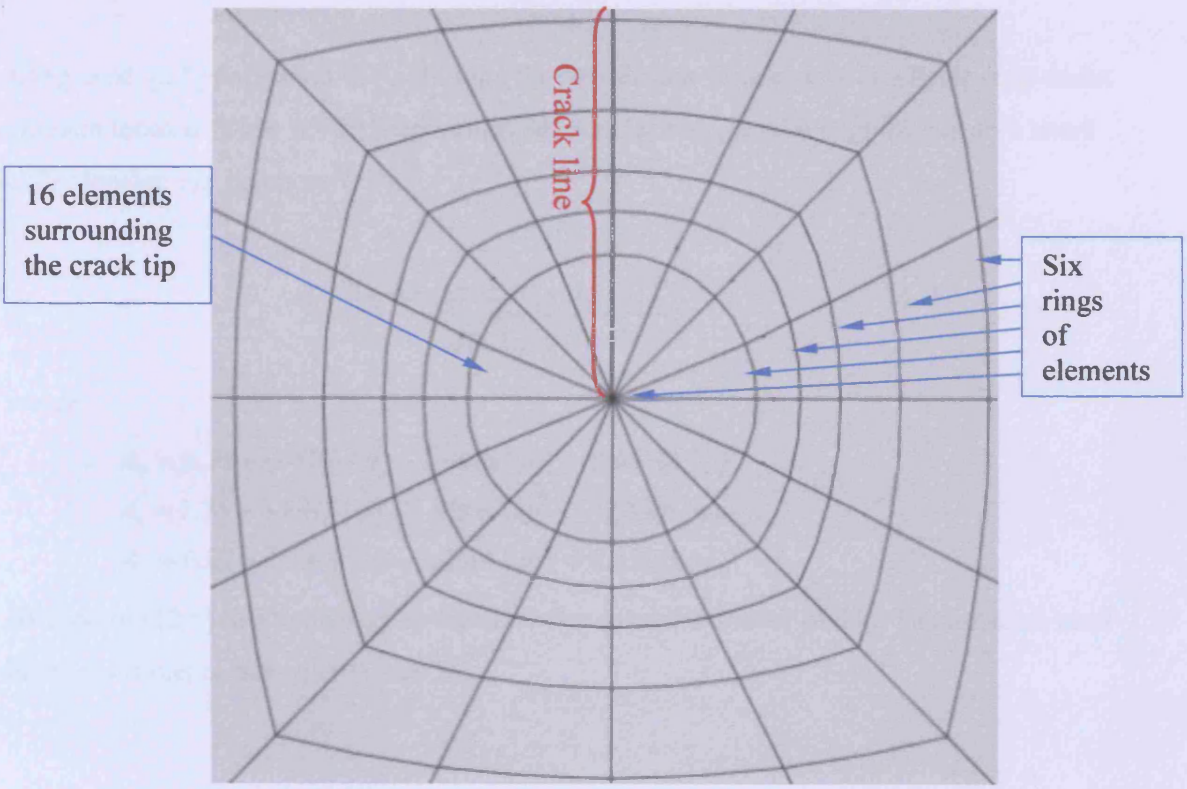

Figure 2.1: Six rings of elements used to evaluate the J-integral values.

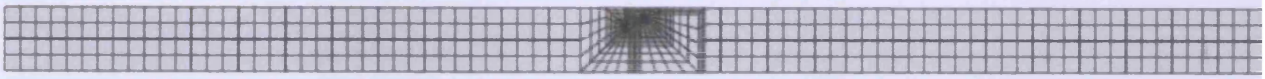

Figure 2.2: FE meshes generated using a mesh generator program.

2.2 SIF Solutions for Two Edge Cracks under Tension

Results of SIFs obtained using FEA were compared with published results [2.5]and[2.6] to demonstrate the reliability of the FE modelling technique used in this thesis. The SIF of the FEA results were normalised in the form below:

$$Y = \frac{K}{\sigma_0 \sqrt{\pi a}} \qquad (2.1)$$

where σ_0 is the remotely applied stress.

Jiang *et al.* [2.5] published SIF solutions for two similar edge cracks in a finite strip under uniform tension. Their normalised values for each of two parallel edge cracks on a sheet under tension are given as:

$$Y=\frac{A_0+A_1(a/T)^{1.5}+A_2(a/T)^4}{\sqrt{1-(a/T)^2}} \tag{2.2}$$

where

$$\begin{aligned} A_0 &= 0.79+0.07(b/a)+0.04(b/a)^2-0.011(b/a)^3 \\ A_1 &= 1.74+2.84(b/a)-1.44(b/a)^2+0.206(b/a)^3 \\ A_2 &= 6.02+2.19(b/a)-3.26(b/a)^2+0.828(b/a)^3 \end{aligned} \tag{2.3}$$

As reported [2.5] this approximate equation has maximum error of 3%. The notation used in the solutions is shown in Figure 2.3.

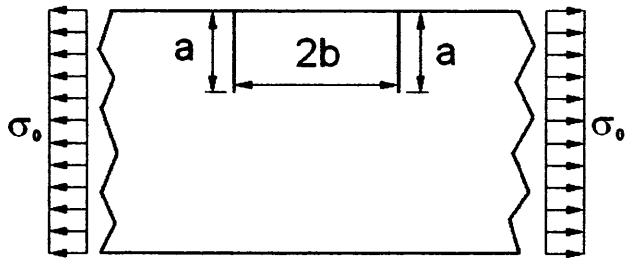

Figure 2.3: Notation used in Ref. [2.5].

There are no closed-form analytical solutions available in the literature for two edge cracks with unequal crack lengths in a finite strip under uniform tension. Jiang *et al.* [2.6] conducted FEA to calculate SIFs of two edge cracks with unequal lengths. The result of their FEA SIFs which are tabulated using different crack geometries were used as a comparison with FEA results obtained in this chapter.

2.2.1 FE Model to Determine SIF of Two Edge Cracks under Tension

Two different mesh generator programs were used to construct FE models for cases of similar and dissimilar crack lengths. This is due to different partitions required for meshing near the crack tip for these two cases. The notations used for FE modelling are shown in Figure 2.4. The strip length used is 10 times longer than its width. This ensured that there was no strip length effect on local stress distribution near the crack tip area. A succession of models for equal and unequal edge cracks of varying crack lengths and separations were generated using the mesh generating program. To model uniform tension, nodes at the end of the strip were constrained and nodes at the opposite end were applied with a point load as shown in Figure 2.4.

Figure 2.5 shows the applied loading and boundary constraints of an FE model. Figure 2.6 shows an example of deformed and undeformed FE model of two equal crack lengths while Figure 2.7 shows a similar case for two unequal crack lengths. Examples of colour contour plot of the y-component of stress for the case of equal and unequal crack lengths is shown in Figure 2.8 and Figure 2.9 respectively.

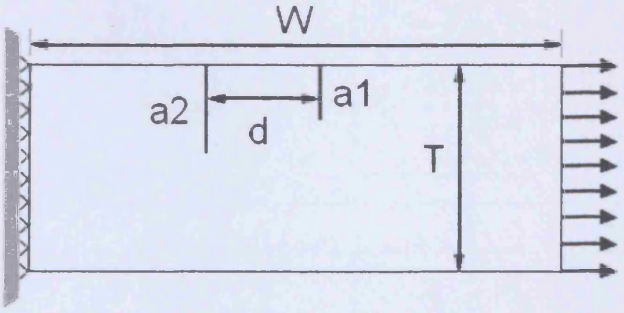

Figure 2.4: Notation used in FE modelling.

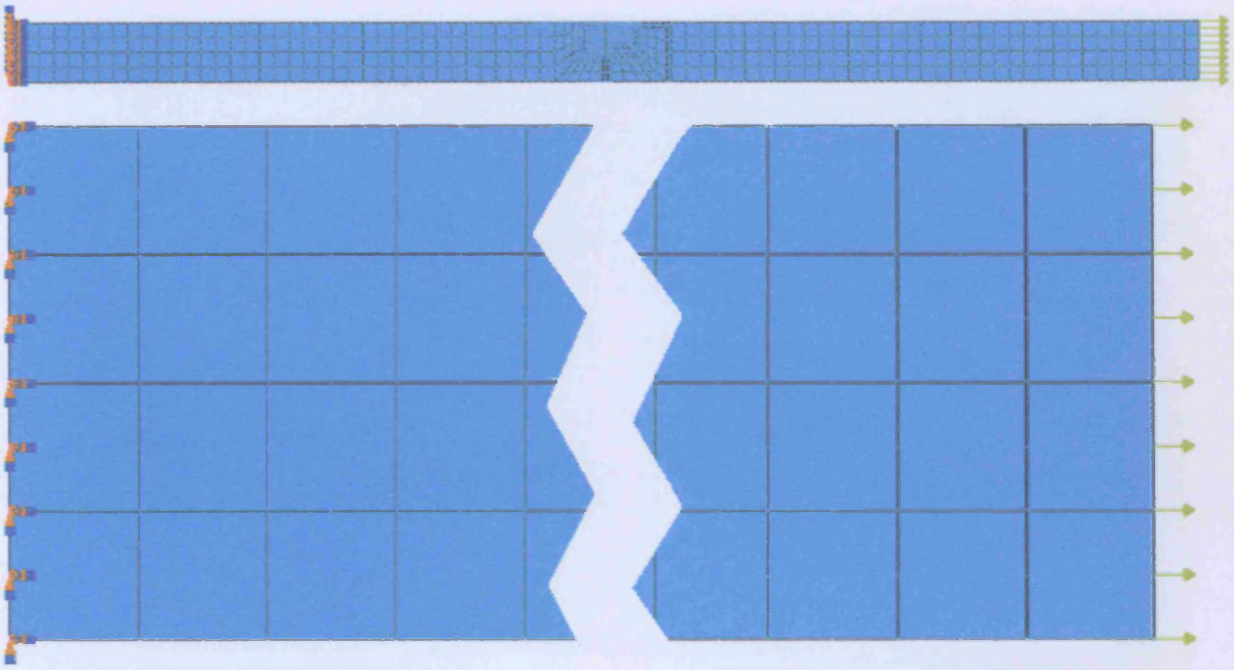

Figure 2.5: FE model showing applied loading and boundary constraints for uniform tension.

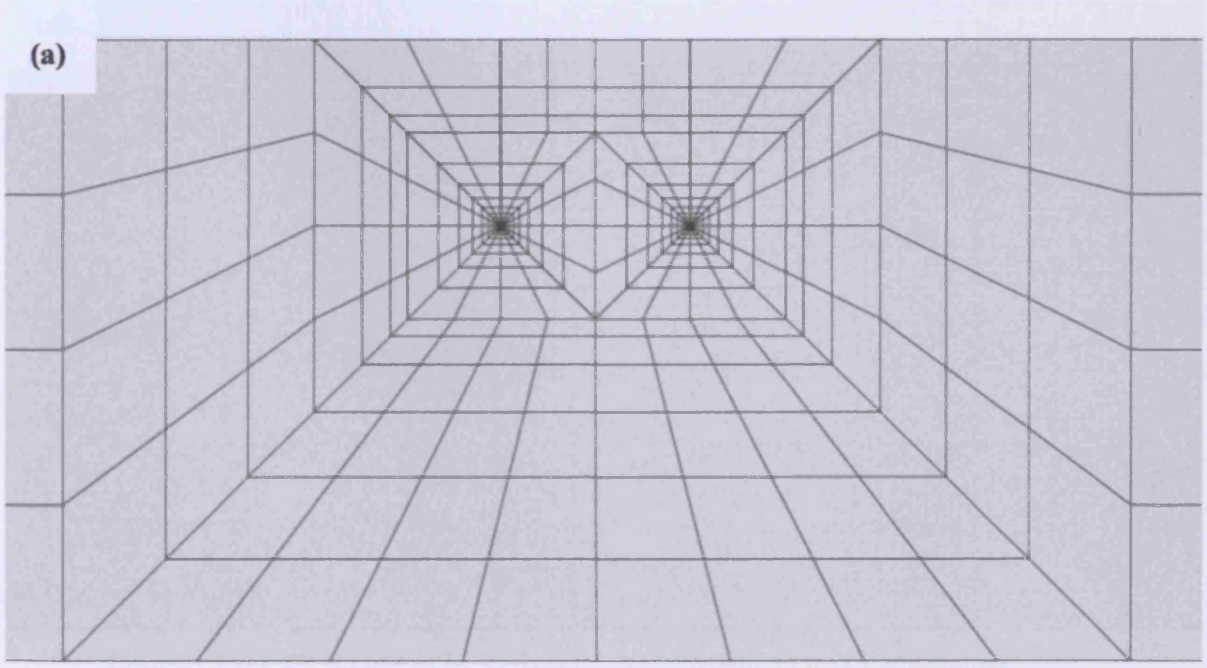

Figure 2.6 (a): FE model of two similar cracks before deformation.

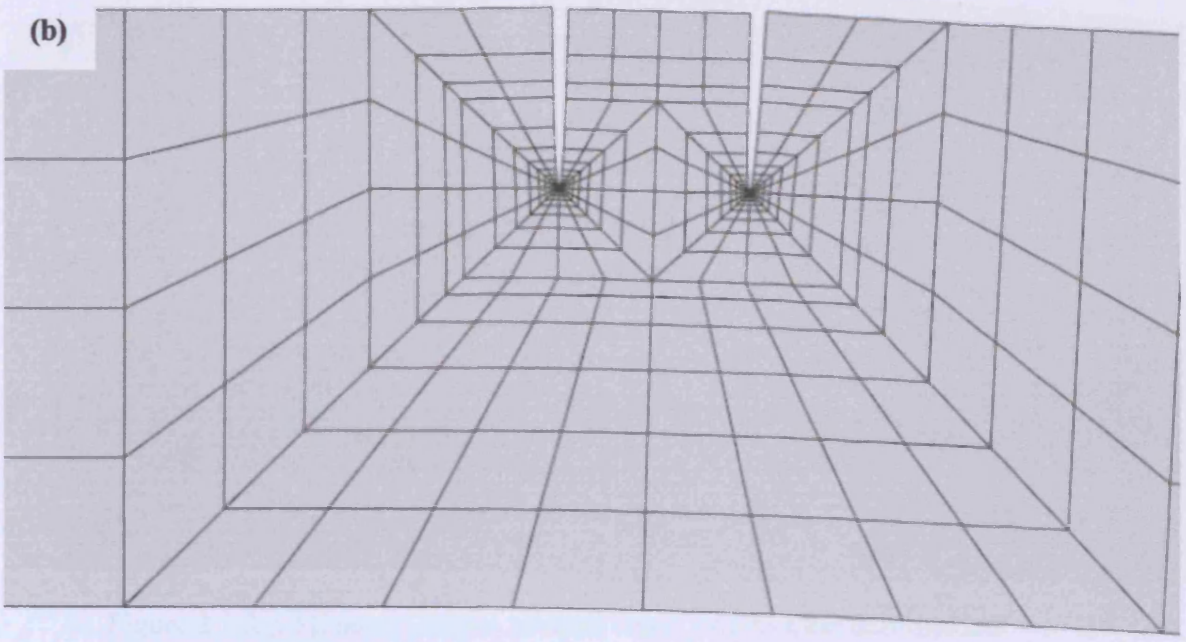

Figure 2.6 (b): FE model of two similar cracks after deformation.

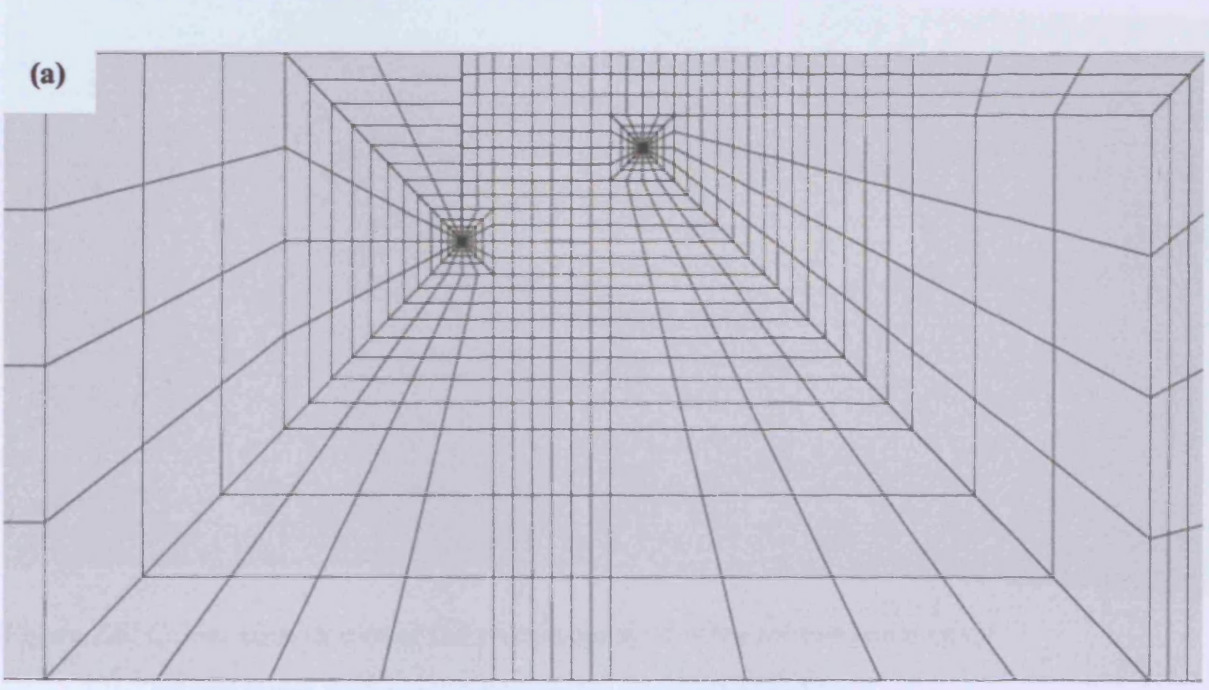

Figure 2.7 (a): FE model of two unequal crack lengths before deformation.

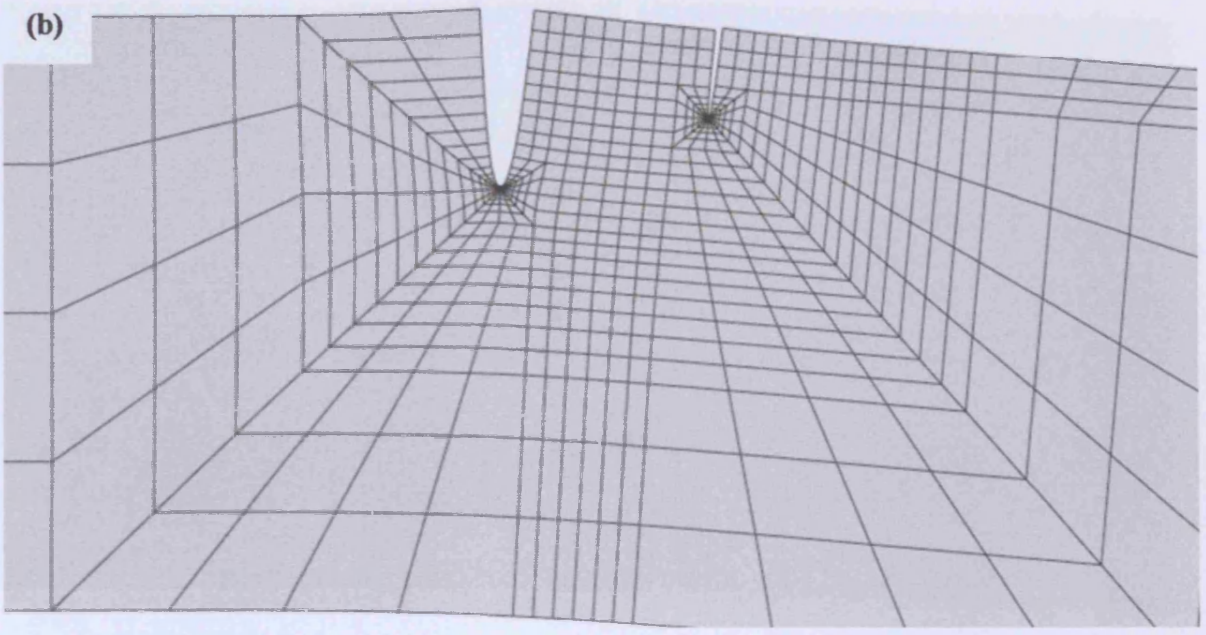

Figure 2.7 (b): FE model of two unequal crack lengths after deformation.

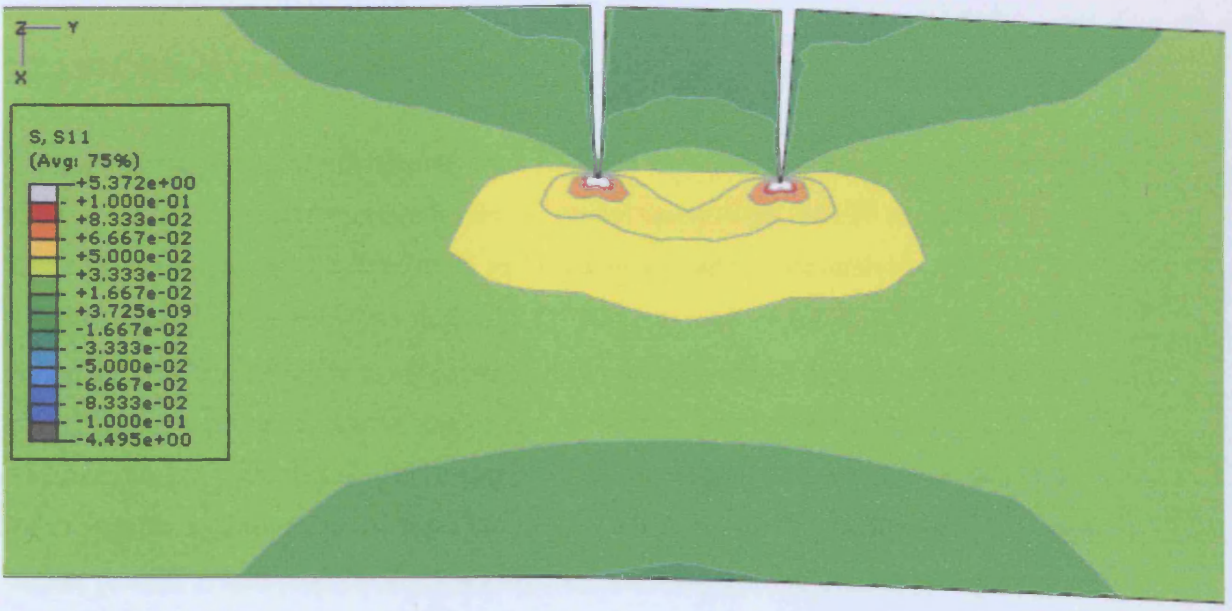

Figure 2.8: Colour contour plot of the y-component of stress for two equal crack lengths under uniform tension (a/T=0.30 and d/T=0.30).

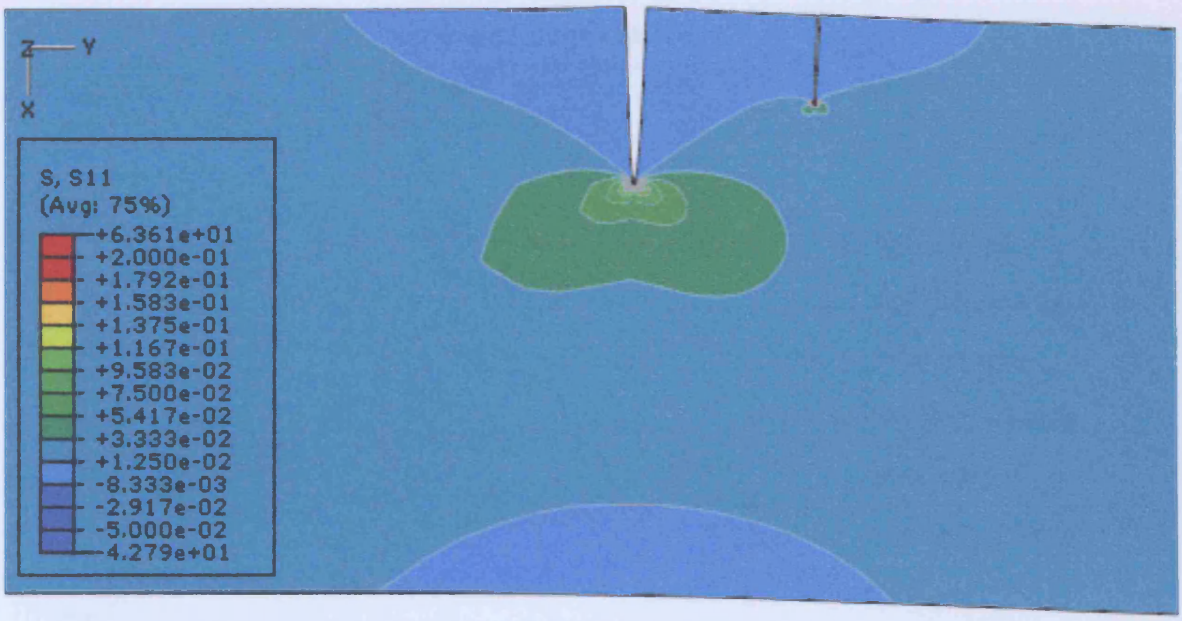

Figure 2.9: Colour contour plot of the y-component of stress for two unequal crack lengths under uniform tension (a2/T=0.30, a1/T=0.15 and d/T=0.30).

2.2.2 SIF Results of Two Edge Cracks

Comparison between FEA results and Ref. [2.5] for two similar edge cracks are shown in Figure 2.10. Each symbol represents one FE model constructed for SIF determination. Three values of a/T equal to 0.05, 0.25 and 0.45 were used for the analysis. FEA results show good correlation with the solution [2.5]. The maximum error for all three different values of a/T is 3% which is equal to the quoted maximum error of the published results [2.5]. The three curves start with low values of SIF and increase to a constant value where at this point the two cracks show no interaction between each other. At this time the two cracks can be treated as two independent edge cracks. The results also show that shorter parallel cracks require larger normalised crack separation, b/a, than longer parallel cracks in order to eliminate the interaction between two cracks. However, overall SIFs for longer parallel cracks are higher than shorter parallel cracks.

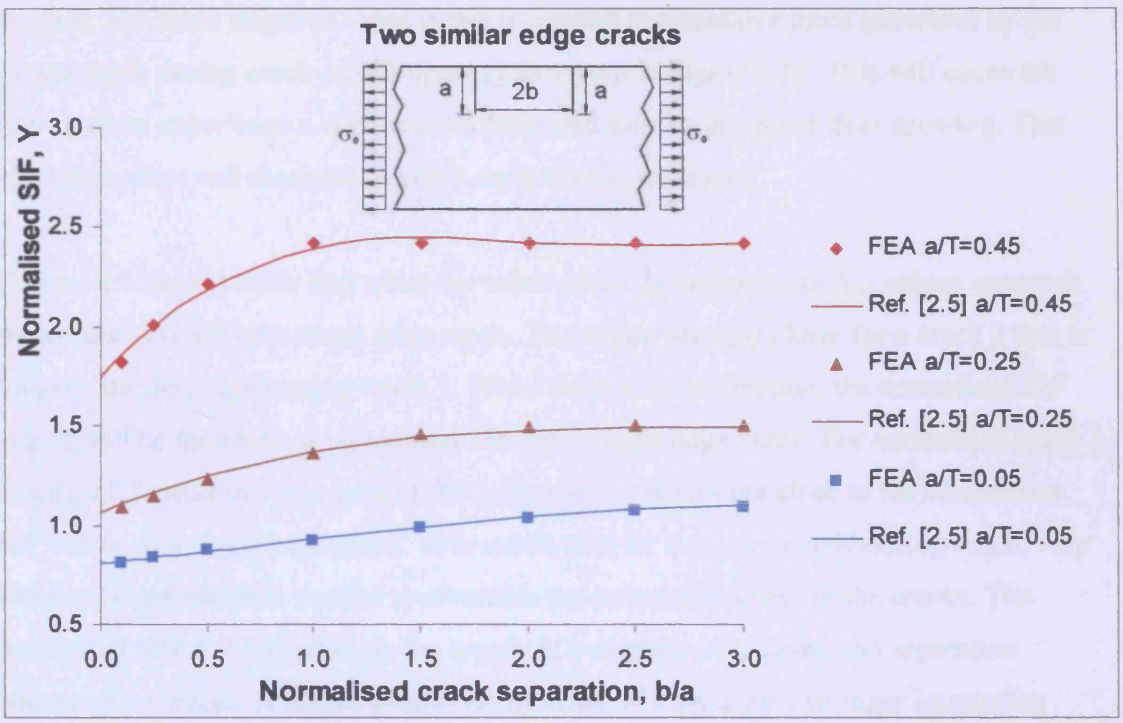

Figure 2.10: Comparison between FEA and Jiang *et al.* [2.5] for two similar edge cracks.

Results of SIFs for the case of two unequal crack lengths are shown in Figures 2.11(a)-(c). The figures show result of normalised SIF of crack 2, Y_{a2} using three a1/T values equal to 0.05, 0.30 and 0.45. Values of normalised crack separation, d/T used to obtain Y_{a2} are equal to 0.2, 0.4 and 0.6. Published [2.6] FEA values were plotted as solid lines to compare with FEA results obtained in this chapter. Solution [2.7] for a single edge crack under tension was also plotted for each graph to observe the interaction effect between two cracks.

Overall results show good correlation with the published values with most of the relative error is less than 2%. A few points have a large error when the crack separation is small (d/T equal to 0.2) and Y_{a2} is close to zero. However, these SIF values are not critical. The chance of these cracks growing is very small because their normalised SIF values are either very small or negative. Values are negative even though the strip was under

tension. The small negative value is due to a small compressive force generated by the longer crack during crack mouth opening as shown in Figure 2.12. This will cause the tiny crack to experience a compressive force and thus be protected from growing. This shielding effect will diminish as crack separation is increased.

Figures 2.11(a)-(c) show that when the value of d/T is increased all Y_{a2} values approach the normalised SIF of a single edge crack. The values are also closer for a crack 2 that is longer than the neighbouring crack 1. When there is no interaction, the normalised SIF values will be the same as normalised SIFs of a single edge crack. For normalised crack 1 length, a1/T equal to 0.05, most of the values of Y_{a2} values are close to the normalised SIF values of a single edge crack. This shows that for a shorter neighbouring crack, very little crack separation is needed to eliminate the interaction effect of the cracks. The interaction effect will depend on the length of a neighbouring crack and separation between two cracks. A longer neighbouring crack will produce a stronger interaction effect while a shorter neighbouring crack will produce a less interaction effect. However with the interaction effect, all normalised SIFs for edge cracks under tension are smaller than single edge cracks under tension.

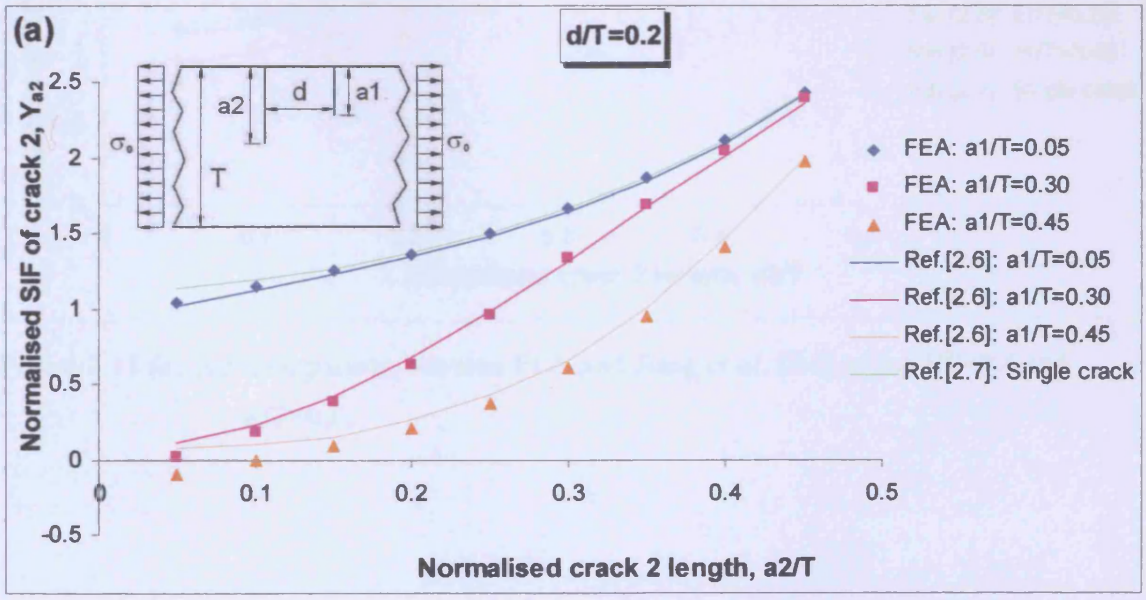

Figure 2.11 (a): Comparison between FEA and Jiang *et al.* [2.6] using d/T=0.2.

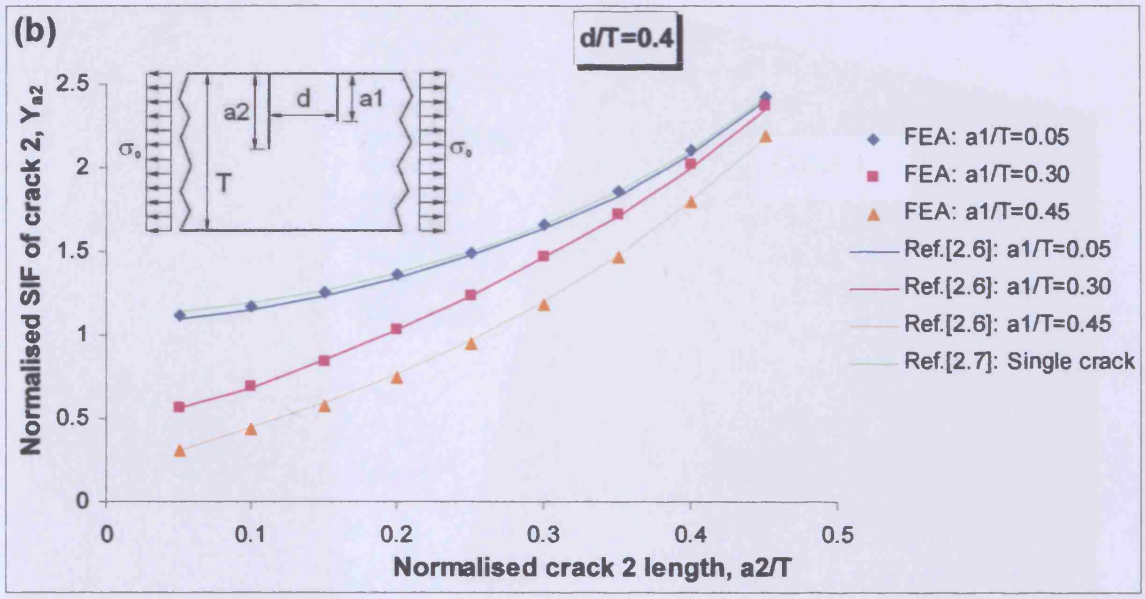

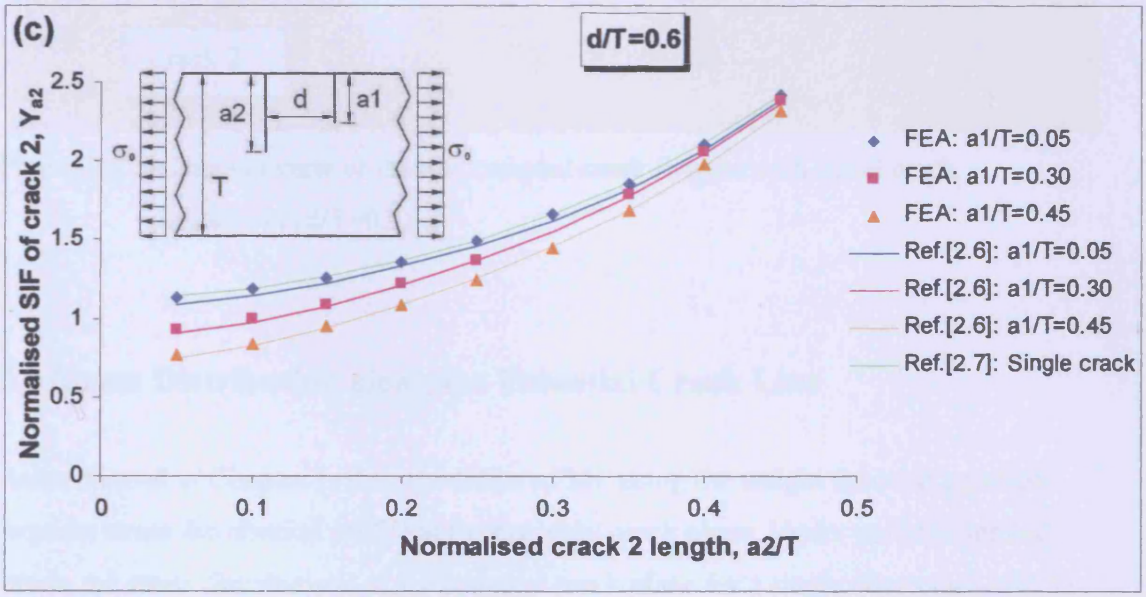

Figure 2.11 (b)-(c): Comparison between FEA and Jiang *et al.* [2.6] using d/T=0.4 and d/T=0.6.

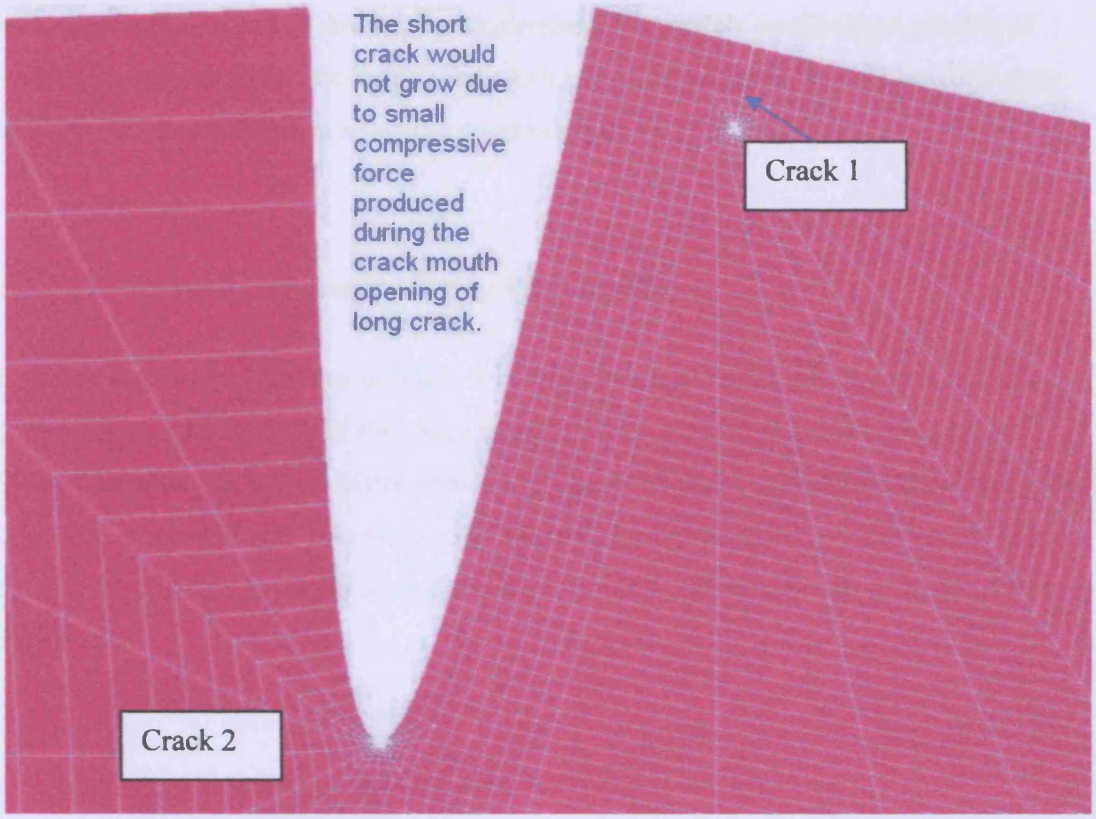

Figure 2.12: Close-up view of the two unequal crack lengths with small crack separation (d/T=0.2).

2.3 Stress Distribution along the Potential Crack Line

As mentioned in Chapter 1, the calculation of SIF using the weight function equation requires stress distribution profile at the potential crack plane. Under uniform applied stress, the stress distributions at the potential crack plane for a single edge crack will be uniform but not for the case of two edge cracks. The stress distributions at the potential crack plane will be non-uniform because of the presence of another crack which causes geometric discontinuities.

The objective of the study of the stress distribution along the potential crack line is to examine whether there is any relation between non-uniform stress distributions and the

interaction effect between cracks. For this reason, FE models containing a crack 1 of varying length were produced using the mesh generator program to examine their non-uniform stress distributions along the neighbouring crack plane 2.

2.3.1 FE Model to Determine Stress Distribution

FE models generated for non-uniform stress distribution are similar to the FE model generated to evaluate SIFs of two edge cracks except it contains only one edge crack. Since the reading of y-component of stress can only be taken at nodal position, the area of interest was meshed with relatively high density in order to provide relatively higher options of locations for stress measurements. The notation used in this model is shown in Figure 2.13.

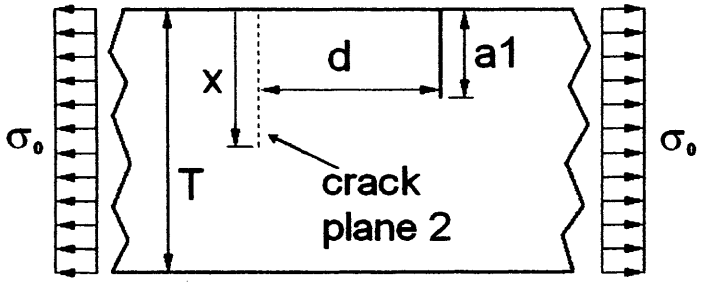

Figure 2.13: Notation used for non-uniform stress distribution study.

A succession of models containing varying crack 1 lengths was generated using the mesh generator program. For each fixed value of crack 1, the y-component of stress, $\sigma(x)$ was measured along the potential crack 2 plane, x at crack separation d. Stress measurements were taken from x/T equal to 0.0 until approximately 0.50. The value of x/T was limited to half of the strip width as the SIFs are only evaluated within this limit. The values of $\sigma 2(x)$ were normalised against the stress remote from the crack plane, σ_0. Using the same FE model, the measurements of $\sigma 2(x)$ were repeated at other d values. A total of nine FE models of varying crack 1 lengths were used for $\sigma 2(x)/\sigma_0$ measurements. A FE model

with a1/T equal to 0.40 was used for the study is shown in Figure 2.14. Figure 2.15 shows the colour contour plot of y-component of stress.

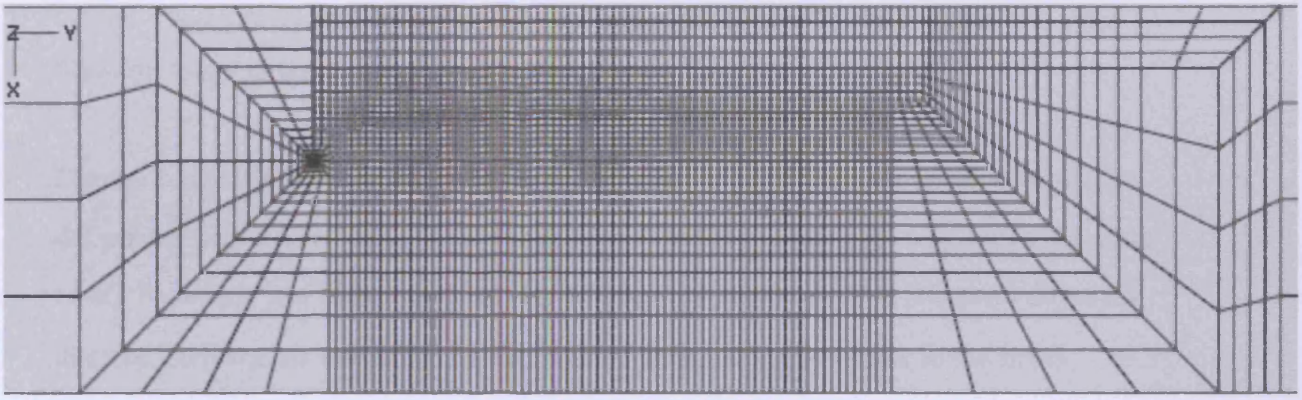

Figure 2.14: FE model used for the non-uniform stress distributions study.

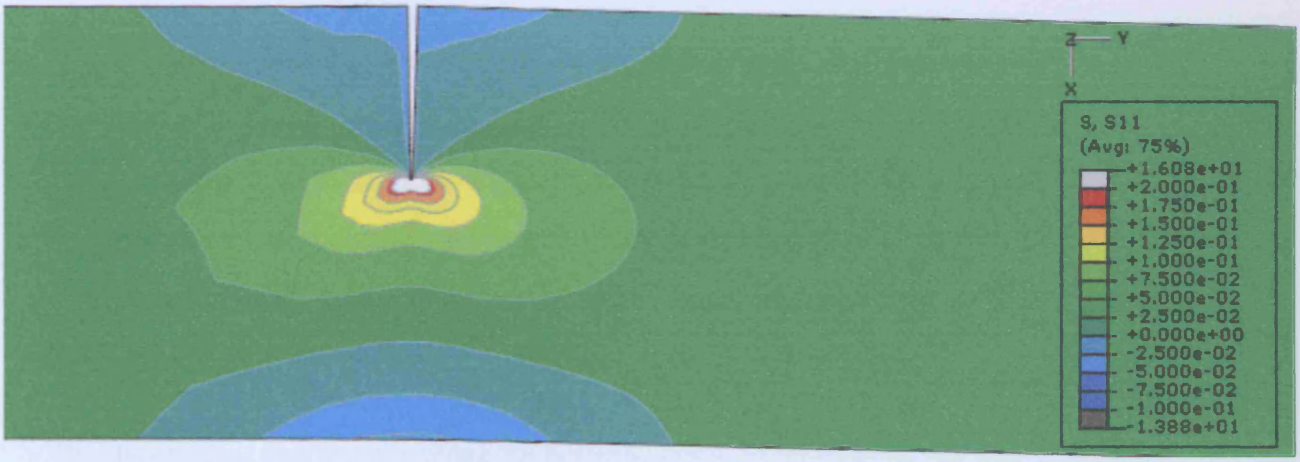

Figure 2.15: Colour contour plot of the y-component of stress for non-uniform stress distributions study (a1/T=0.40).

2.3.2 Results of the Stress Distribution

Results of $\sigma 2(x)/\sigma_0$ are shown in Figures 2.16(a)-(i) using a1/T equal to 0.05 up to 0.45. Values of d/T depend on the nodal position chosen for the stress readings along the x/T values. Their values vary between 0.06 and 1.02. Stress distributions beyond d/T equal to 1.0 were found to be uniform for all a1/T values.

Figures 2.16(a)-(i) shows that the variation of $\sigma 2(x)/\sigma_0$ and its stress gradient at smaller d/T values is relatively high. Both variation and stress gradients are reduced as the value of d/T increases. The values of $\sigma 2(x)/\sigma_0$ will approach 1.0 where at this point the stress distribution becomes uniform. The distribution of $\sigma 2(x)/\sigma_0$ is similar to the stress distribution of nominal stress which is used for a single edge crack. The value of d/T required for $\sigma 2(x)/\sigma_0$ to be uniform depends on the a1/T value. A larger a1/T value will need a larger d/T value in order eliminate the variation of the distribution of $\sigma 2(x)/\sigma_0$.

The variation of $\sigma 2(x)/\sigma_0$ also depends on the value of a1/T. As the value of a1/T is increased, the variation of $\sigma 2(x)/\sigma_0$ is also increased. For example, by comparing between Figure 2.16(a) and Figure 2.16(b), for a1/T equal to 0.05 the distribution of $\sigma 2(x)/\sigma_0$ varies approximately between 0.48 and 1.15 while for a1/T equal to 0.10 it varies approximately between -0.2 and 1.58. The largest variation occurs when a1/T is equal to 0.45 as shown in Figure 2.16(i).

Results of stress distributions along the potential crack 2 plane shows that their variation is similar to characteristics of interaction effects as illustrated by the SIF results of two edge cracks in Section 2.2.2. The variation of $\sigma 2(x)/\sigma_0$ and the interaction effects depend on crack 1 size and its separation. The variation of $\sigma 2(x)/\sigma_0$ could be used as an indicator of the interaction effect. A large variation of $\sigma 2(x)/\sigma_0$ indicates strong interaction effect between two cracks. Chapter 4 discusses more the approach used in order to relate this

variation with the interaction effect. All results in Figure 2.16 were used to establish a general form of the interaction effect between two cracks.

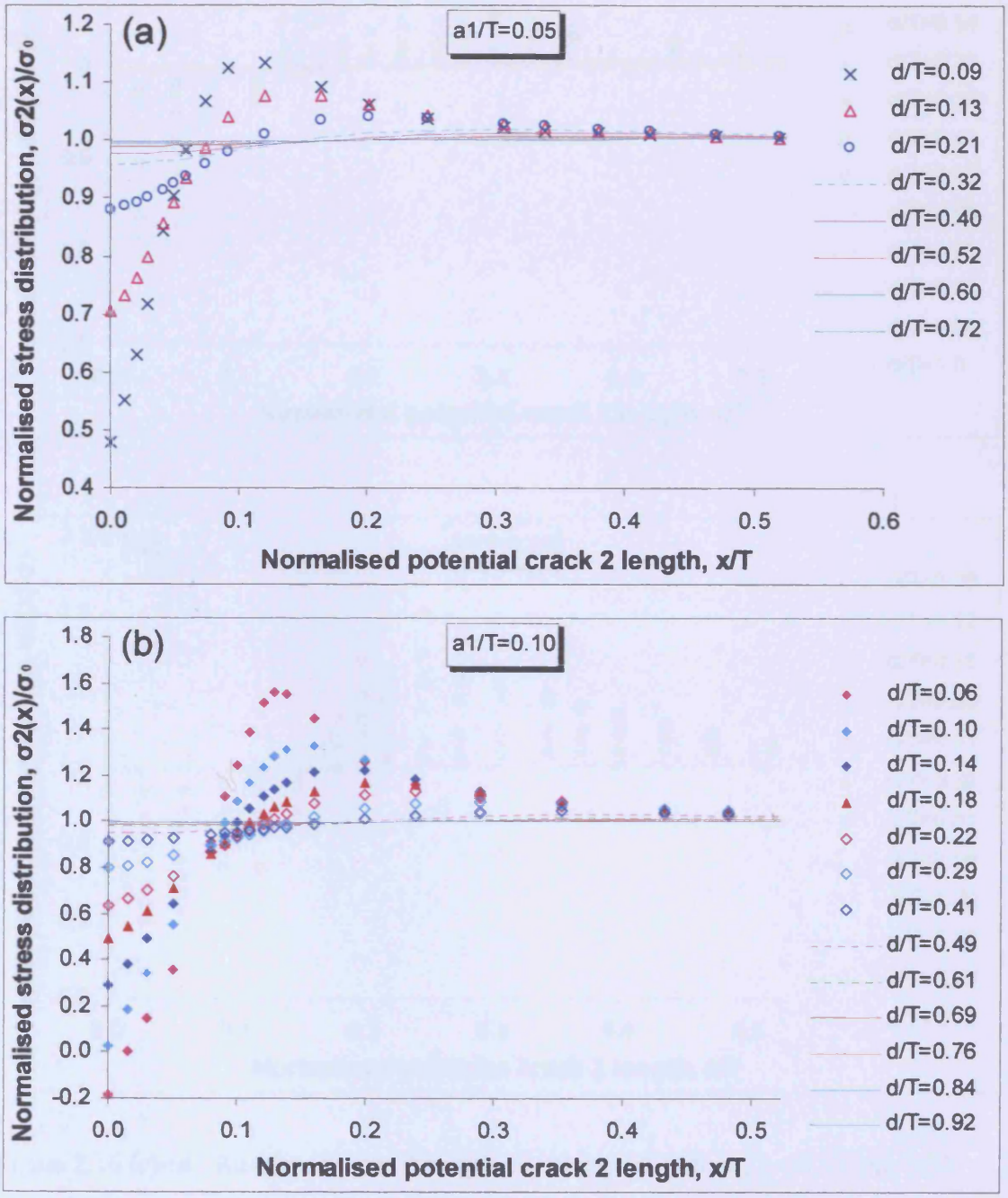

Figure 2.16 (a)-(b): Results of stress distributions along x/T with a1/T = 0.05 and 0.10.

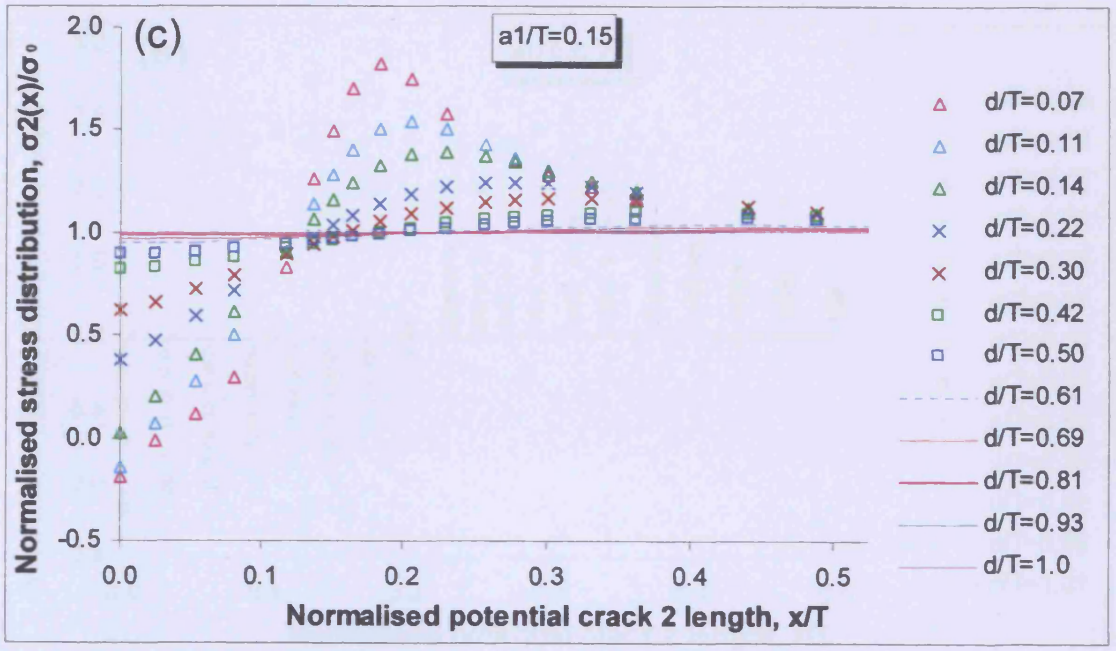

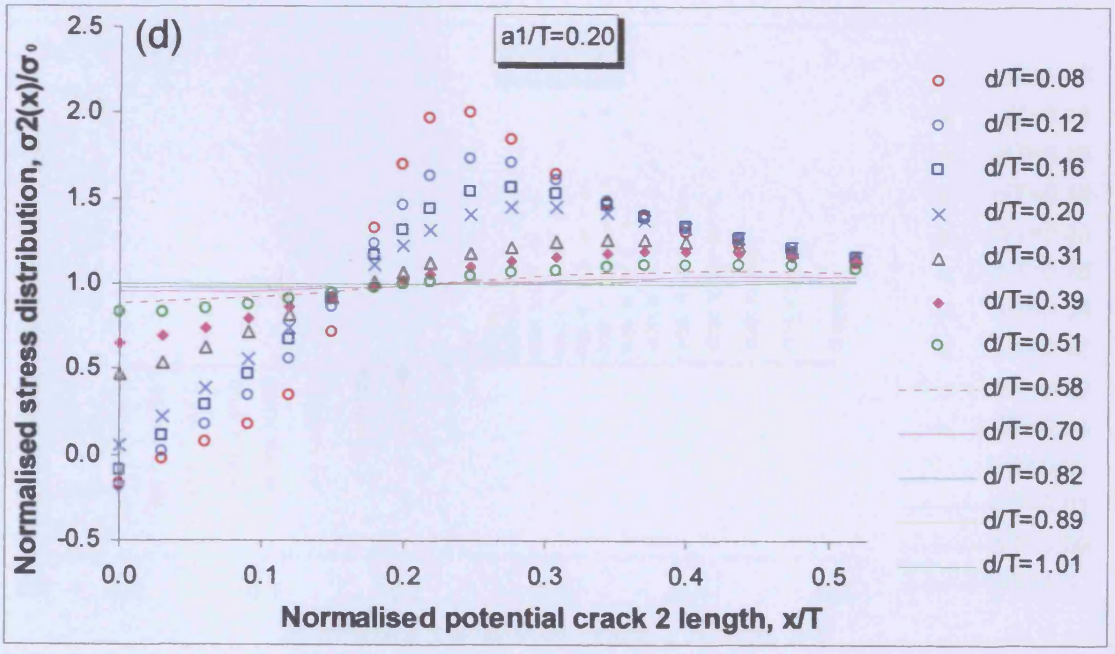

Figure 2.16 (c)-(d): Results of stress distributions along x/T with a1/T = 0.15 and 0.20.

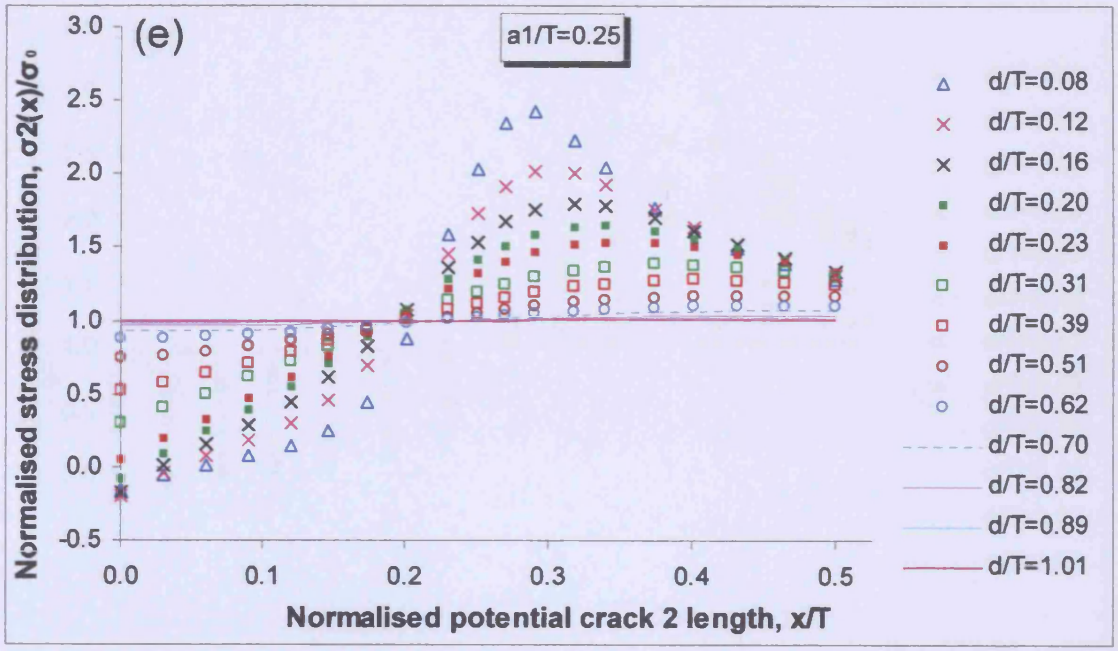

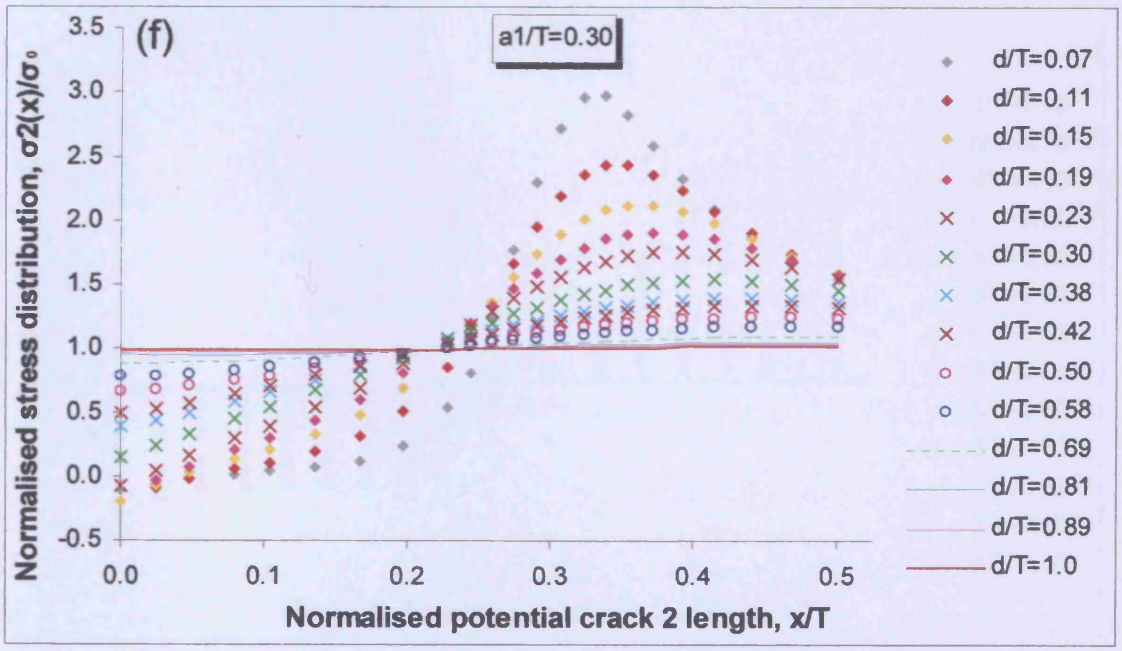

Figure 2.16 (e)-(f): Results of stress distributions along x/T with a1/T = 0.25 and 0.30.

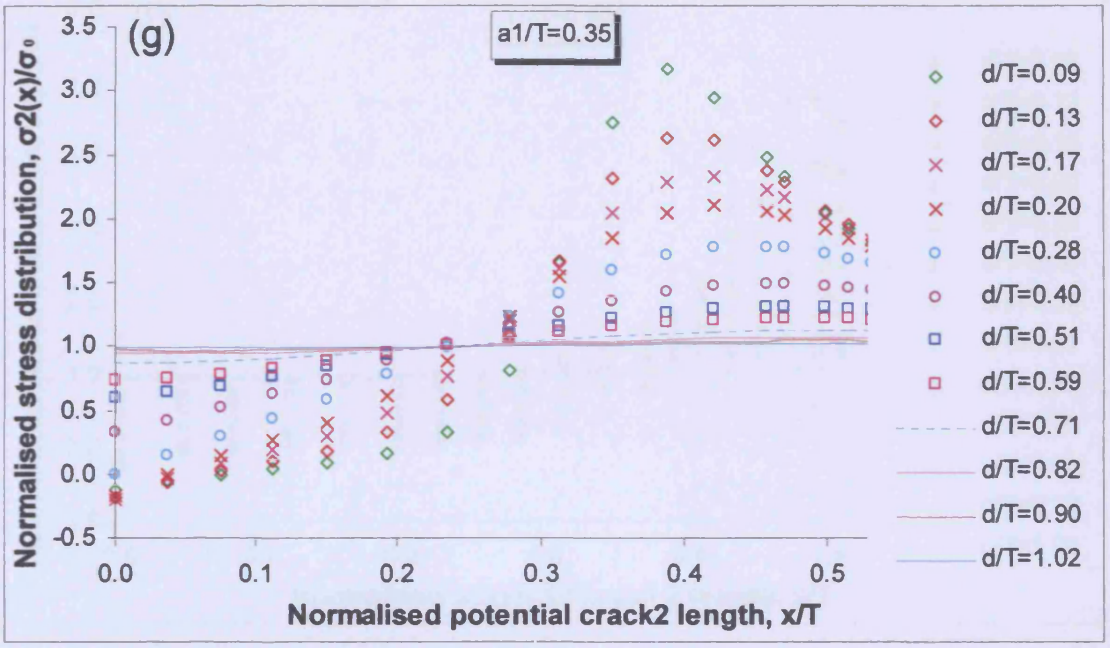

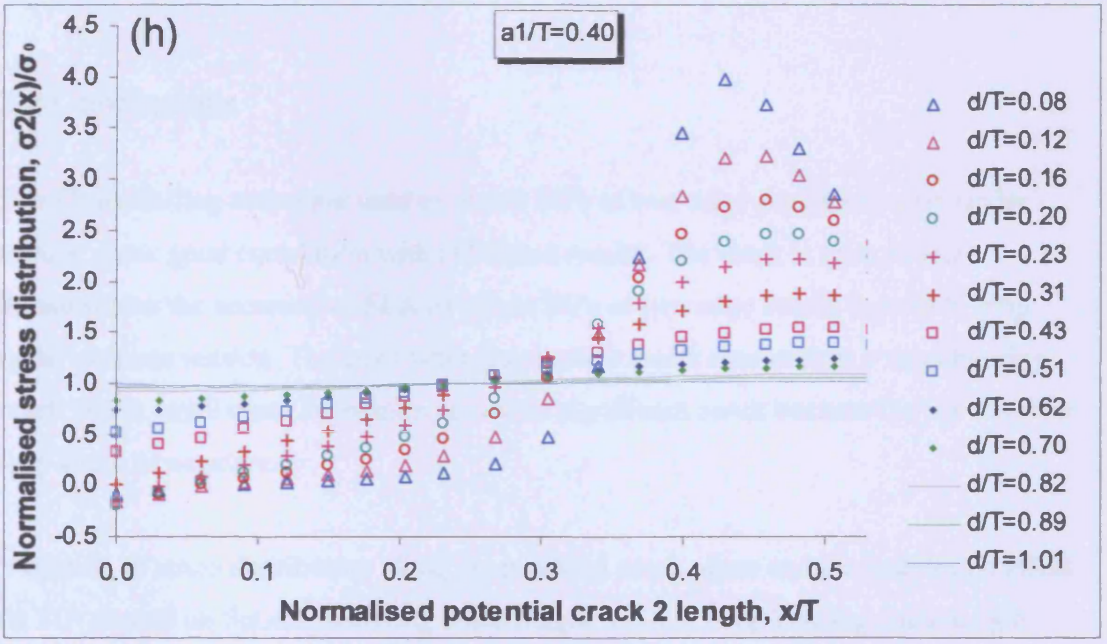

Figure 2.16 (g)-(h): Results of stress distributions along x/T with a1/T = 0.35 and 0.40.

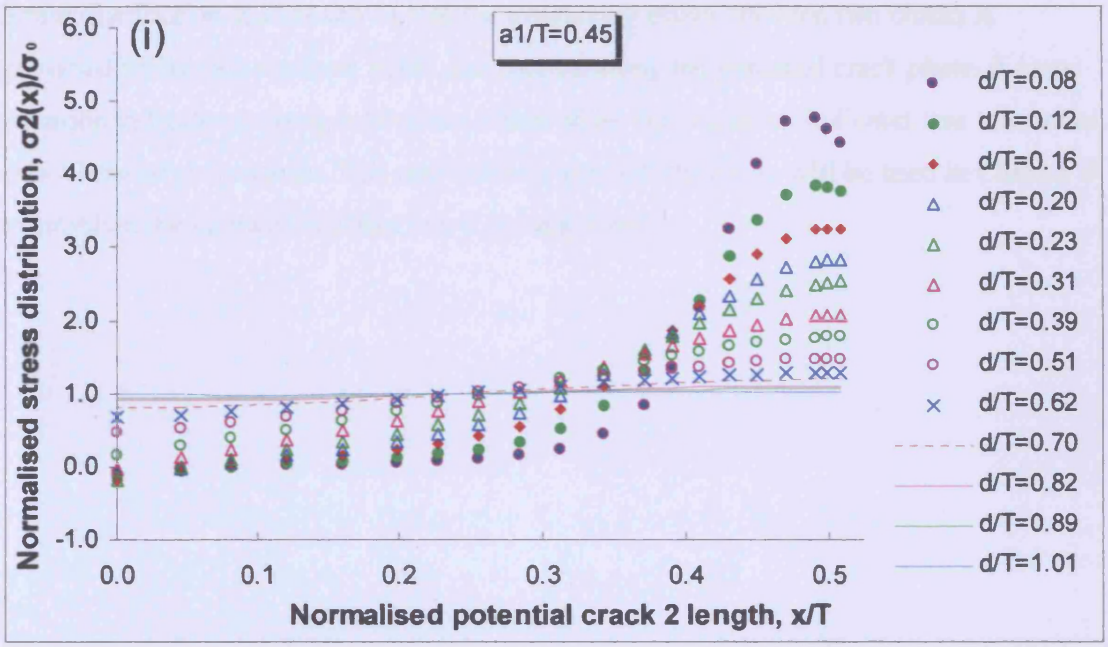

Figure 2.16 (i): Results of stress distributions along x/T with a1/T = 0.45.

2.4 Conclusions

The FE modelling technique used to obtain SIFs of two edge cracks in a strip under tension show good correlation with published results. The work in this chapter demonstrates the accuracy of FEA to obtain SIFs of two edge cracks in a finite strip under uniform tension. The error when the crack is much shorter than a neighbouring crack and at small crack separation shows no significant result because the SIF is either very small or negative.

Variation of stress distribution along the potential crack plane and the interaction effect on SIF depend on the neighbouring crack length. Longer neighbouring crack length produces stronger interaction or larger variation of stress distribution. A longer neighbouring crack needs larger crack separation in order to eliminate the interaction effect or stress distribution variation.

Stress distribution studies shows that the interaction effect between two cracks is governed by the non-uniform stress distribution along the potential crack plane. A large variation indicates a strong interaction effect while less variation indicates less interaction effect between two cracks. This non-uniform stress distribution will be used in Chapter 4 to establish the interaction effect into a general form.

2.5 References

2.1 ABAQUS, version 6.4. Hibbitt, Karlsson and Sorensen, Inc.

2.2 DIGITAL™ Visual Fortran, Profession Edition Version 5.0 for Windows NT and Windows 95, Digital Equipment Corporation (now COMPAQ), 1997.

2.3 Love, A.J., Interpolation of SIF weight functions in fracture mechanics analyses. PhD Thesis, University College London, 2005.

2.4 Teh, L.S., Love, A.J. and Brennan, F.P., Mode I stress intensity factors for edge cracks emanating from 2-D U-notches using composition of SIF weight functions. International Journal of Fatigue, 2006, 28, pp. 355-365.

2.5 Jiang, Z.D., Zeghloul, A., Bezine, G. and Petit, J., Stress intensity factors of parallel cracks in a finite width sheet. Engineering Fracture Mechanics, 1990, 35, pp.1073-1079.

2.6 Jiang, Z.D., Petit, J. and Bezine, G., An investigation of stress intensity factors for two unequal parallel cracks in a finite width plate, 1992, 42, pp. 129-138.

2.7 Brown, W.F. and Srawley, J.E., Plane strain crack toughness testing of high strength metallic materials. ASTM STP 410, 1966.

Chapter 3: Experimental Work of Multiple Edge Cracks

3.0 Introduction

SIFs obtained using FEA or numerical methods are fast and accurate but it is essential to be able to verify these against experimental or other evidence. The FEA technique relies on continuum theory. A continuum does not contain voids, micro cracks, grain boundaries, dislocations, atoms or any other microscopic features that control fracture behaviour in engineering materials. Unlike a mathematical model, an experiment will follow all laws of nature. Thus an experiment often gives important information that FEA overlooks.

A comprehensive literature search revealed very little published material on experimental tests carried out on multiple cracks with unequal crack length. This is likely to be due to the fact that preparation of a multiple cracked specimen is not a trivial task. It is important to consider the SIF ranges for all cracks and thus a suitable load range to ensure all cracks grow during the fatigue testing. To prepare more than one crack at a required length and crack separation is also extremely complicated in addition to the normal difficulties associated with monitoring and measuring fatigue cracks.

In this chapter, two edge cracks located on the same side of a rectangular plate were prepared for fatigue testing to study the interaction effect between two edge cracks under tension loading. A total of seven specimens with different geometries were conducted for the tests. To avoid any major modification to the specimens, two test machines were used separately for fatigue precracking and fatigue tensile testing. Specimens were precracked with one crack using three-point bending then the crack was pinned using welded straps in order to precrack another crack either at the weld toe or notch depending on the crack separation. Completed precracked specimens were machined to reduce their width in order to remove any surface damage before conducting fatigue testing. Crack lengths were measured using travelling microscopes which were fixed to a frame. The material

used for the experiment was Mild Steel which has minimum yield strength of 275MPa. Two end fittings used to hold the specimens during fatigue testing were machined from high strength steel. Besides conducting fatigue tensile testing, CT tests were also conducted to obtain material constants *c* and *m* of the Mild Steel. These results were used in the Paris Law equation to obtain the SIFs of the two edge cracks. Results of the SIFs obtained using experiment were compared with results obtained using FEA. In this thesis only the mode I SIF was considered.

3.1 Test Design

Material used for the fatigue tensile tests was Mild Steel, Grade S275JR [3.1] with minimum yield strength, σ_y equal to 275MPa. Material properties and chemical composition are shown in Table 3.1. The objective of the test was to obtain experimental SIF values of two edge cracks with different crack lengths in a plate under tension loading. Crack separations were also varied to see the interaction effect between two cracks. A total of seven specimens were completed for the tests with parameters as shown in Table 3.2. Notations used are as shown in Figure 3.1.

The tests were divided into two stages. The first stage was to precrack the specimens using three-point bending followed by fatigue testing. The dimensions of the specimens for precracking are shown in Figure 3.2. The dimensions of the specimen were based on calculation of SIF ranges and stresses calculations. Once precracking was completed the width of the specimen was reduced to the dimensions shown in Figure 3.3 for fatigue tensile testing. The reason of this reduction after precracking is to eliminate surface damage due to the notch which was introduced to initiate a crack. The crack geometries that are shown in Table 3.2 were measured after this width reduction. The test machine used for fatigue tensile testing was an Instron model 1251. An Instron model 1362 was used for fatigue precracking. Both machines have maximum loading capacity of 100kN.

It is also important to keep the two cracks in the region remote from the applied tensile load to ensure the nominal stress is uniformly distributed in the crack region. Jiang *et al.* [3.2] kept the ratio of crack depth to the distance from the crack to the loading pin, H greater than 3. This is shown in Figure 3.4. Based on a crack length of 45mm, the maximum crack separation allowed is 100mm. All cracks were grown within this region.

FEA was also conducted using ABAQUS [3.3] to observe the stress distributions within the crack region. A FE half model and a point load with 50kN was modelled as shown in Figure 3.5. The result of the FEA in Figure 3.6 shows that the x-component of stress within the crack region is uniform. Figure 3.7 shows the same result but with a smaller scale of stress magnitude range. It shows that the x-component of stress varies at both edges but the variation is very small and negligible. The stress values are very close to 62.5MPa which is equal to the nominal stress value.

Mechanical Properties

Yield 0.2% (MPa)	U.T.S. (MPa)
≥275	410-560

Chemical composition of Mild Steel (%).

C	Si	Mn	S	N	Cu
0.24	-	1.60	0.045	0.014	0.60

Table 3.1: Material properties and chemical composition of the Mild Steel, Grade S275JR [3.1].

Test	Short crack length, a1 (mm)	Long crack length, a2 (mm)	Distance between cracks, d (mm)	Plate width, T (mm)	a1/T	a2/T	d/T
1	19.61	31.90	31.7	80.45	0.24	0.40	0.39
2	24.40	24.47	33.6	80.30	0.30	0.30	0.42
3	20.02	24.03	34.1	80.20	0.25	0.30	0.43
4	17.13	24.58	26.2	80.65	0.21	0.30	0.32
5	16.10	24.42	49.5	80.25	0.20	0.30	0.62
6	16.12	24.02	64.7	80.50	0.20	0.30	0.80
7	16.13	24.11	81.5	80.08	0.20	0.30	1.02

Table 3.2: Parameters that are used for fatigue tests.

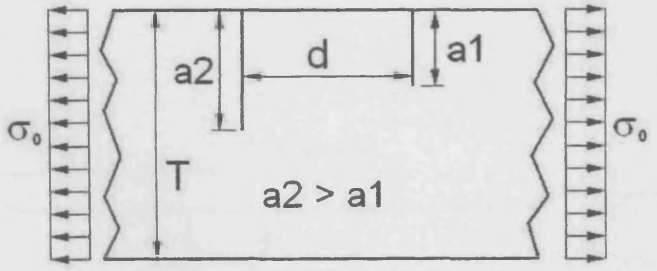

Figure 3.1: Notation used for fatigue testing.

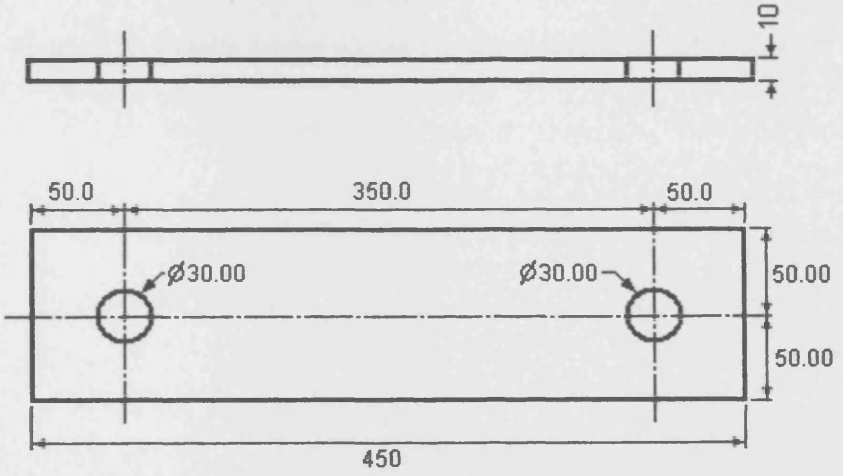

Figure 3.2: Dimensions of the specimens for fatigue precracking (units in mm).

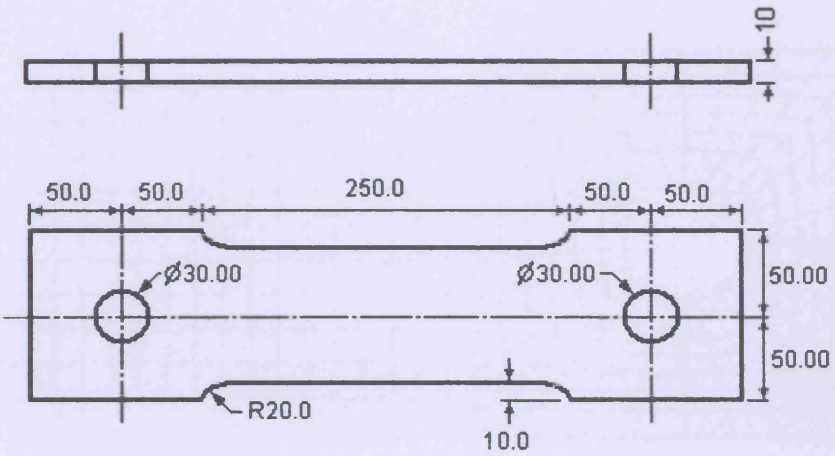

Figure 3.3: Dimensions of the specimens for fatigue testing (units in mm).

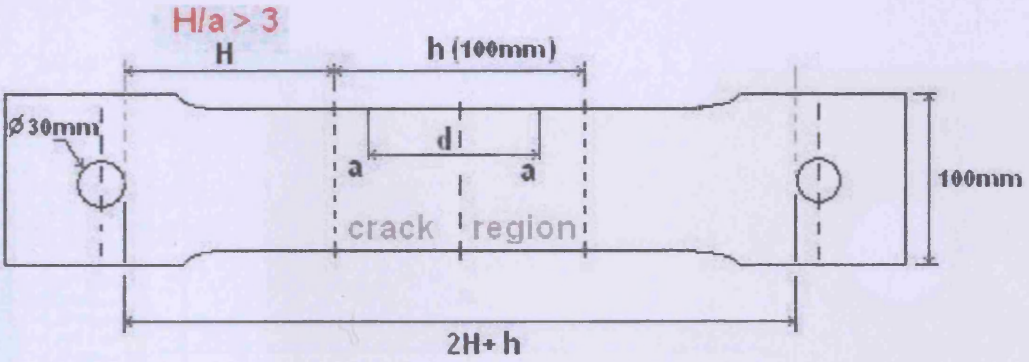

Figure 3.4: Cracks grown within the crack region of 100 x 80 mm^2.

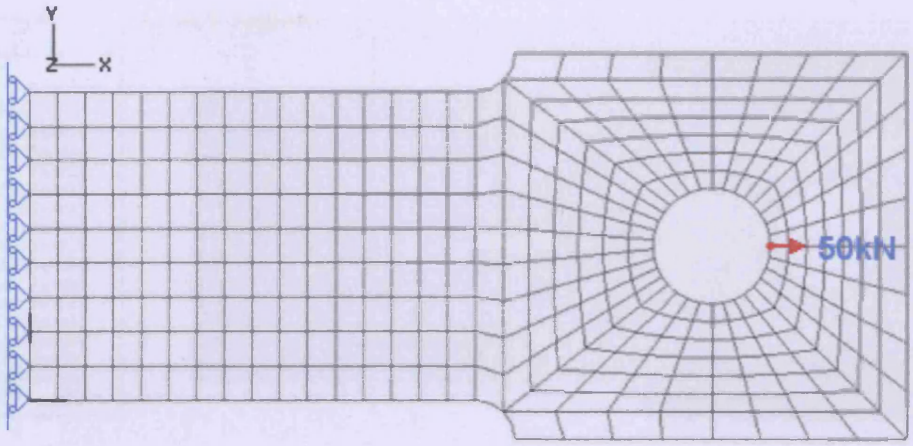

Figure 3.5: FE half model constructed to observe stress distributions at the crack region.

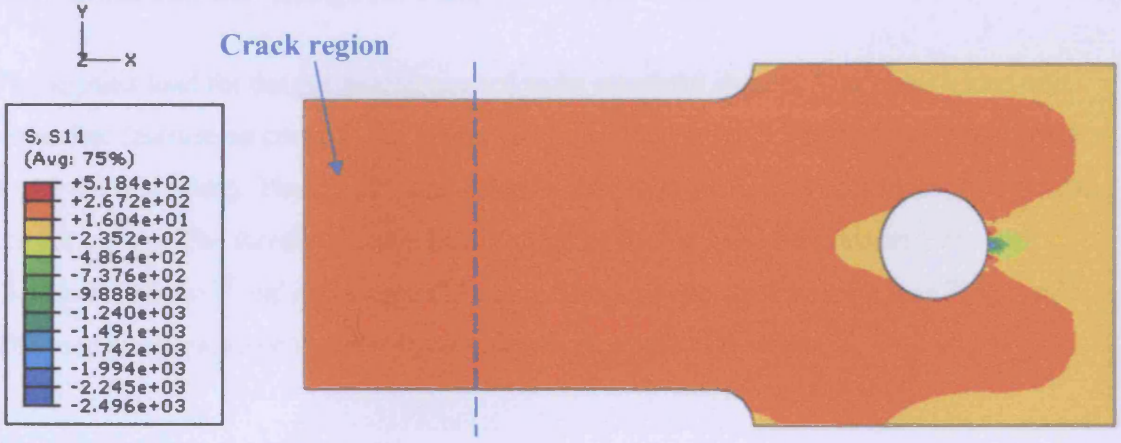

Figure 3.6: FEA results show the x-component of stress distributions.

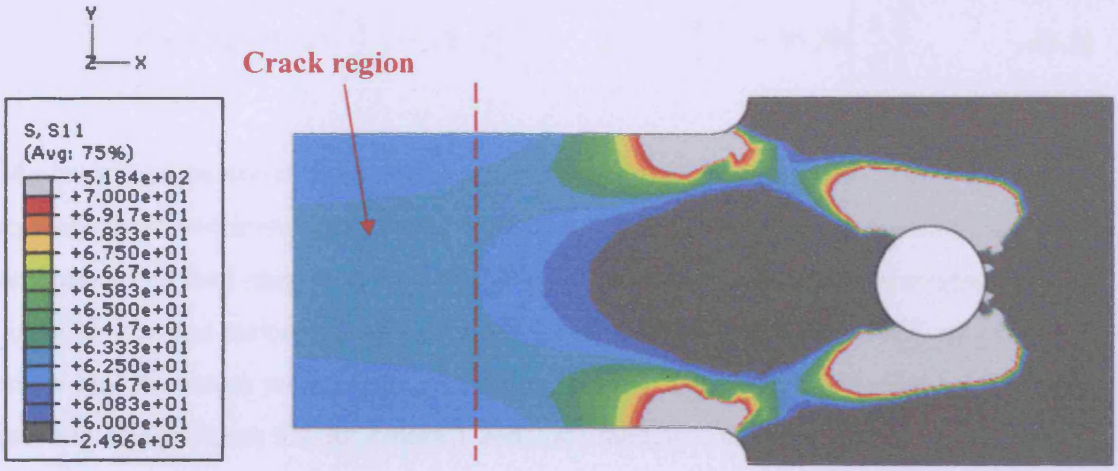

Figure 3.7: Reduced stress magnitude scale shows a small variation in stress within the crack region.

3.1.1 Load and SIF Range for Fatigue Tensile Test

The applied load for fatigue testing needed to be carefully chosen. Too large a load will cause fast fracture on crack 2 (the longer crack) and too small a load will not grow crack 1 (the shorter crack). The chosen load must be able to grow both cracks during the fatigue tensile testing. The threshold value of SIF range, ΔK_{th} for Mild Steel taken from Ref. [3.4] is 8.6MN/m$^{3/2}$ and maximum SIF range, ΔK_{max} taken from Ref. [3.5] is 70MN/m$^{3/2}$. The load range required for testing was chosen from this SIF range.

The SIF range can be written as:

$$\Delta K = \Delta\sigma\, Y \sqrt{\pi a} \qquad (3.1)$$

From Eqn.(3.1) and together with values of ΔK_{th} and ΔK_{max}, minimum and maximum load range can be determined by:

$$\Delta P = A\, \Delta K/(Y\sqrt{\pi a}) \qquad (3.2)$$

where A is cross section of the plate. The normalised SIF solution for an edge crack under tension, Y of Brown and Srawley [3.6] is used for this geometry. The solution is in the form:

$$Y = 1.12 - 0.231\left(\frac{a}{T}\right) + 10.55\left(\frac{a}{T}\right)^2 - 21.72\left(\frac{a}{T}\right)^3 + 30.39\left(\frac{a}{T}\right)^4 \quad (3.3)$$

Minimum and maximum load range was calculated for cracks 1 and 2. The two sets of minimum and maximum load ranges were then combined to get the required minimum and maximum load range that are possible to grow both cracks. The load ranges selected for minimum and maximum were checked for their equivalent value of SIF range to make sure the values were suitable for fatigue testing. Load range was selected for every test and its equivalent SIF for cracks 1 and 2 are tabulated in Table 3.3.

Test	Short crack, crack 1		Long crack, crack 2		Chosen Load Range, ΔP (kN)	Equivalent SIF (crack 2) range ΔK ($MN/m^{3/2}$)	Equivalent SIF (crack 1) range ΔK ($MN/m^{3/2}$)
	Min.Load Range, min ΔP (kN)	Max.Load Range, max ΔP (kN)	Min.Load Range, min ΔP (kN)	Max.Load Range, max ΔP (kN)			
1	19	153	10	85	40	33	18.41
2	15	121	15	121	33	19	18.94
3	18	149	15	123	40	23	18.98
4	21	174	15	121	47	27	18.83
5	22	182	15	121	48	28	18.62
6	22	183	15	124	48	27	18.33
7	22	181	15	122	49	28	18.91

Table 3.3: Load range selected for every test and the equivalent SIF for short and long cracks.

3.1.2 Fatigue Test Stress Calculations

It is important to check the stresses on the specimen before conducting an experiment to avoid damage to the specimen. The dimensions of the plate were selected based on the stress calculations. The stress was kept below yield strength of Mild Steel which equal to 275MPa. The maximum tensile load that was used for the stress calculation is 50kN. The

stress calculations are as shown in Appendix A. All calculated stresses are below the yield strength of the plate. The highest stress is the stress on ligament width i.e. 176MPa.

3.1.3 Crack Length Measurement

A travelling microscope was used to measure the crack length on one side of a specimen. The magnification of the microscope used is ×20 and the accuracy of the vernier scale of the travelling microscope is ±0.01mm. Two travelling microscopes were mounted to a frame to measure the two crack lengths on the specimen during fatigue testing. Only one travelling microscope was used for precracking because the crack was grown individually using three-point bending. The crack length measurement and its equivalent total cycles were recorded for approximately every 0.25mm of crack growth. At this point the specimen was kept under a mean value of sinusoidal cyclic load. A cross-hair engraved on the eyepiece of the scope was used to target the crack tip before reading the crack length on the vernier scale. Crack lengths on both sides were also measured using a ruler at approximately every 5mm of crack growth to record any dissimilarity in order to check any asymmetrical crack growth. The accuracy of the ruler used is ± 0.5mm.

3.1.4 End Fittings

The specimen was held by two end fittings together with two pins as shown in Figure 3.8. The test machine gripped both end fittings to apply a sinusoidal cyclic tensile load. The end fitting and the 30mm diameter pin were machined from high strength steel with a minimum yield strength of 700MPa. The dimensions of the end fitting are shown in Figure 3.9. The stresses on the end fittings are not critical as the total width and thickness are almost double those of the specimens.

Figure 3.8: Two end fittings and the two pins that were used to hold the specimen during fatigue tensile testing.

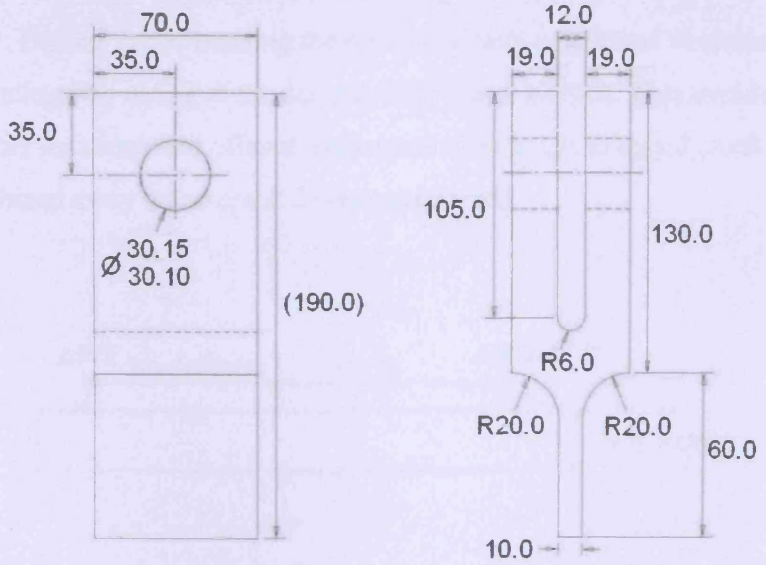

Figure 3.9: Dimensions of the end fitting (all units in mm).

3.2 Fatigue Precracking

The most difficult part of the test programme was to precrack a specimen with two desired crack lengths and with a desired crack separation. Cyclic loading with three-point bending was used to grow cracks 1 and 2 in each specimen as shown in Figure 3.10 and Figure 3.11. A V-shape notch was cut as shown in Figure 3.12 with a 2mm depth to initiate a crack at the desired location during cyclic bending loading.

After crack 1 (or the short crack) was grown to a required depth it was then pinned by using three welded straps as shown in Figure 3.13 to arrest its growth during further cyclic bending. One strap was welded on the top and two straps were welded at both sides of the specimen. The sizes of the straps used were 50 x 10 x 10mm and 30 x 10 x 5mm. It is much easier to stop a shorter crack than a longer crack as longer cracks have higher SIF values. The weld toe was then machined at a desired distance from the crack 1 to make sure crack 2 would grow with the correct crack separation. The technique to grow crack 2 from a weld toe is only suitable for small crack separation. For a larger crack separation, approximately more than 40mm, the crack 2 was grown from a V-shape notch as shown in Figure 3.14. During cyclic bending the point load was positioned to ensure the maximum bending was acting at the desired weld toe or a notch. This avoided a crack growing at other locations and offered extra protection to the strapped crack. The strap was then machined away when crack 2 was completed.

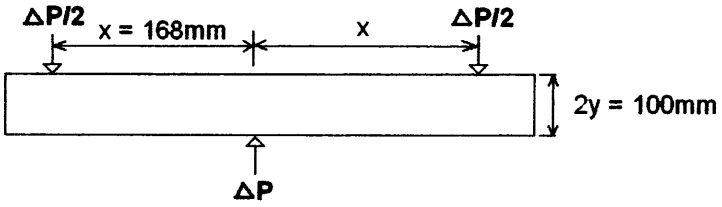

Figure 3.10: Three-point bending used to precrack specimens with the required crack length.

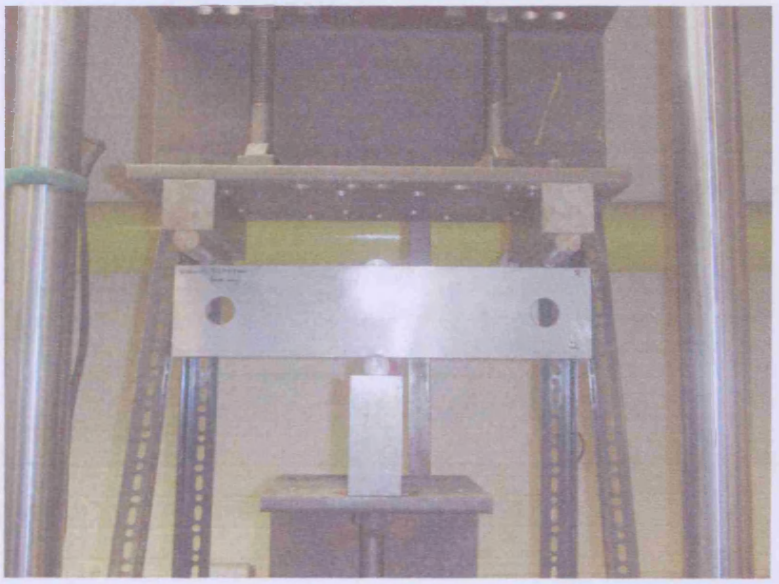

Figure 3.11: Photo of a specimen under cyclic bending loading.

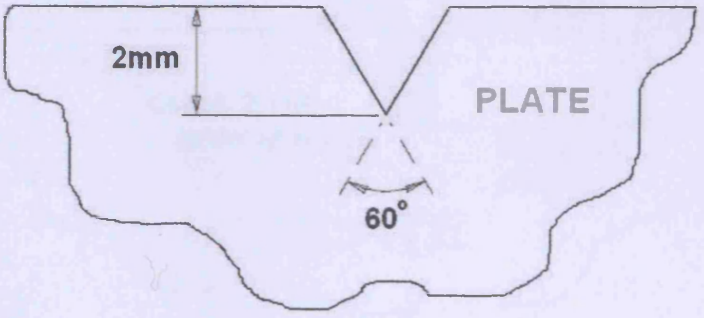

Figure 3.12: V-shape fine cut on an edge of the specimen to initiate a crack.

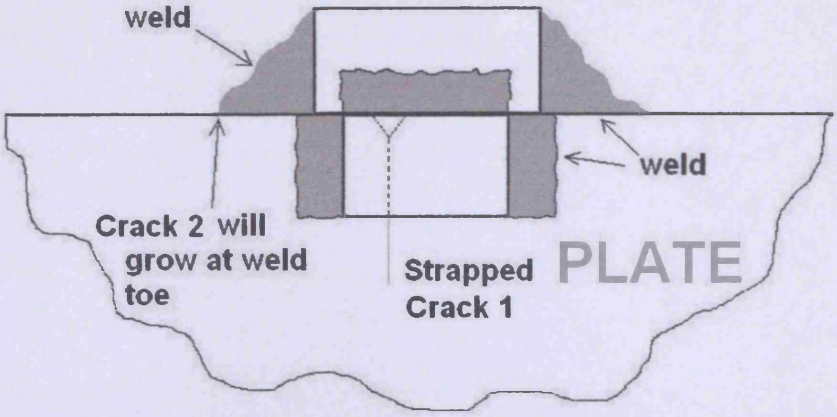

Figure 3.13: Three mild steel straps welded to stop the first crack from growing before starting to grow a second crack at the weld toe.

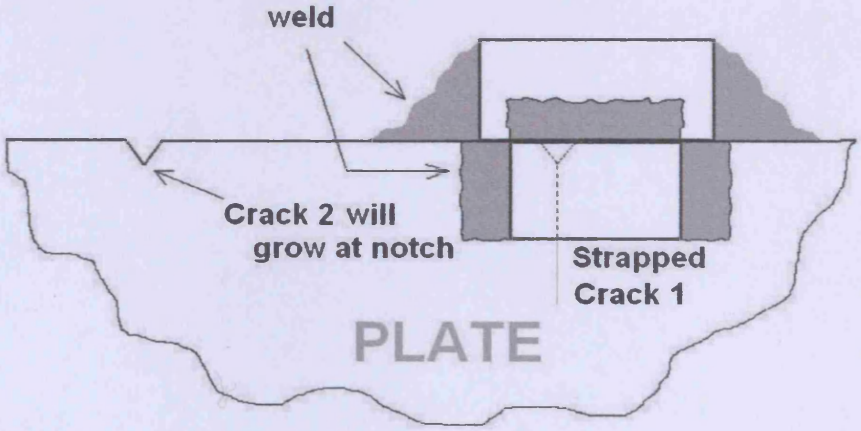

Figure 3.14: For a crack separation more than 40mm the second crack was grown from a V-notch.

The load range, ΔP required for bending moment was calculated by using Eqn.(3.2) and equations below:

$$My = \Delta\sigma I \quad (3.4)$$

and

$$\Delta P = M/x \quad (3.5)$$

where x is equal to 168mm, half of distance between two point load contact as shown in Figure 3.10; I is the second moment of area; and y is half of the plate width. In Eqn.(3.2) the threshold value of SIF range required to initiate a crack, ΔK is equal to $8.6MN/m^{3/2}$. The normalised SIF solution for an edge crack under bending, Y obtained from Ref. [3.7] is used:

$$Y = 1.107 - 2.120\left(\frac{a}{T}\right) + 7.71\left(\frac{a}{T}\right)^2 - 13.55\left(\frac{a}{T}\right)^3 + 14.25\left(\frac{a}{T}\right)^4 \qquad (3.6)$$

The calculated minimum load range, ΔP required for cyclic bending loading is equal to 18.5kN. The bending load was cycled using a sinusoidal wave between -1kN and -31kN with a load range of 30kN during precracking. Its mean value was 16kN. The maximum stress generated on the plate edge by this load setting was 170MPa which is below the yield strength of the Mild Steel. The total number of cycles taken to produce a 1mm crack from the machined notch was approximately 100,000 cycles. This load setting was only used to precrack the crack 1. The load range used for precracking the crack 2 was lower in order to reduce the bending effect on the crack 1 which was strapped to stop it from growing. The bending load was cycled between -1kN and -27kN with a load range of 26kN. Using this load setting it is estimated that an average of 100,000 cycles were required to initiate a 0.2mm crack length from a notch tip or weld toe.

3.2.1 Fatigue Precracking Procedure

A precrack test set-up on an Instron 1362 100kN servo-hydraulic fatigue test machine is as shown in Figure 3.15. The testing was conducted at ambient temperature at a frequency of 1.5Hz. During precracking, readings of crack length, a and number of fatigue cycles, N for each crack were recorded. A travelling microscope was mounted vertically to measure the crack length on one side of the specimen during the cyclic three-point bending loading. The crack length measurement and its equivalent number of cycles were recorded approximately every 0.25mm of crack growth. The readings were taken under a static mean value of cyclic load. Graphs of a versus N were plotted and its crack growth rate, da/dN was determined from the gradient of the curve by using an

incremental polynomial method which uses a third order polynomial and seven data points. Finally the value of ΔK was determined using Eqn.(3.1).

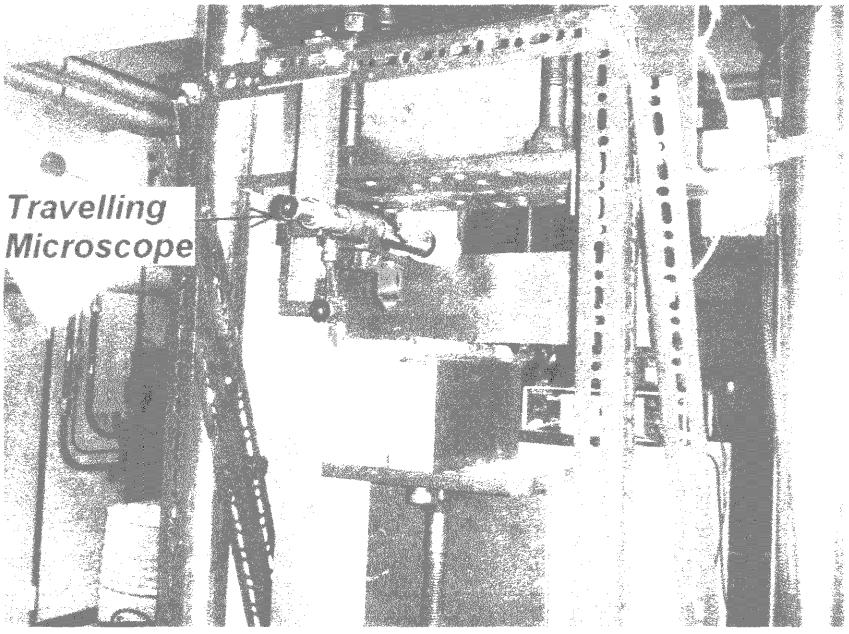

Figure 3.15: A precrack test set-up on an Instron 1362 100kN fatigue test machine.

3.2.2 Fatigue Precracking Results

Figure 3.16 shows the total fatigue cycles taken to precrack the crack 1 for all test specimens. Crack 1 lengths shown in the figure include the notch depth of approximately 2mm. The total number of fatigue cycles taken to precrack vary from approximately 160,000 to 660,000 cycles. This depends on the crack 1 initiation length before taking the reading, total precracked length, variation in notch qualities and test set up variation for each specimen. The total number of fatigue cycles does not including the fatigue cycles taken to initiate a crack. All test specimens were initiated between 2.2 and 3.5mm (including a notch depth of 2.0mm) of crack length before taking readings of their fatigue crack growth data. Fatigue crack growth data for test specimen 2 was started after 5mm of crack initiation due to unexpected machine stoppage that prevented data being taken.

Figure 3.17 shows the total number of fatigue cycles taken to precrack the crack 2. The total number of fatigue cycles varies from 150,000 to 580,000 cycles.

Figure 3.18 shows a plot of crack growth rate versus SIF range for all precrack tests of crack 1 and crack 2. The plot also includes crack propagation data obtained from ESDU 81011 [3.5] which shows limits and mean of the crack propagation data for a group of low-strength alloy steels with yield strength between 250MPa and 350MPa. Most of the fatigue precrack data are within these limits. The data is scattered with a large range at the early crack growth but reduced after the SIF range of the crack tip reaches approximately $30MN/m^{3/2}$.

Figure 3.19 shows separate results for fatigue crack growth rate data of (a) crack 1 and (b) crack 2 for each precrack test. Fatigue crack growth rate data for crack 1 as shown in Figure 3.19(a) are good except for precrack test 2, 4 and 5 which demonstrate slower crack growth rates at the early stage of crack growth. However, the crack growth rate is increased as the crack grows longer. This is probably due to the set up of these specimens during precracking using three-point bending. It is not an easy task to align a specimen with a thickness of 10mm and length of 450mm on three contact points for fatigue bending. During the cyclic loading, the specimen is not only bending in the specimen plane but also tend to bend slightly in the normal direction of the specimen plane. Other factors such as blunt notches and variation in material properties also cause deviation. Figure 3.19(b) shows the fatigue crack growth rate data during precracking crack 2. Most of the data are well scattered within the limits and in close proximity to the mean line. The crack growth rate data for precrack test 1 to 4 are higher than the mean line at early crack growth. Most probably this is due to the effect of the weld toe that was used for crack 2 initiation still affecting the crack growth rate at the early stage. All the crack 2s were grown from a weld toe except test specimen 5, 6 and 7 which show no similar effect during early crack growth.

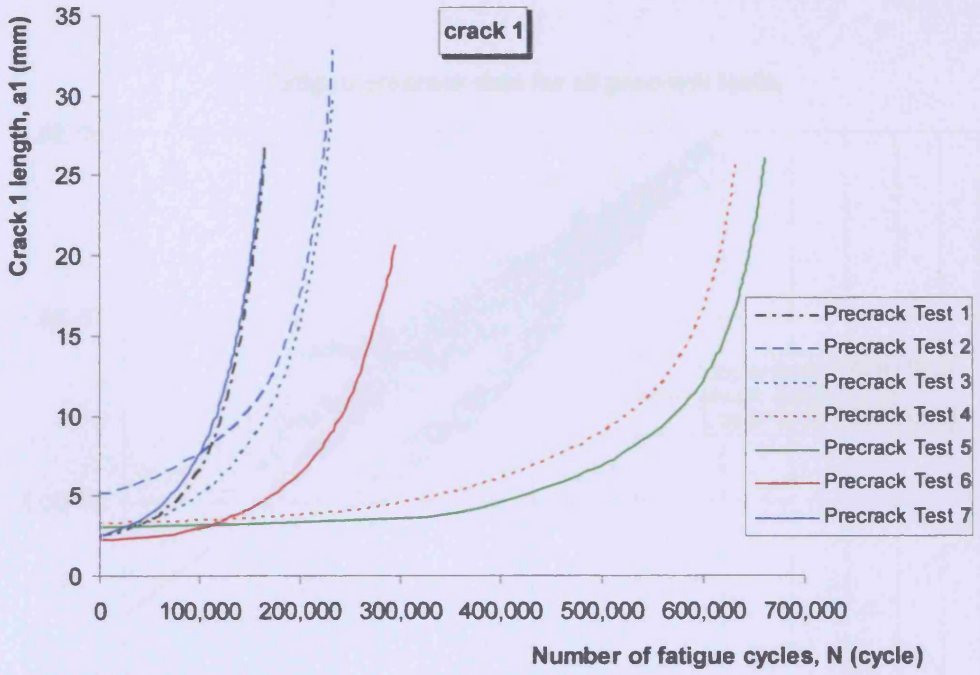

Figure 3.16: Number of fatigue cycles of crack 1 for every precrack test.

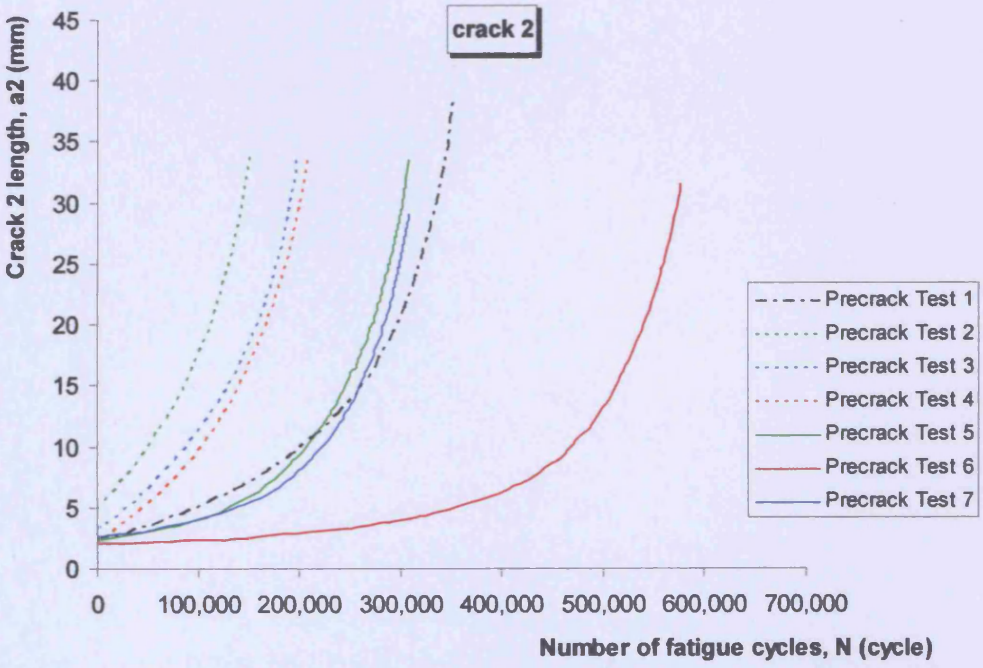

Figure 3.17: Number of fatigue cycles of crack 2 for every precrack test.

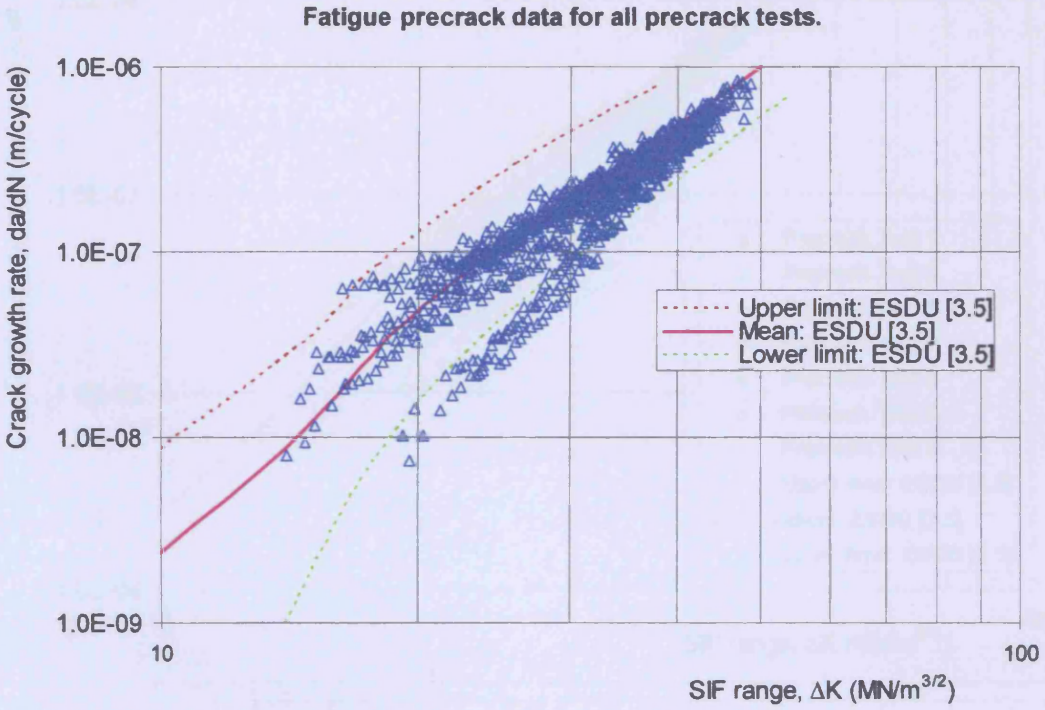

Figure 3.18: Fatigue crack growth rate data of crack 1 and crack 2 for all precrack tests.

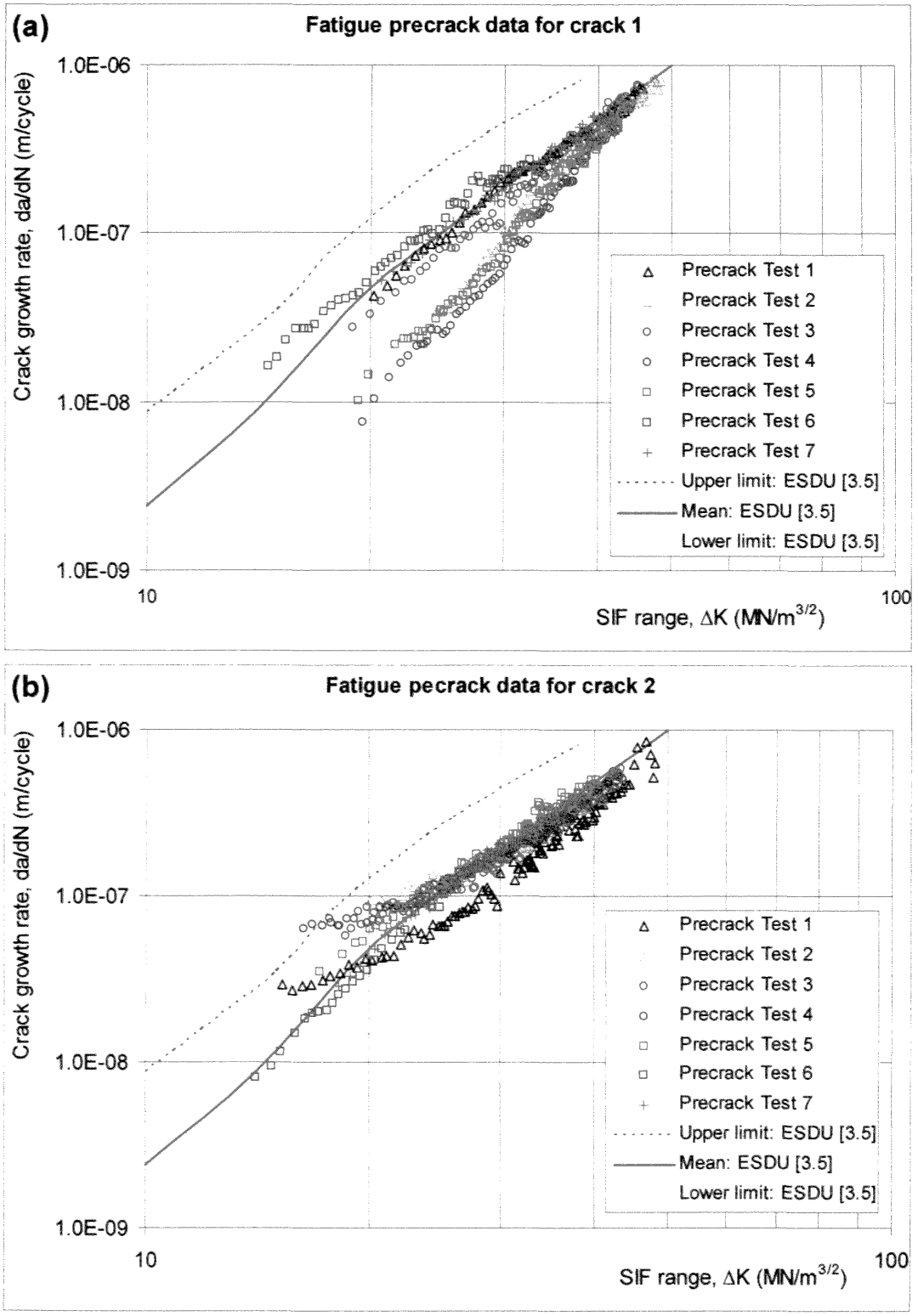

Figure 3.19: Fatigue crack growth rate data of (a) crack 1 and (b) crack 2 during precrack test.

3.2.2.1 Development of the Precracking Procedure

This is the first time multiple cracked specimens were attempted and for this reason the procedure to introduce a second crack, crack 2 had to be developed. This section reports details of the first specimen to be precracked. Initially the first crack, crack 1 was pinned using welded strap as shown in Figure 3.20. During the cyclic bending loading to grow this crack 2, the crack 1 or the strapped crack was found to be still growing. However this was growing at a much slower rate than before it was strapped. The crack growth rate was about 0.1mm every 5000 cycles. The load range was then reduced from 32kN to 26kN to reduce the crack growth rate. The reduced value of load range was checked to make sure the SIF value at the weld toe was greater than the threshold SIF. It was important to ensure the new crack would grow at the weld toe. With this new value of load range, the strapped crack was growing at a rate of less than 0.05mm for 270,000 cycles. The crack 2 appeared at the weld toe after about 275,000 cycles. At this time the strapped crack also showed a significant increase in crack growth rate. This was now growing at about 0.35mm in only 28,000 cycles. This rate is very high as compared with 0.05mm for the preceding 270,000 cycles with the same load range setting.

The specimen was inspected and it was found that the weld strap had itself cracked as shown in Figure 3.21. The specimen was removed from the test machine and the crack at weld material was machined away as shown in Figure 3.22 and re-welded. Clearly it was essential to have additional straps to resist the fatigue loading. In addition to re-welding the removed section, the specimen was also welded with extra small plates at both sides of the specimen as shown in Figure 3.13. The figure also shows that the small plates at both sides were welded together with a small plate on the top to further support it from fatigue loading.

With these extra straps in place to hold the crack 1, the cyclic bending loading was continued to grow the crack 2 to the required crack length. The crack 2 was grown as shown in Figure 3.23. It grew in a curve before stabilising into a straight line. With this knowledge the data for next specimen was taken by locating the microscope at the

potential straight line. With both cracks grown on a specimen, the welded material was removed and polished. The width of the precracked specimen was reduced to the dimensions shown in Figure 3.3 before fatigue testing. From this experience subsequent test specimens used this method to pin the crack 1 before precracking the crack 2.

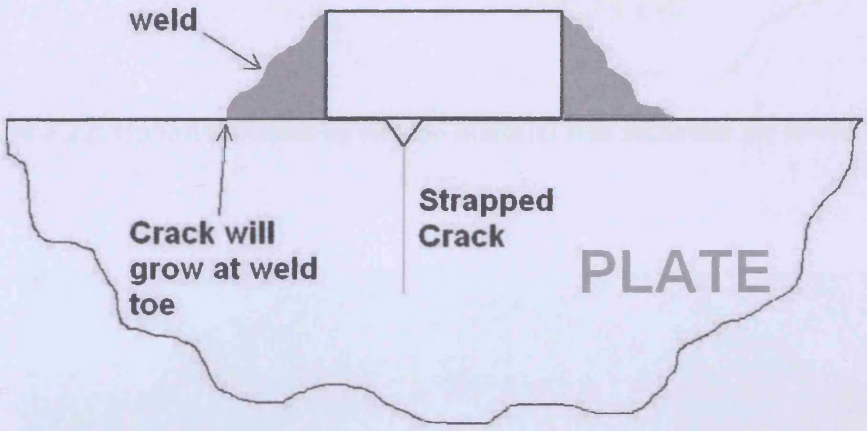

Figure 3.20: Strap welded to the top of the specimen.

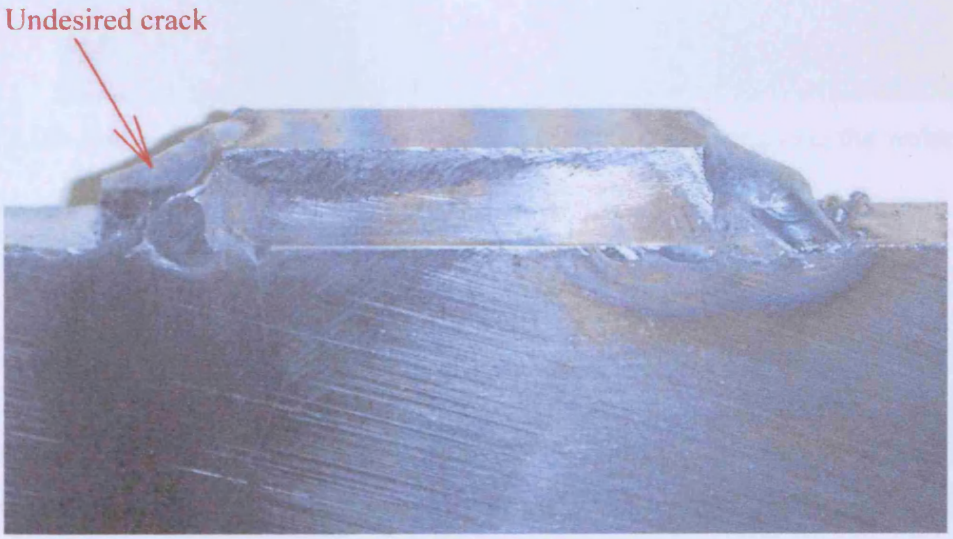

Figure 3.21: Photo shows the cracked welded strap.

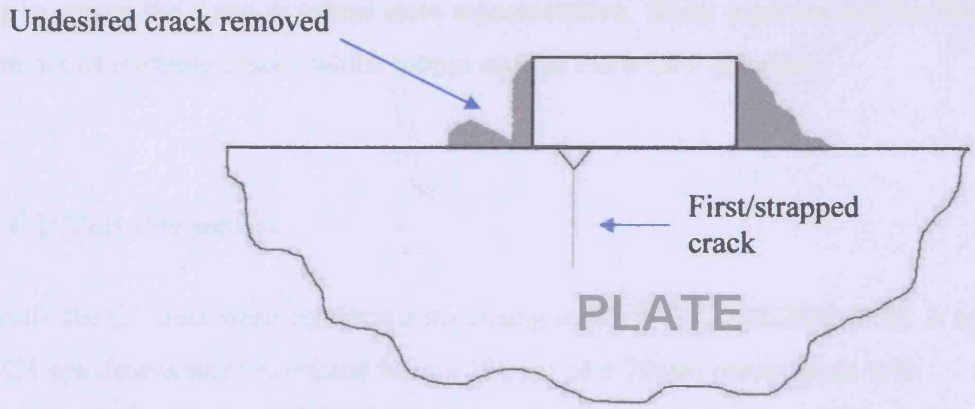

Figure 3.22: Undesired crack in welded material was removed for re-welding.

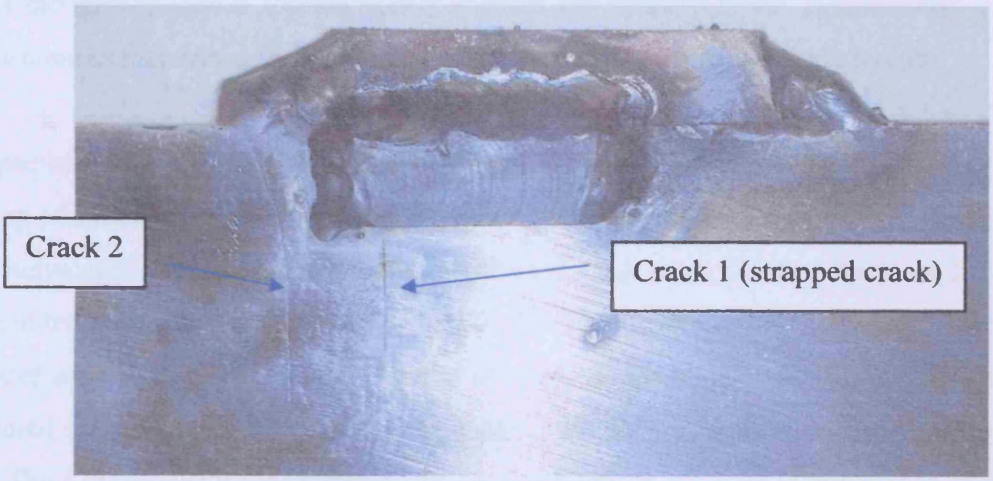

Figure 3.23: Photo shows the specimen with two cracks before removing the welded straps.

3.3 Compact Tension (CT) Test

CT tests were conducted to obtain actual material constant values of c and m for Mild Steel, Grade S275JR [3.1]. The published values of c and m from ESDU 81011 [3.5] may vary even though the same material was used during the CT test. A total of three CT specimens were removed from the same batch of material that was used for fatigue

testing to ensure the *c* and *m* values were representative. These were needed for SIF range calculation of multiple cracks which would use the Paris Law equation.

3.3.1 CT Test Procedure

Generally the CT tests were conducted according to BS ISO 12108:2002 [3.8]. A total of three CT specimens were extracted from a 170 x 120 x 70mm parent plate with dimensions shown in Figure 3.24. A set-up of a CT test on an Instron 1251 100kN servo-hydraulic fatigue test machine is shown in Figure 3.25. The CT specimen was loaded using two sets of pin and clevis assemblies which allow a three-dimensional movement to ensure the tension load is applied axially without any bending effect. A travelling microscope as mentioned in Section 3.1.3 was used to measure the crack length.

CT specimens were initially precracked to approximately 3.20mm before taking the reading of fatigue crack growth data. The CT specimen was cycled using load range of 8kN, between 0.6kN and 8.6kN throughout the tests. All three CT tests were conducted in ambient temperature at a frequency of 2.5Hz. The fatigue cycles and crack length were recorded approximately for every 0.25mm of crack extension. Total crack length was measured from the reference plane of the loading pin holes centreline as shown in Figure 3.26. The final results were plotted as ΔK versus da/dN in a log scale. From this graph the value of *c* and *m* can be determined based on Y-axis intersection and gradient respectively.

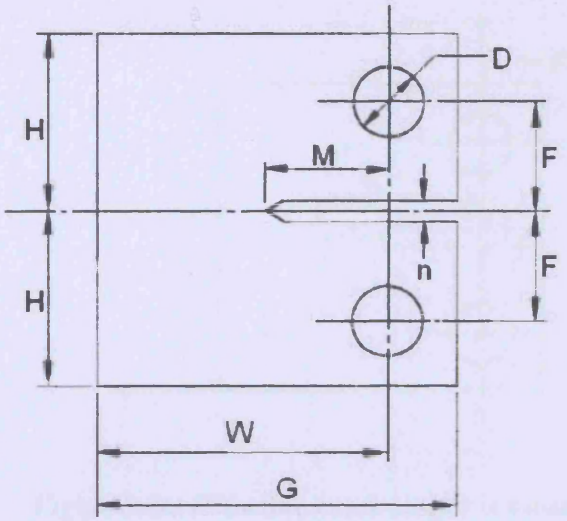

Dimensions:
W = 48.4 mm
H = 29.04 mm
G = 60.5 mm
D = 12.1 mm
F = 13.31 mm
n = 3.146 mm
M = 9.68 mm
Thickness, B = 17.3 mm

Figure 3.24: Dimensions of CT specimen according to BS ISO 12108:2002 [3.8].

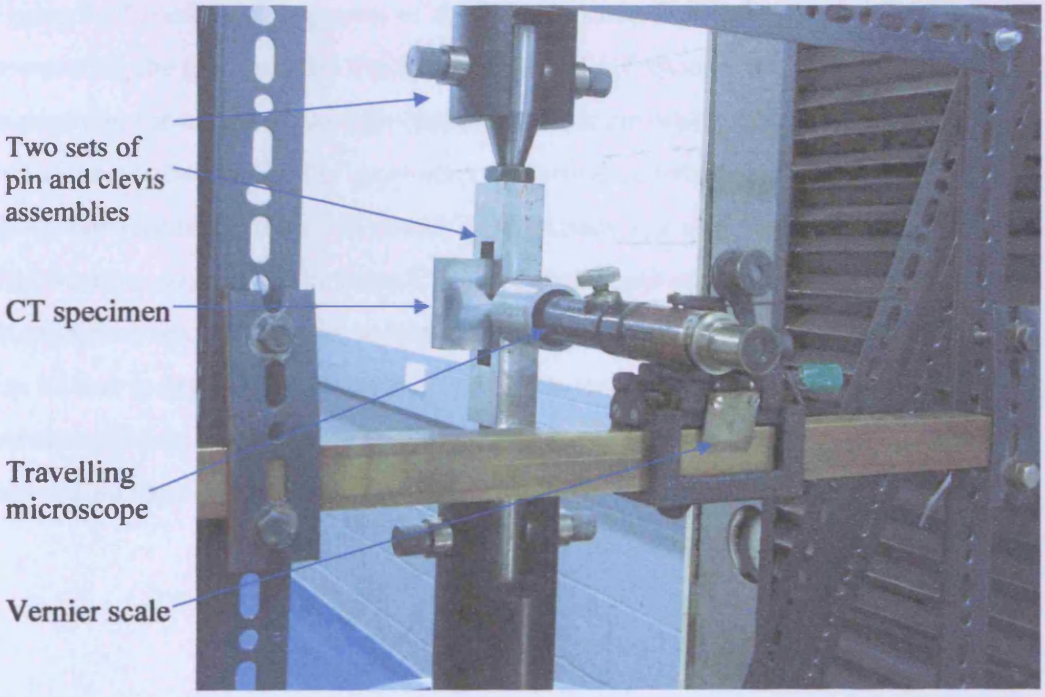

Figure 3.25: A set-up of a CT test on an Instron 1251 100kN fatigue test machine.

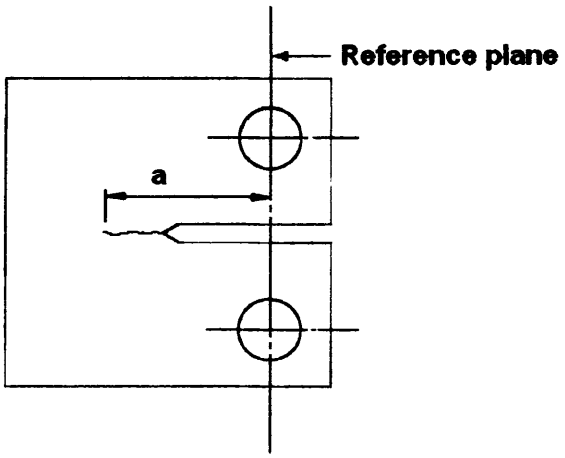

Figure 3.26: Effective crack length is measured from the reference plane.

3.3.2 CT Test Results

Figure 3.27 shows crack growth of the CT specimen during fatigue loading. After completing the CT tests, the fracture surfaces of CT specimens 1, 2 and 3 were observed to examine the extent of through-thickness crack curvature. Since no visible crack contour was observed in the specimens, the crack curvature correction was not employed [3.8]. The fracture surfaces of three CT specimens 1, 2 and 3 are shown in Figure 3.28. The fracture surfaces of the three CT specimens show no visible asymmetrical crack fronts which indicate that no asymmetrical crack growth occurred during the tests. This can be due to asymmetrical loading during the tests as a result of possible uneven contact between the loading pin and the CT specimen. This was avoided by adequately lubricating the pin-and-hole assembly prior to the starting the tests.

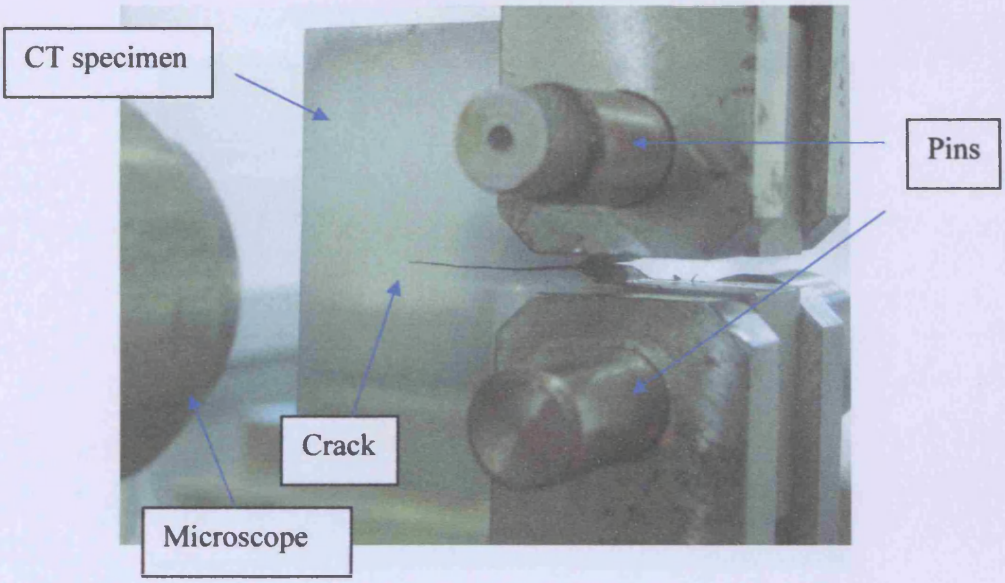

Figure 3.27: Crack propagation during fatigue loading.

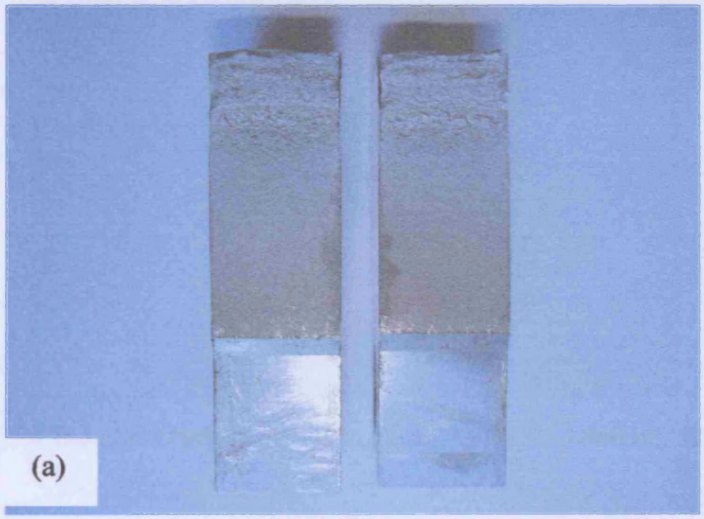

Figure 3.28 (a): Fracture surfaces of Test CT 1.

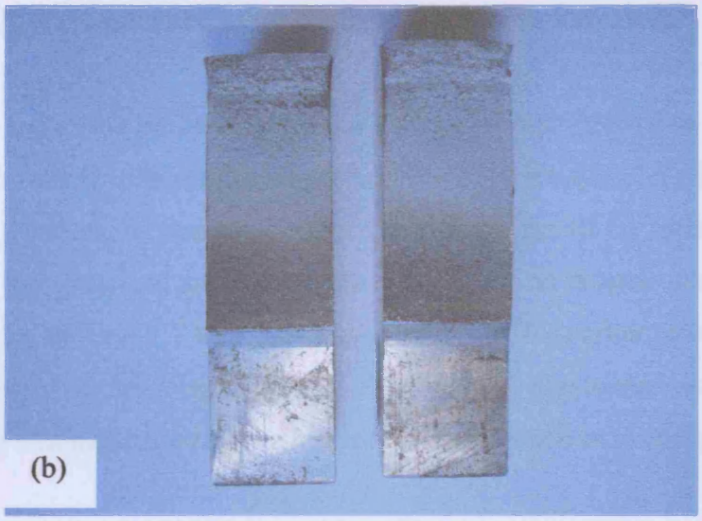

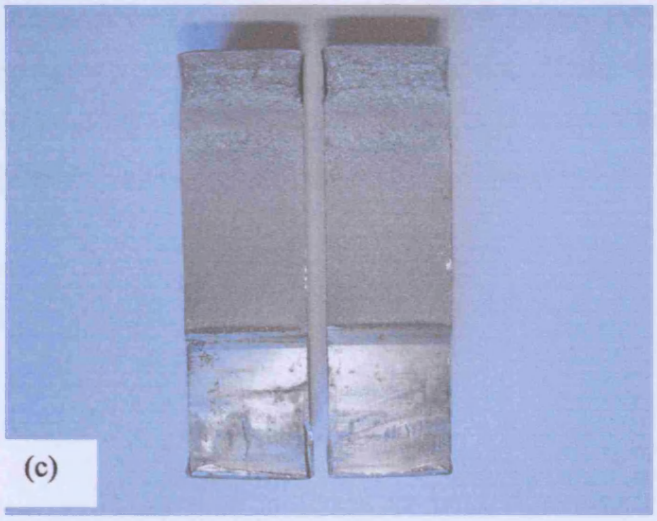

Figure 3.28 (b)-(c): Fracture surfaces of (b) Test CT 2 and (c) Test CT 3.

Figure 3.29 shows the fatigue crack growth data for test CT specimens 1, 2 and 3. Cracks grow from approximately 13mm to 33mm. Their life cycles to failure are between approximately 1.03×10^6 to 1.73×10^6 cycles. Figure 3.30 shows fatigue crack growth rate, da/dN versus SIF range, ΔK plotted using a log scale for all CT tests. The values of da/dN were calculated from the gradient of the curve in Figure 3.29 by using an incremental polynomial method which uses a second order polynomial and five data

points. They were calculated using a program coded in Visual Fortran [3.9]. The corresponding ΔK was calculated using the formula given in Ref. [3.8].

Figure 3.30 also shows the limits and mean of the crack propagation data for a group of low-strength alloy steels with yield strength between 250MPa and 350MPa obtained from ESDU 81011 [3.5]. It can be observed that the data points for all CT tests are well scattered within the limits and are close to the mean line. The fatigue crack growth rate data obtained from all three CT tests are consistent except for earlier crack growth for SIF range less than approximately 16.8MN/m$^{3/2}$. This could be due to the crack growth at early stage being still influenced by the machined starter notch or precracking load history.

Figure 3.31 shows a combination of all test data within the valid SIF range as outlined in Ref. [3.8] for calculation of the material constants c and m values. The values were calculated by fitting a power series line to the combined data. Using the least square method, the material constant were calculated to be $c = 3.72$ and $m = 4.97 \times 10^{-13}$. These values were used in Paris Law equation to obtain the SIF ranges of the multiple cracks in Section 3.4.

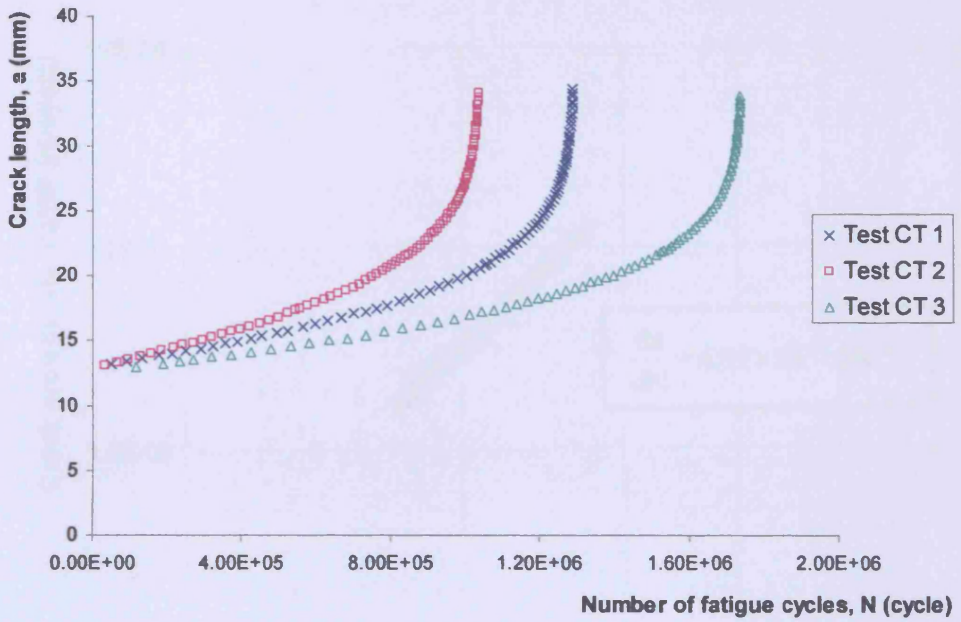

Figure 3.29: Fatigue crack growth data for all CT tests.

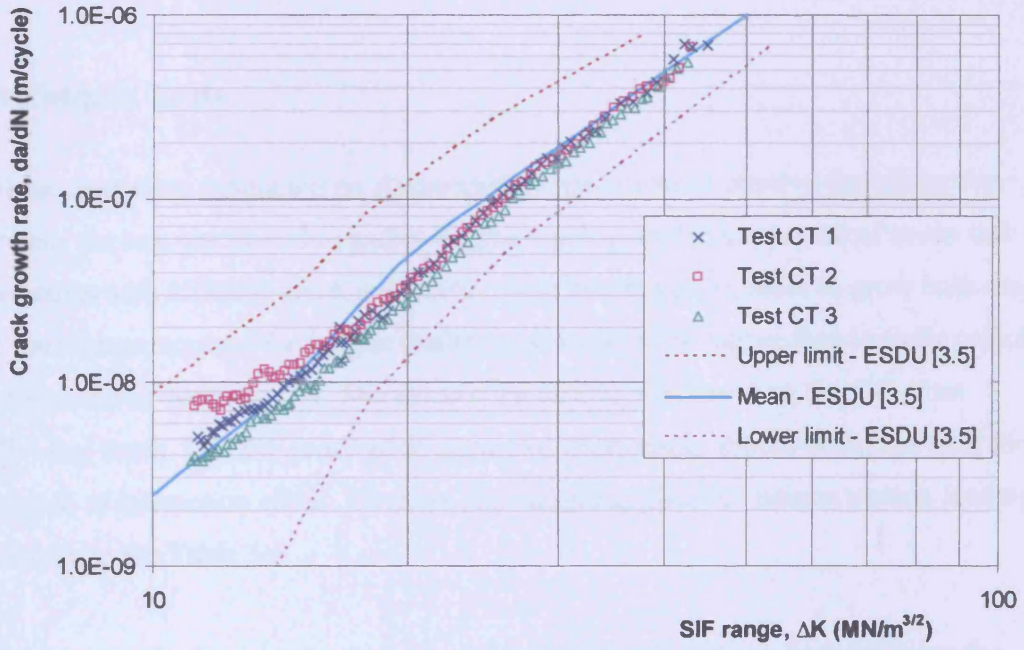

Figure 3.30: Fatigue crack growth rate vs. SIF range for all CT tests plotted on a log scale.

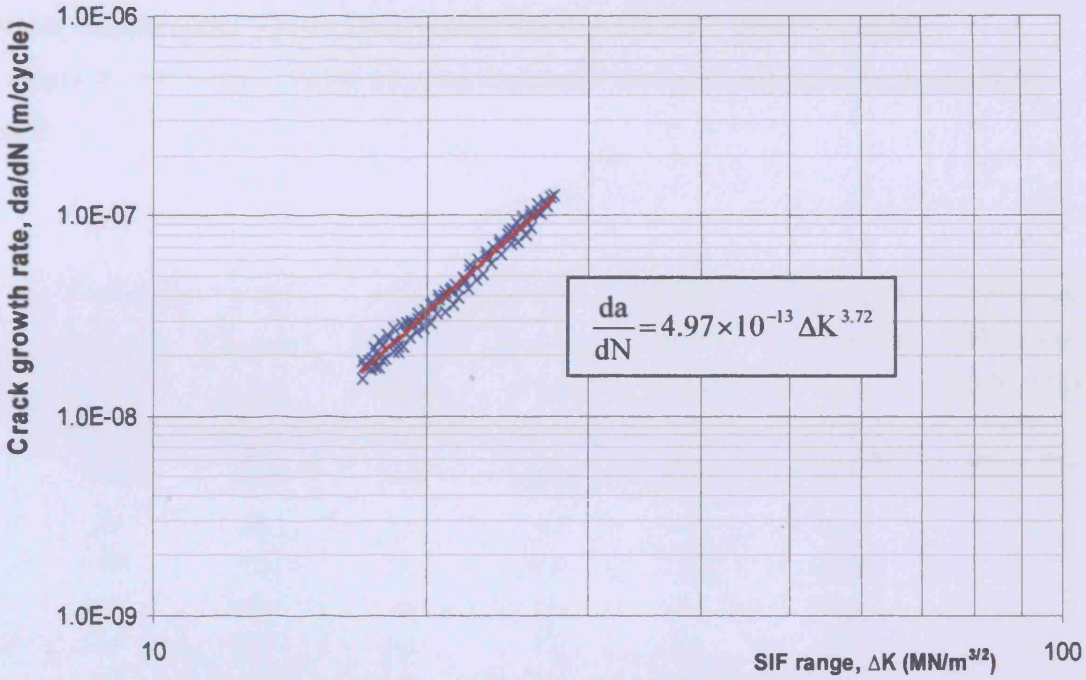

Figure 3.31: Combined fatigue crack growth data of Tests CT 1 to CT 3 for *c* and *m* calculations.

3.4 Fatigue Tests

Fatigue tests were conducted on all precracked specimens to observe the interaction between the two cracks and to gather fatigue crack growth data. A total of seven test specimens with different crack geometries were completed. In order to grow both cracks, the load range required for fatigue loading was found to be higher than initially calculated as discussed in Section 3.1.1. The calculation of load was based on the SIF of an individual crack. The SIF required to grow two edge cracks should be higher with the presence of interaction effect. The new load ranges applied for fatigue tension loading are as shown in the Table 3.4.

With this new load range, the stresses on the specimens were recalculated using the maximum applied load of 61kN. Using an applied load of 61kN, the maximum applied

stress at cross-sectional area in the crack region is approximately 76MPa which is within the linear elastic region. This is to ensure the validity of Linear Elastic Fracture Mechanics (LEFM) theory which assumes the plastic zone deformation near the crack tip is small.

Test	Short crack, crack 1		Long crack, crack 2		Applied Load Range, ΔP (kN)	Equivalent SIF (crack 2) range ΔK_L ($MN/m^{3/2}$)	Equivalent SIF (short crack) range ΔK_S ($MN/m^{3/2}$)
	Min.Load Range, min ΔP_S (kN)	Max.Load Range, max ΔP_S (kN)	Min.Load Range, min ΔP_L (kN)	Max.Load Range, max ΔP_L (kN)			
1	19	153	10	85	60	49.2	27.5
2	15	121	15	121	57	33.0	32.9
3	18	149	15	123	57	32.4	26.7
4	21	174	15	121	60	34.7	24.2
5	22	182	15	121	60	34.7	23.1
6	22	183	15	124	57	32.2	21.9
7	22	181	15	122	60	34.7	23.4

Table 3.4: New fatigue tensile test load range.

3.4.1 Fatigue Tensile Test Procedure

A set up of a specimen on an Instron 1362 100kN servo-hydraulic fatigue test machine is as shown in Figure 3.32. The two pins that used to join the end fittings and specimen holes were adequately lubricated prior the test. The fatigue testing was conducted in ambient temperature with frequency of 2.5Hz. Two travelling microscopes were mounted horizontally on a frame to measure the two crack lengths. Only cracks on one side of the specimen were measured using travelling microscopes as discussed in Section 3.1.3.

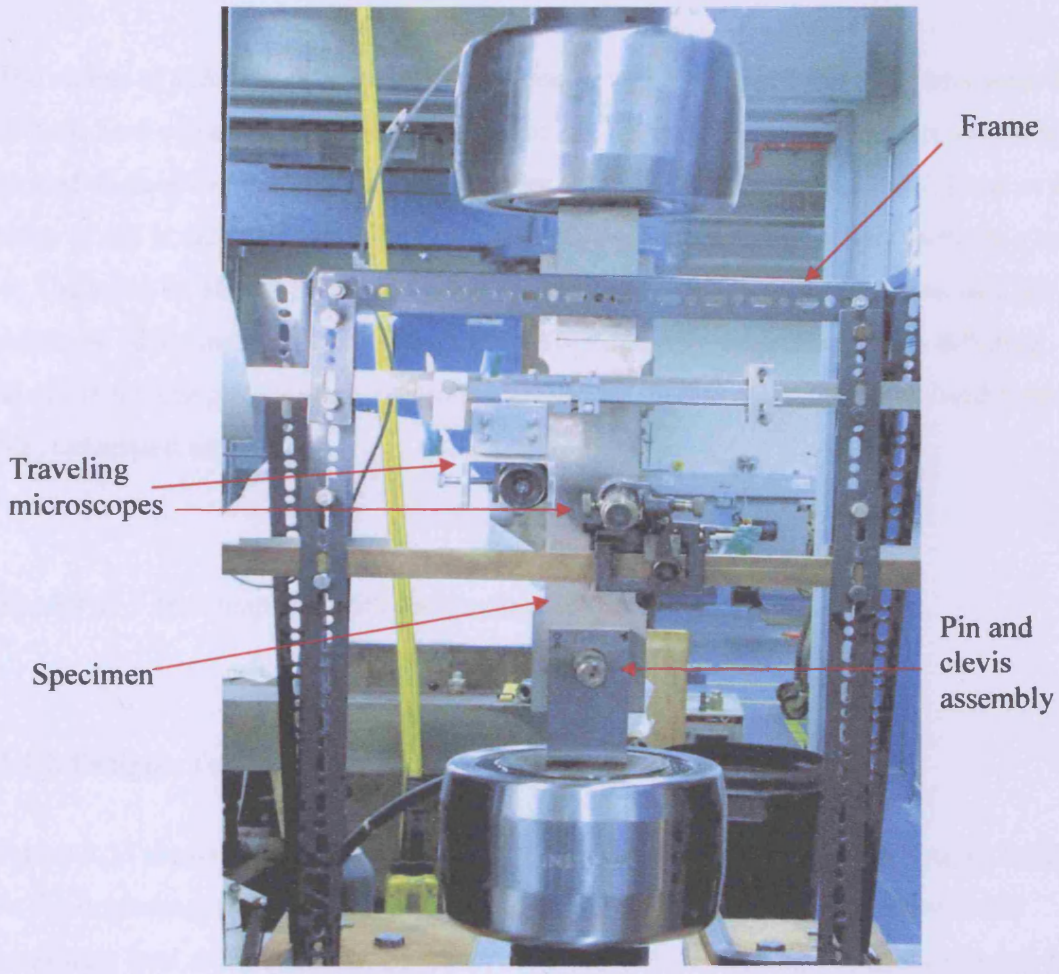

Figure 3.32: A set up of fatigue tensile test on an Instron 1362 100kN fatigue test machine.

Before the start of every test, the two crack lengths were measured using travelling microscopes to obtain actual crack geometries. The crack geometries were slightly different after machining following precracking. The test parameters as tabulated in Table 3.2 in Section 3.1 were measured just before the fatigue testing began. During fatigue testing the readings of the two crack lengths and the number of fatigue cycles were recorded approximately every 0.25mm of crack extension. The readings were taken under a static mean value of cyclic load. The readings were recorded until the crack 2 length was equal to at least half of the plate width. Graphs of a versus N were plotted and its crack growth rate, da/dN was determined from the gradient of the curve by using an incremental polynomial method described earlier.

The values of da/dN and the material constants *c* and *m* obtained from CT tests were used in Paris Law equation to obtain the values of ΔK for each crack. The results cannot be plotted as da/dN versus ΔK similar to results obtained for precracking and CT test as the value of ΔK is calculated directly using the value of da/dN and material constants *c* and *m*. The value of ΔK for precracking and CT tests were using available normalised SIF, Y solutions. Since there are no Y solutions available for two edge cracks with differing length in a finite plate under tension, the results are plotted using the normalised form of SIF, calculated as:

$$Y = \frac{\Delta K}{\left(\Delta\sigma\sqrt{\pi a}\right)} \tag{3.7}$$

Results of Y are compared with results obtained using FEA.

3.4.2 Fatigue Test Results

Figure 3.33 shows Test 6 specimen which contains two cracks during the fatigue loading. At the beginning of the test, when the specimen was cycled between minimum and maximum load using a sinusoidal wave, the crack mouth opening of both cracks can be visually observed. However the crack 2 shows relatively larger crack opening than crack 1. The crack 2 opening becomes dominant when it starts growing and no crack 1 mouth opening can be seen.

Figure 3.34 shows a typical crack as seen through a travelling microscope with the help of indirect lighting. As the crack 2 approaches half of the plate width, crack branches can be observed. This is due to the size of the deformed plastic zone. The crack branches become severe when the crack length exceeds the width of the plate. At this time the test was completed as the crack tip could not be recognised for crack length measurement. When the test specimen was stopped under mean cyclic load, the crack 2 mouth also can be seen wide open indicating that the deformed plastic zone is large. Figure 3.35(a)

shows the completed Test 6 specimen with crack 2 length approximately equal to 42mm and Figure 3.35(b) shows the equivalent crack 2 as seen through a microscope.

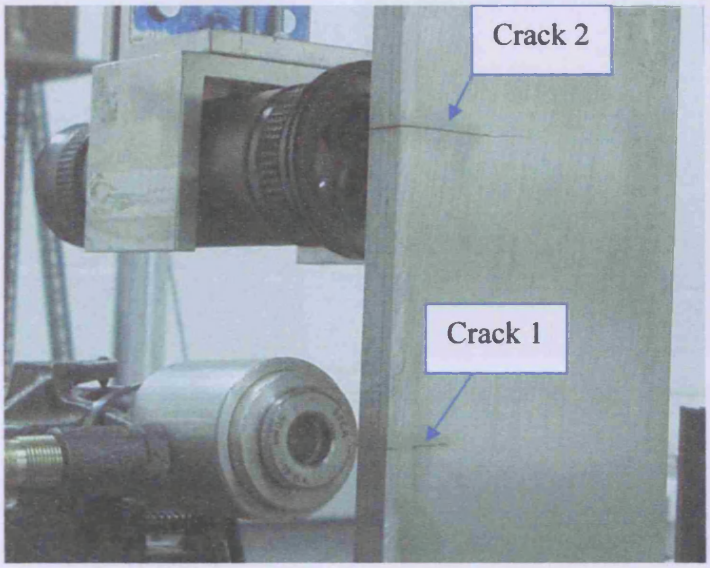

Figure 3.33: Two edge cracks of Test 6 specimen during fatigue testing.

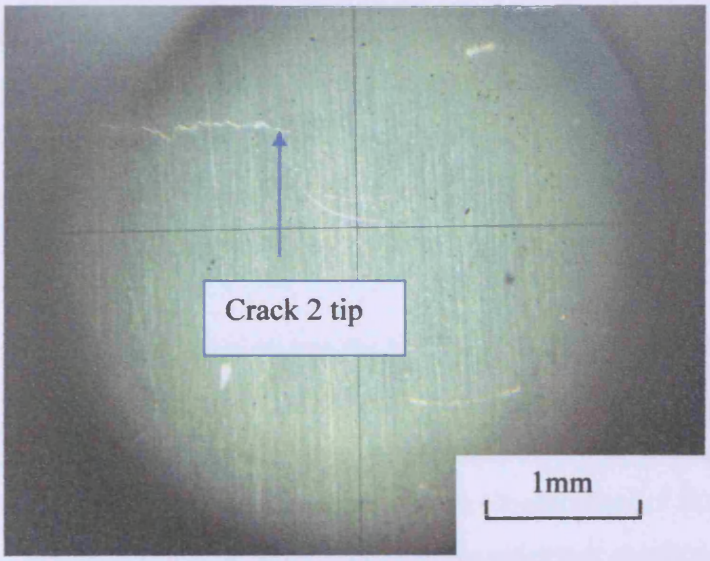

Figure 3.34: Typical crack tip as seen through a microscope during fatigue testing.

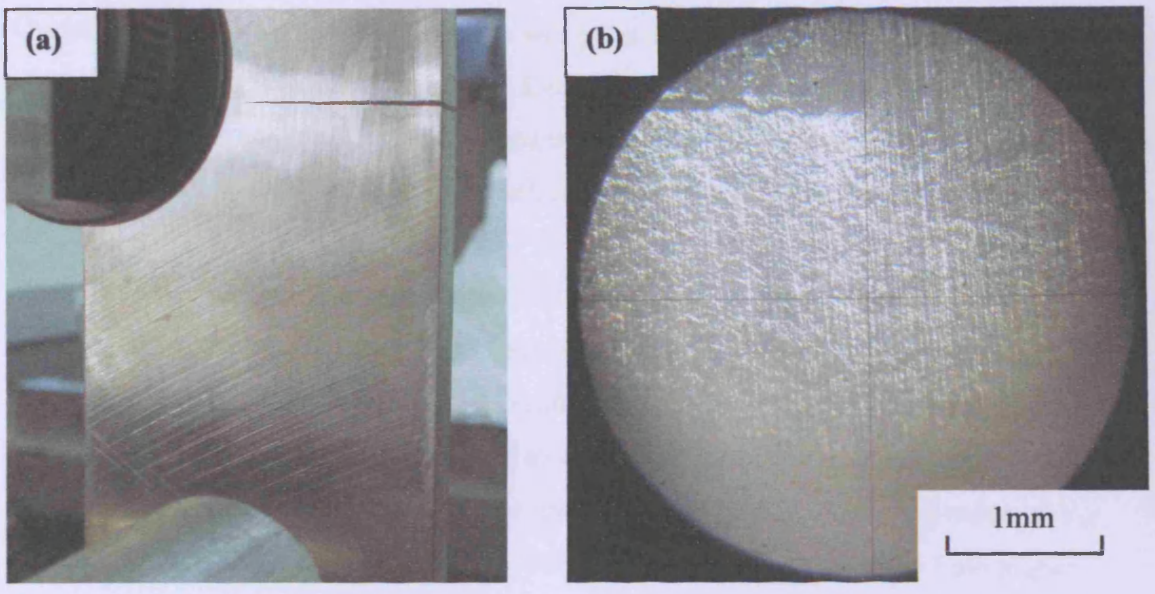

Figure 3.35: (a) A complete fatigue Test 6 specimen, and (b) crack 2 tip as seen through a microscope (a2 ≈ 42mm)

Figure 3.36 shows the results of fatigue crack growth data for (a) crack 1 and (b) crack 2 under fatigue loading. The number of fatigue cycles required to complete the test varies depending on the crack geometries and other factors such as material variation and the test set up. Test 1 required less fatigue cycles because it was precracked with the longest crack 2. The ratio of crack 2 to plate width, a2/T was 0.40. Test 3 demonstrated the largest number of fatigue cycles taken during the fatigue tensile loading. The two cracks required more fatigue cycles at early crack growth possibly due to the strong interaction effects. It required a large number of fatigue cycles for a small crack growth. The crack 2 started to grow as normal when the crack 1 arrested.

All cracks 1 grew less than 0.7mm except for test 2 and 7. Crack 1 for test 2 and 7 grew 1.86mm and 0.99mm respectively. Crack 1 from test 2 grew slightly longer than other tests because the two edge cracks were precracked to almost similar length. As shown in Table 3.2 the two crack lengths are 24.40mm and 24.47mm. Crack 1 from test 7 was precracked with largest crack separation compared to other test specimens. It allows crack 1 to grow slightly longer than other tests because of the smaller interaction effect.

Overall results show that the short crack will grow a small length compared to the longer crack which grows until fracture occurs. Even where two cracks were almost at the same length, the longer crack always dominated leaving the shorter crack to arrest. The short crack growth depended on the initial crack length and crack separation.

Figure 3.37 shows results of normalised SIF for crack 1, Y_{a1} for all fatigue tensile tests compared to Y_{a1} obtained using FEA. Experimental results show that the values of Y_{a1} obtained are low compared to the FEA results. The values of Y_{a1} also shows a large reduction as the crack 1 grows compared to FEA results which show negligible reduction. The value of Y_{a1} reduces to a small value until the crack arrests. The initial value of Y_{a1} depends on crack lengths and separation. Initial values of Y_{a1} for test 5 to 7 are higher than test 1, 3 and 4 because of the larger separation. The initial value of Y_{a1} for test 2 is high because of the two cracks that are precracked approximately with the same length.

Figure 3.38 compares Y values of crack 1 and crack 2 together with their FEA results. Each graph from Figure 3.38 also shows the Y solution for an edge crack under tension from Ref. [3.6] to highlight the difference or interaction effect between two cracks. Similar to crack 1, crack 2 Y_{a2} values obtained from the experiments are low compared to the FEA results. At the early test stages, the normalised SIF for crack 2 reduce to a low value before starting to increase eventually approaching Y of a single edge crack [3.6]. This trend that causes a U-shape can be observed for all fatigue tests. Values of Y_{a2} obtained using FEA are similar to Y [3.6] for cases where there is little interaction between cracks. Results of the FEA also show that Y_{a2} values are higher than Y_{a1} values throughout the crack propagation. Experiments show similar results except for test 7 where during early crack growth, the value of Y_{a1} is slightly higher than Y_{a2}. The experimental results also show the values of Y_{a2} are scattered unevenly as the crack 2 approaches half of the specimen width. This is because of the large plastic deformation zone at the crack tip. The disparities between experiment and FEA in some cases are possibly due to the shape of cracks that are not perfectly straight. The separation between cracks is also inconsistent with the curve shape.

Figure 3.39 shows a combination of experimental Y_{a2} values for all fatigue tests and a solid line that represent a single edge crack solution [3.6]. It can be seen that test 7 which contains the largest crack separation will start to have less interaction at a2/T approximately equal to 0.35. It is not really obvious for other tests to estimate their limit of interaction effects as the entire values of Y_{a2} are lower than the solid line. By considering the entire values of Y_{a2} for each test in relation to the solid line, it can be estimated that test 6 and 5 which have larger separation require less a2/T compared to test 1 to 4 which have smaller crack separations.

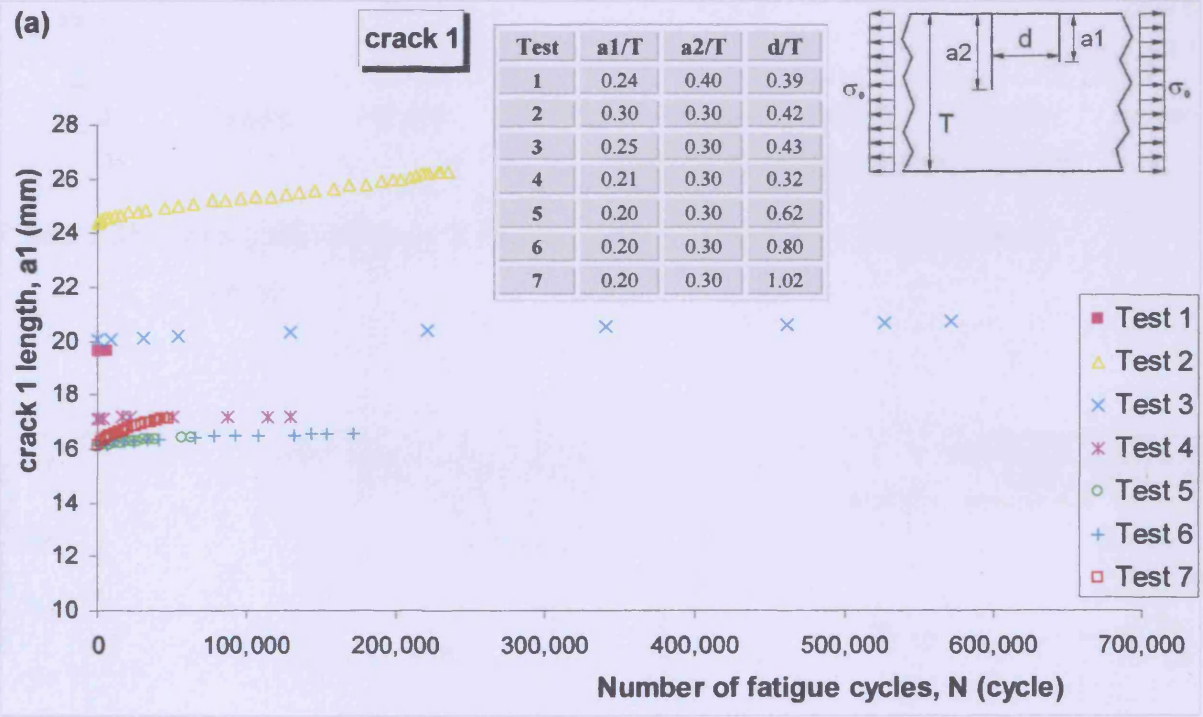

Figure 3.36 (a): Fatigue crack growth data for crack 1 under fatigue tensile loading testing.

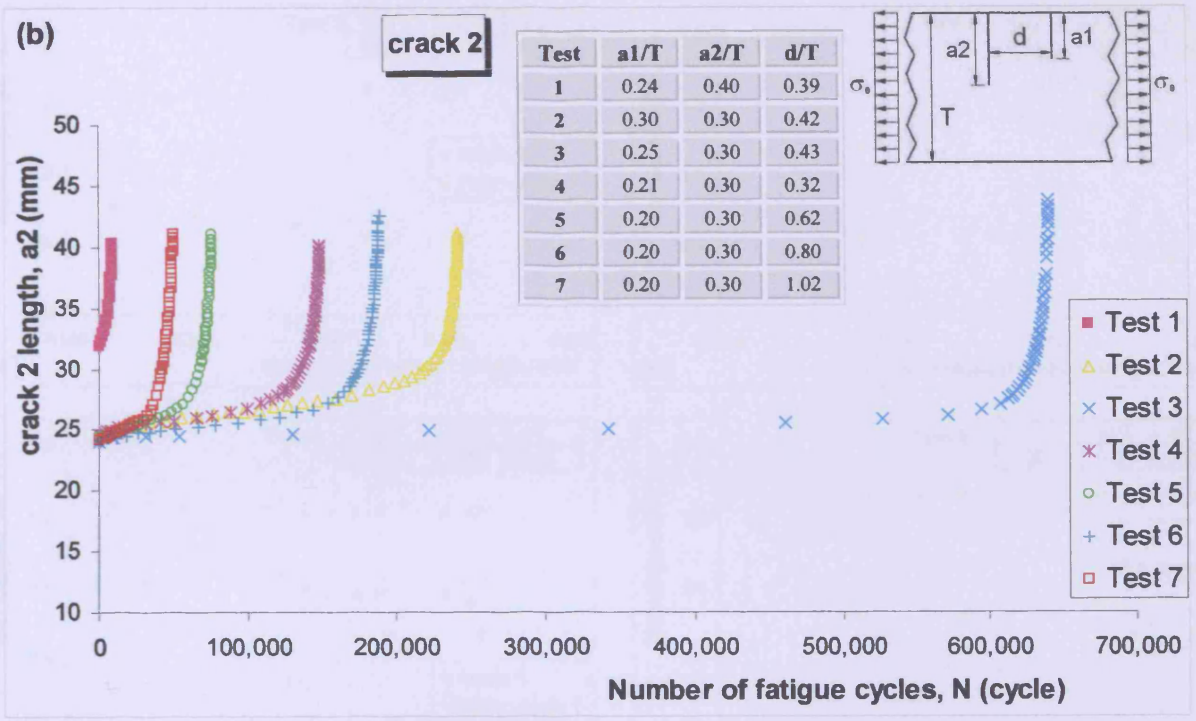

Figure 3.36 (b): Fatigue crack growth data for crack 2 under fatigue tensile loading testing.

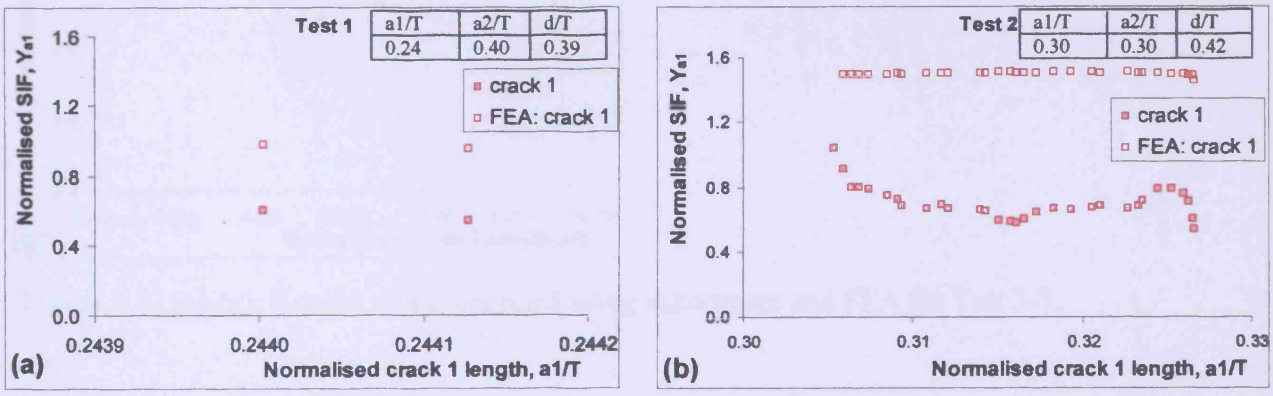

Figure 3.37 (a)-(b): Results of Y_{a1} obtained using experiment and FEA for Test 1 and 2.

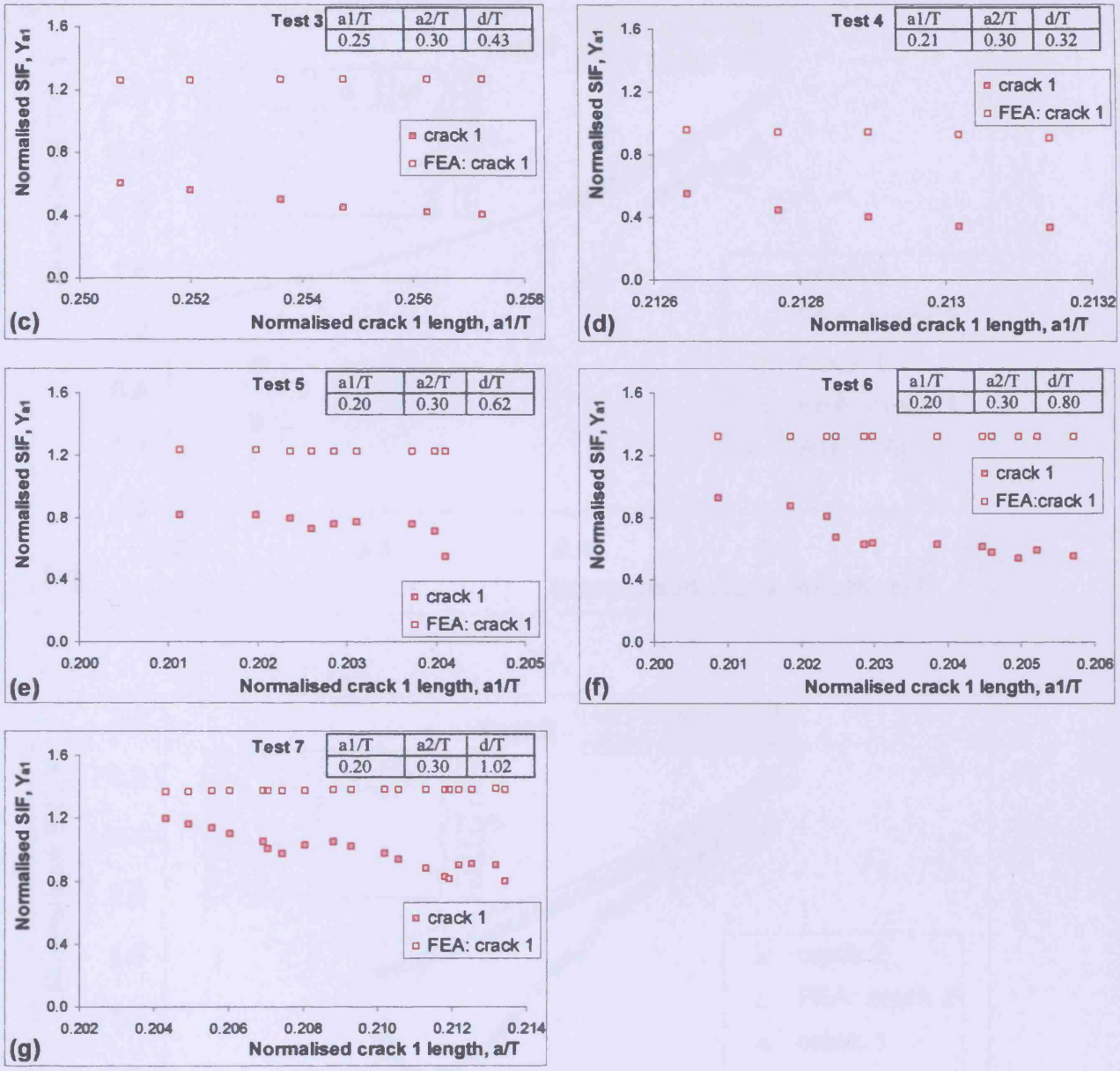

Figure 3.37 (c)-(g): Results of Y_{a1} obtained using experiment and FEA for Test 3-7.

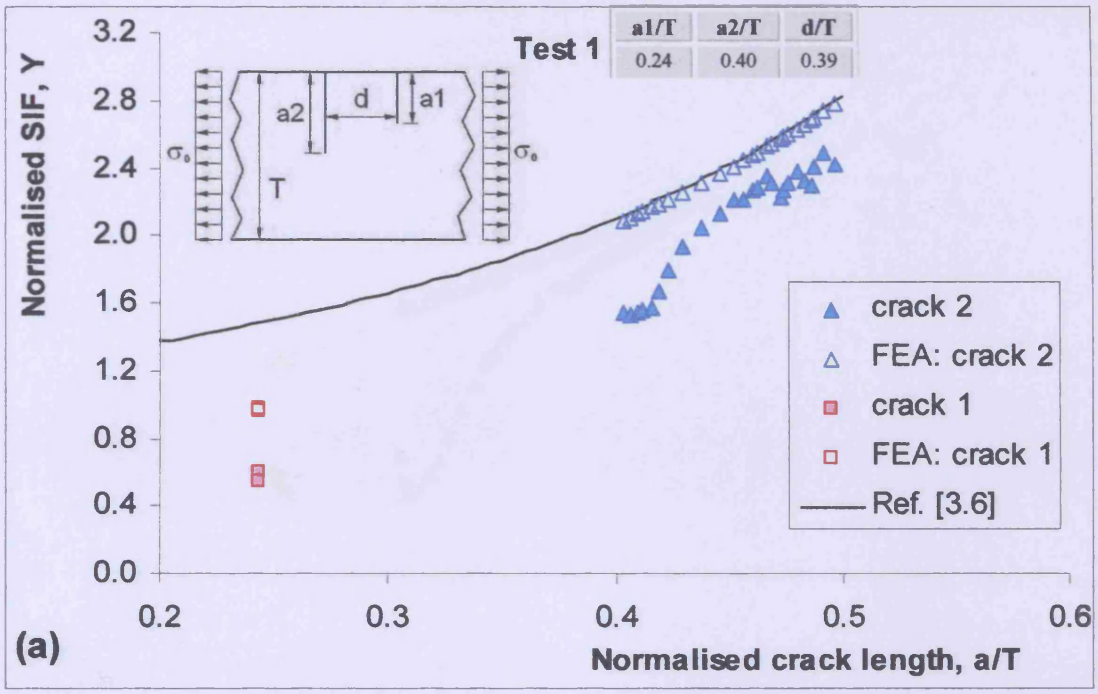

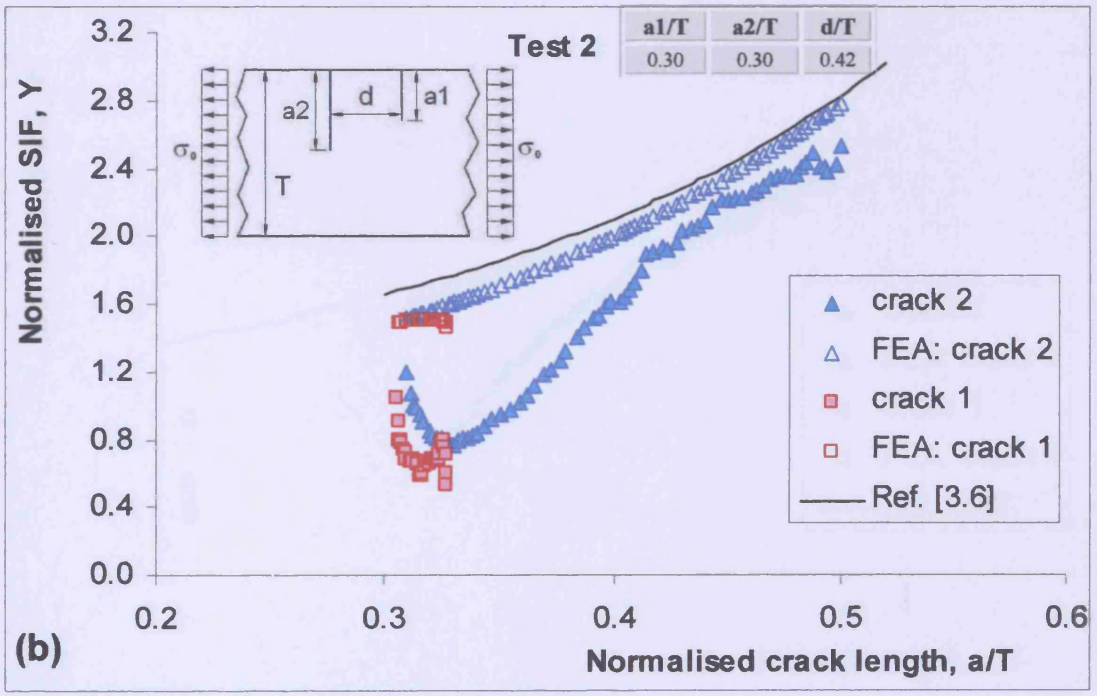

Figure 3.38 (a)-(b): Results of Y for short and long cracks obtained using experiment and FEA for Test 1 and 2.

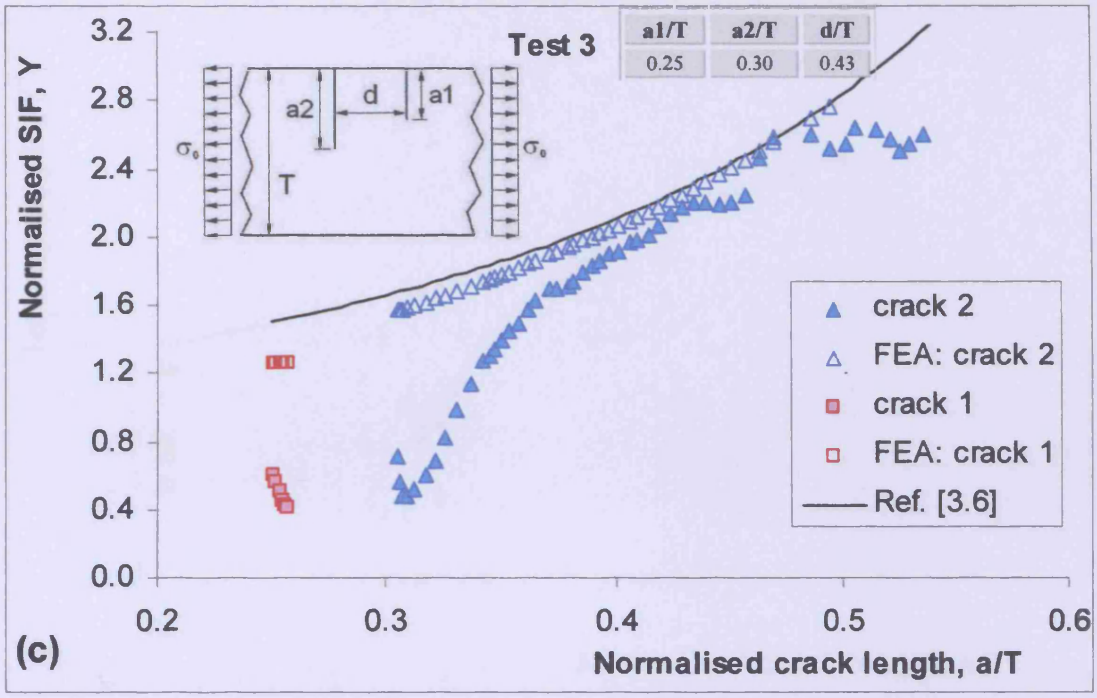

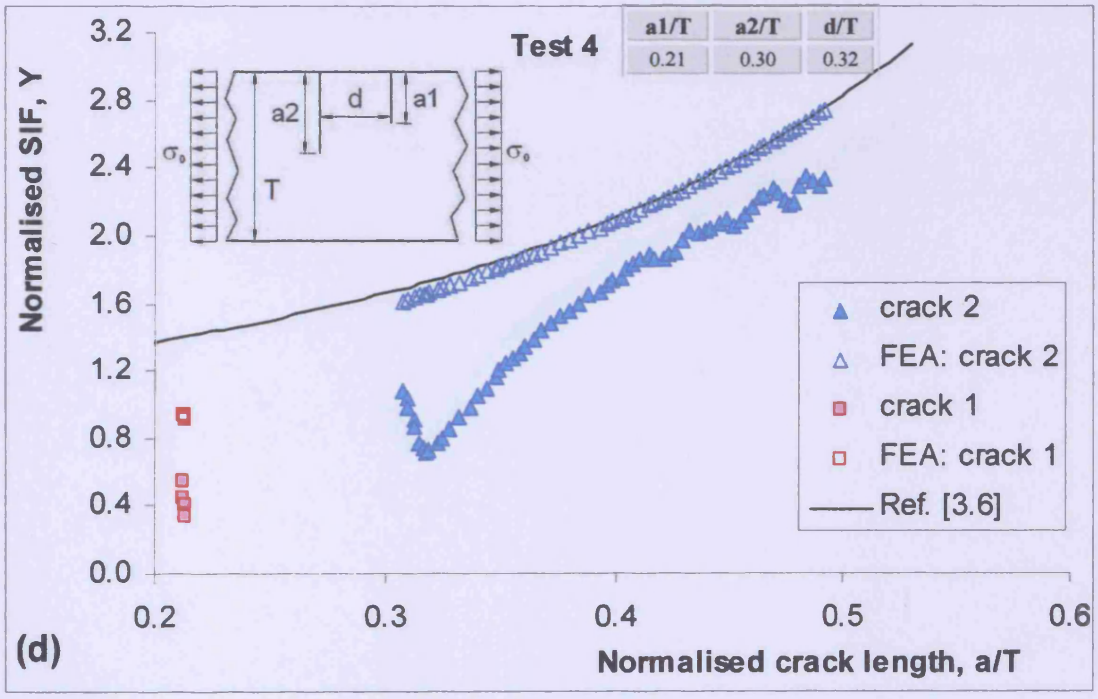

Figure 3.38 (c)-(d): Results of Y for short and long cracks obtained using experiment and FEA for Test 3 and 4.

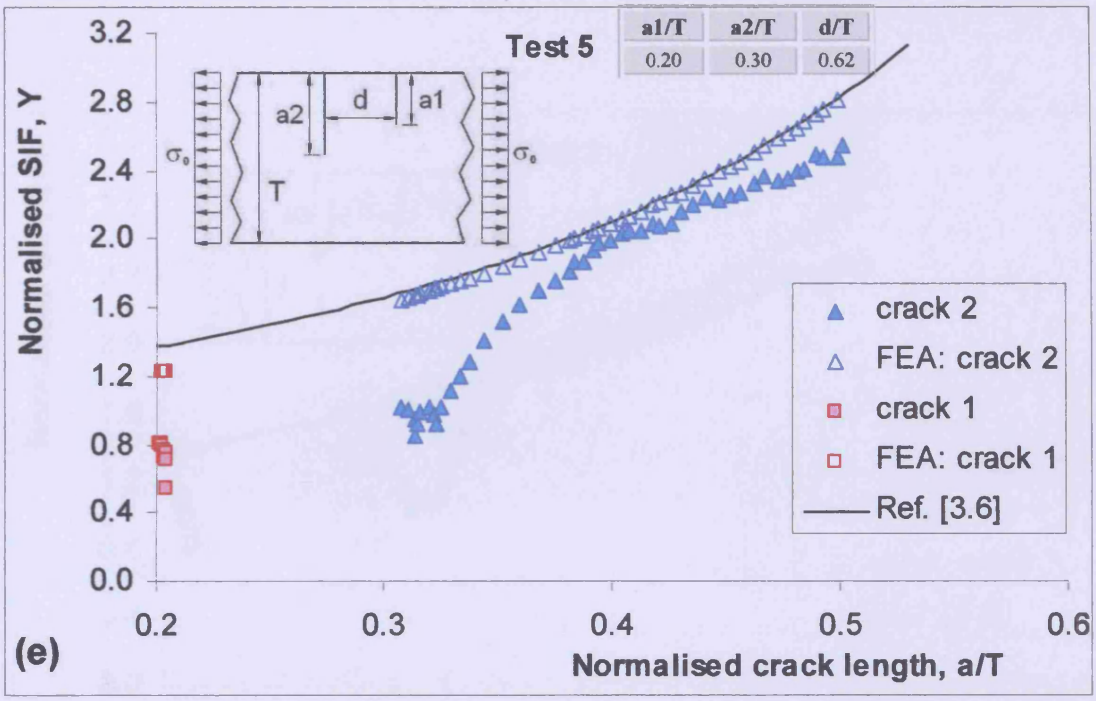

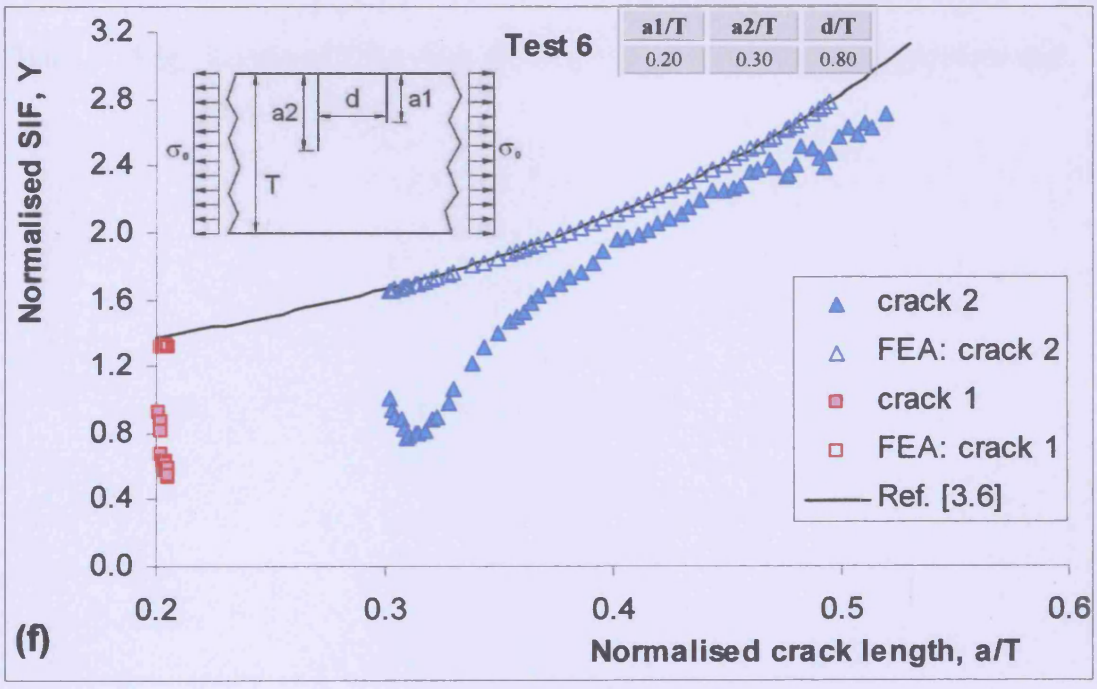

Figure 3.38 (e)-(f): Results of Y for short and long cracks obtained using experiment and FEA for Test 5 and 6.

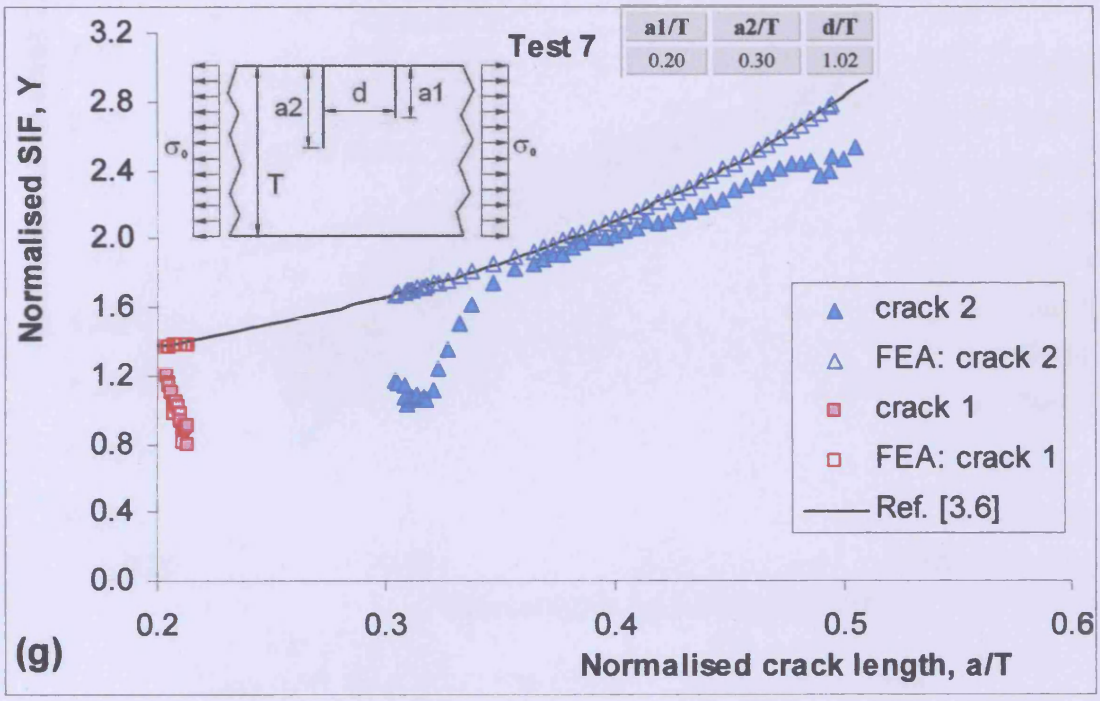

Figure 3.38 (g): Results of Y for short and long cracks obtained using experiment and FEA for Test 7.

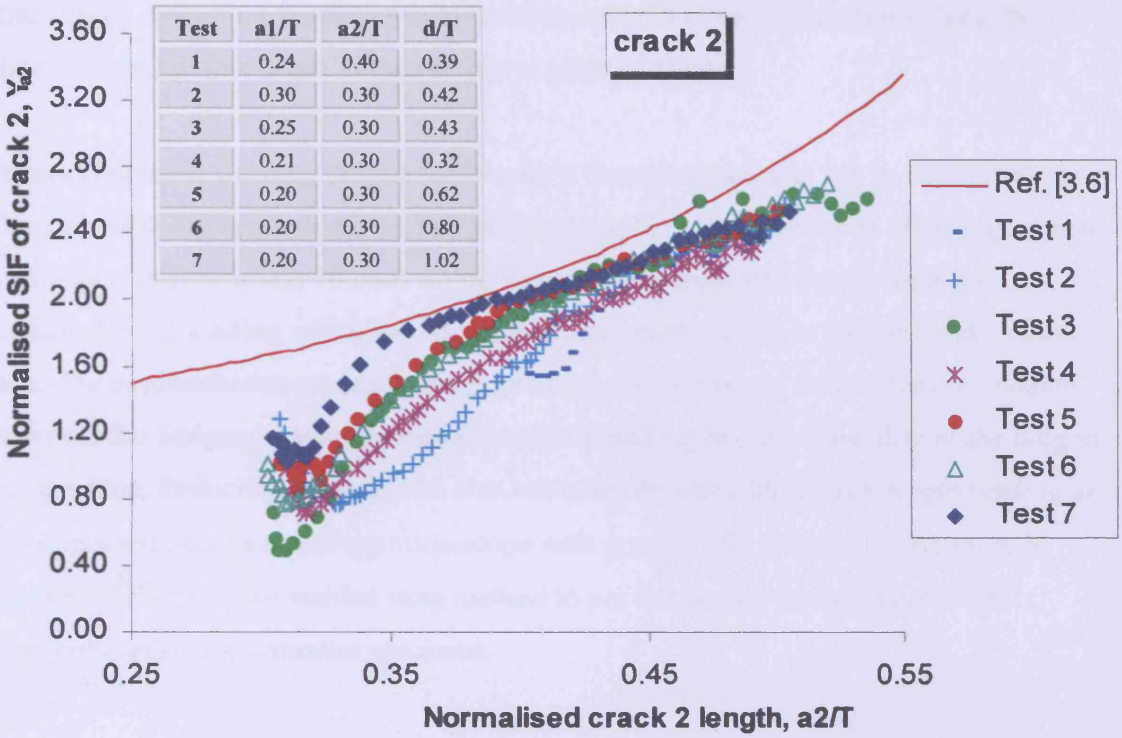

Figure 3.39: Results of experimental Y_{a2} values for all tests.

3.5 Discussion

The work in this chapter shows that a specimen with two edge cracks of differing length can be individually precracked. Welded straps which consist of three small plates can be used to pin a crack before precracking another crack. Precracking results as shown in Figure 3.18 look satisfactory even though some specimens produce large disparities compared to published fatigue crack growth data for steel with yield strength between 250MPa and 350MPa [3.5]. One reason for these disparities is that precrack testing was not designed according to the published standard where it was carefully designed in order to obtain *c* and *m* values. Precracking using three-point bending is also not necessarily the same as under tension. The idea of using three-point bending was to control the location of maximum bending force. This was to provide maximum force at a potential crack initiation site either at a notch or a weld toe and also to give extra protection to welded

strap. Using four-point bending would result in uniform stress distributions along the plate surface, but this could initiate cracks at other locations.

Precracking using bending fatigue loading for a thin specimen also has its own problems. The ratio of thickness to width of the specimen was 0.1. It is difficult to align a specimen with 10mm thickness and 100mm width. Any error in alignment would cause non-uniform fatigue loading which would in turn contribute to errors in fatigue crack growth data. The best method to precrack this type of specimen is to use fatigue tension loading. However the designed specimen would require a load beyond the capability of the fatigue test machine. Reducing the specimen size increases the error for a crack length reading as it is measured using a travelling microscope with accuracy ±0.01mm. Furthermore it could be difficult to use welded strap method to pin the crack 1 and to remove the damaged surface for a smaller specimen.

There are several possibilities for the U-shape during the early crack growth of Y_{a2} as observed for all fatigue tensile tests results. One of the possibilities could be due to the crack arrest of the crack 1. To examine this clearly, the plot of normalised SIF, Y versus fatigue cycles, N is compared between crack 2 and crack 1 for every test as shown in Figure 3.40. It should be noted that the total points that represent the number of fatigue cycles shown in Figure 3.40 are less than shown in Figure 3.36 because of the usage of an incremental polynomial method to calculate da/dN and hence Y values. The figure shows that during the early fatigue cycles, values of Y_{a2} decrease similar to Y_{a1} values. While Y_{a1} values continue to decrease, Y_{a2} values start to increase with increasing number of cycles. Perhaps as the crack 1 arrests, the crack interaction between the two cracks becomes less causing the crack growth rate for crack 2 to start increase.

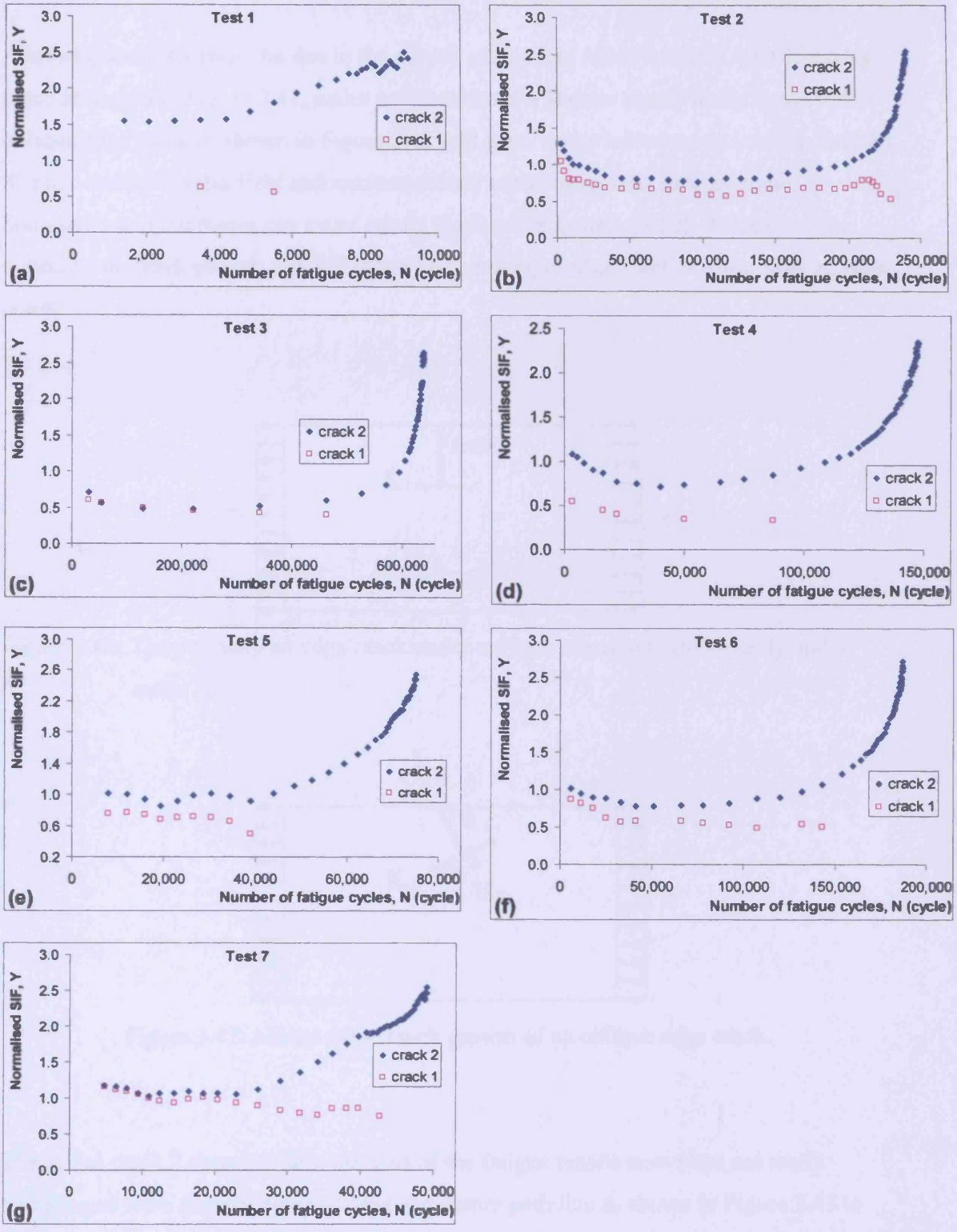

Figure 3.40 (a)-(g): Y against N for all tests.

Another possibility could be due to the curved precracked crack 2 shape. A perfect edge crack as shown in Figure 3.41, under uniform stress will grow purely under mode I. An oblique edge crack as shown in Figure 3.42 will grow under mixed mode I and II. Factors like non uniform stress field and microstructural inhomogeneities such as grain boundaries and interfaces can cause mixed mode crack growth [3.10]. Because of the mixed mode crack growth, the SIF mode I of an oblique edge crack is lower than an edge crack.

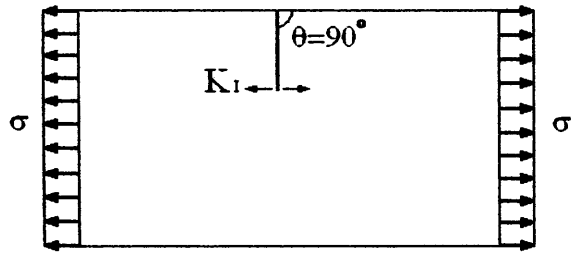

Figure 3.41: Theoretically an edge crack under uniform stress will grow purely under mode I.

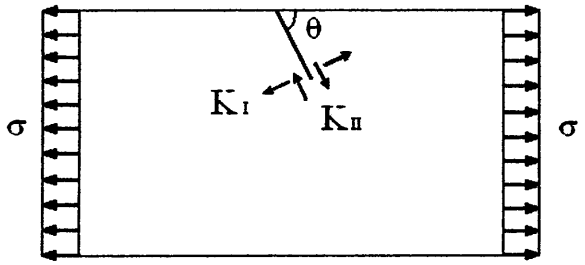

Figure 3.42: Mixed mode crack growth of an oblique edge crack.

The initial crack 2 shapes before the start of the fatigue tensile tests were not really straight and were slightly deviated from the centre path line as shown in Figure 3.43 to form an oblique edge crack. This occurred during fatigue precracking under three-point bending. Ma *et al.* [3.11] predicted that an oblique edge crack under uniform stress will

grow towards the centre path line to form a kinked crack. Ma *et al.* [3.11] shows that the mode I SIFs, K_I will be reduced as the crack angle increases as shown in Figure 3.44. Similar to an oblique crack, a kinked crack will grow under mixed mode I and mode II and thus reducing the K_I compared to a crack that grow purely under mode I. All seven specimens had oblique precracks estimated approximately 5 to 15 degrees before the start of every fatigue test.

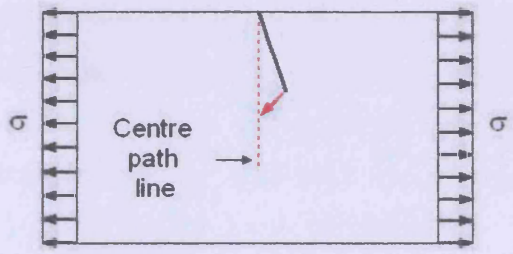

Figure 3.43: An oblique edge crack will move towards the centre path line under uniform stress to form a kinked crack.

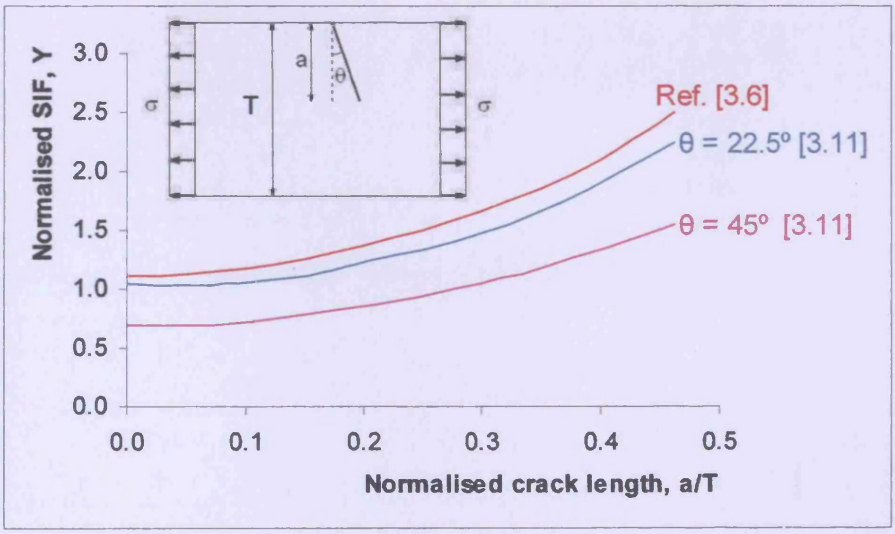

Figure 3.44: Normalised K_I of an oblique edge crack [3.11] with two different crack angles compared to an edge crack [3.6].

Considering the seven specimens, the crack 2 shape can be divided into three stages as shown in Figure 3.45. The three stages are as follows:

1. Oblique, where the crack 2 grows at an angle from the normal edge crack. This occurred during the fatigue precracking using three-point bending.
2. Kinked, where the crack 2 deviates from oblique crack towards the centre path line.
3. Second kinked, when the crack 2 deviates again from the kinked crack to follow the centre path line in order to grow as a normal edge crack.

Perhaps the worst crack 2 shape is from Test specimen 4 as shown in Figure 3.46. The large deviation of the long oblique edge crack from the centre path line caused a large kinked length in order to return towards the centre path line.

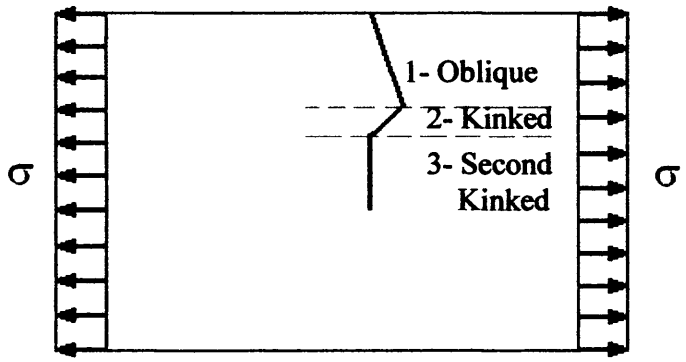

Figure 3.45: Three stages of crack 2 shape.

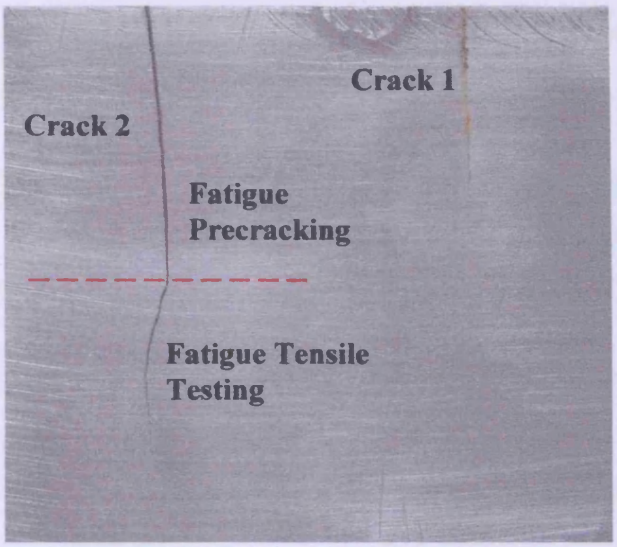

Figure 3.46: A photo of the two cracks from test specimen 4.

To correlate between Y_{a2} values and crack 2 shape, the results of Y_{a2} were mapped to the equivalent crack 2 path. Figures 3.47 (a)-(g) show the results of Y_{a2} together with their equivalent crack 2 path for every specimen. The crack 2 path shown in the figure begins from a2/T equal to 0.2. The first point of Y_{a2} value is equivalent to the start of crack path under fatigue tensile testing or the start of the kinked crack. The figure shows that every specimen has a small kink at the early fatigue cycles. The angle of the kinked crack is approximately between 5 and 30 degrees. During the fatigue tensile test the initial crack 2 will grow towards the centre path line to form a kink before it forms another kink to continue growing as a normal edge crack. At the start of the kinked crack the Y_{a2} value is reduced before it starts to increase. The turning point where the Y_{a2} value starts to increase does not correspond to the start of the second kinked crack. Other factors could affect the location of the turning point possibly due to the boundary effect of the finite plate. Figure 3.48 illustrates the comparison of the SIF profile for an edge crack in a finite and semi-infinite body under uniform tension [3.6]. The SIF for a finite body will increase rapidly as it approaches the plate edge while the SIF for a semi-infinite body will be the same because of no boundary effect on the crack tip.

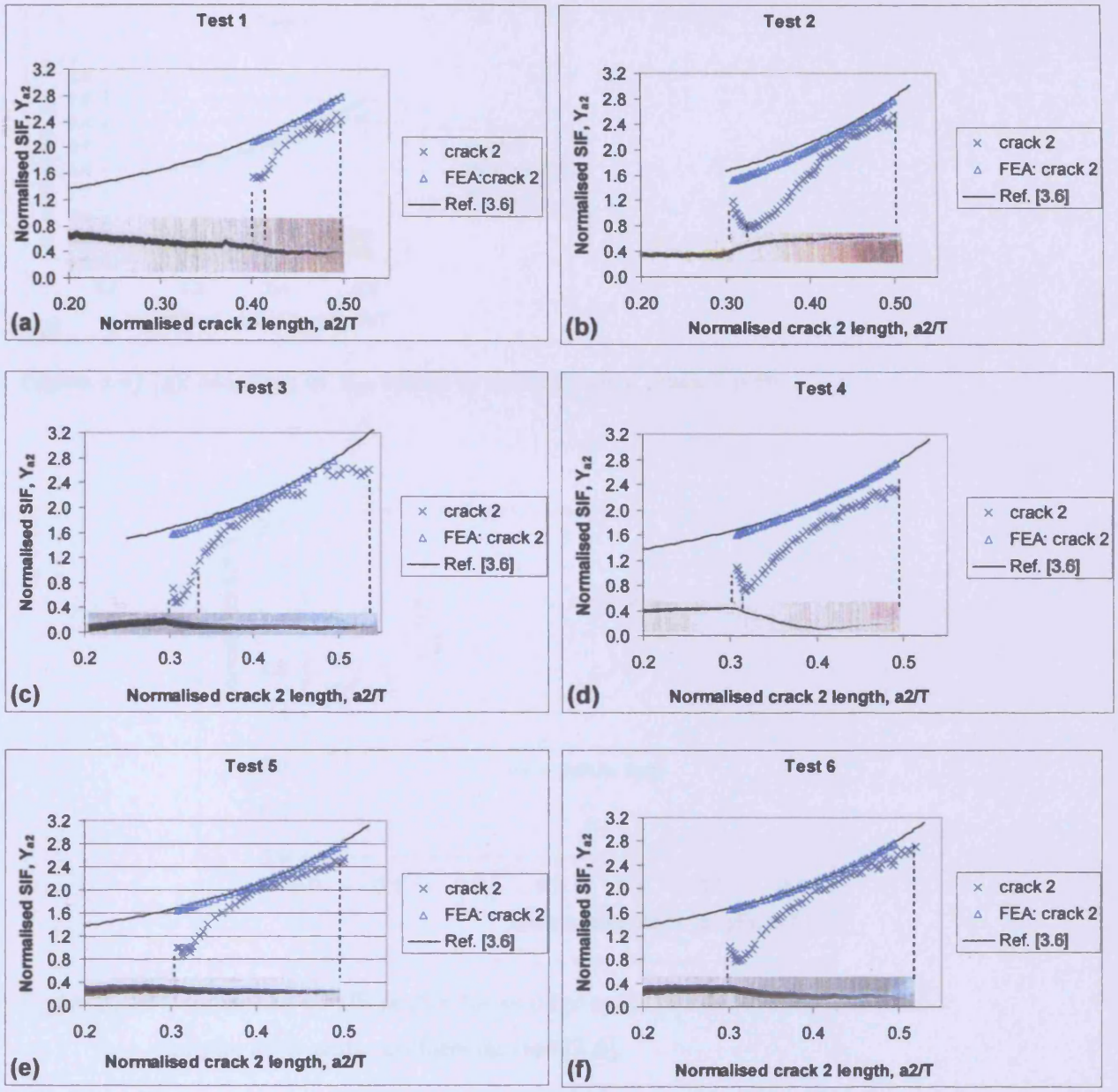

Figure 3.47 (a)-(f): Mapping of Y_{a2} values to the equivalent crack 2 path.

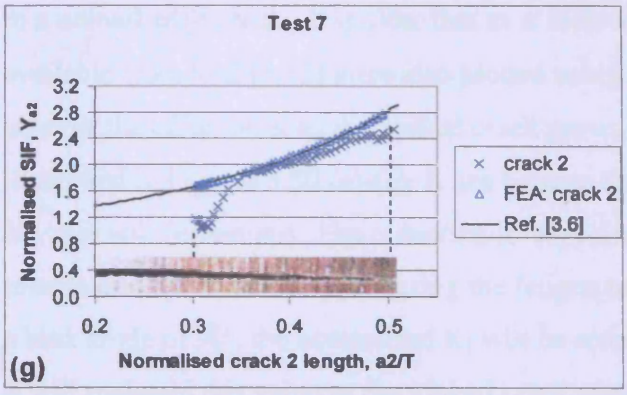

Figure 3.47 (g): Mapping of Y_{a2} values to the equivalent crack 2 path.

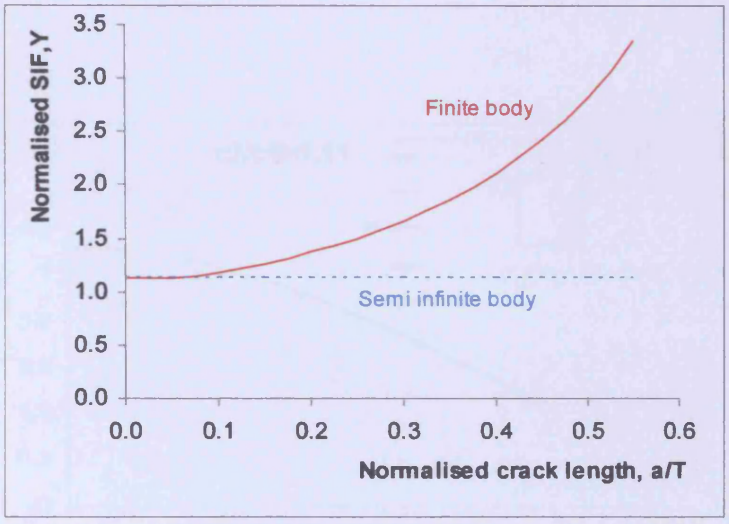

Figure 3.48: Comparison of SIF profile for an edge crack in a finite body and semi-infinite body under uniform tension [3.6].

There are no stress intensity factor (SIF) solutions available for a kinked edge crack in a finite body found in the literature. Most of the solutions are for a kinked edge crack in a semi-infinite body [3.12] and a kinked central crack in an infinite body [3.10], [3.13] and [3.14]. Data for a kinked edge crack in a semi-infinite body in Ref. [3.12] was plotted as shown in Figure 3.49 with different kink angles, α. With limited angle available for the initial crack, angle θ equal to 90 degree is chosen assuming that the initial crack is similar

to a normal edge crack. It is clear that as α increases the Y values will be reduced. Data available from Ref. [3.12] were also plotted using various normalised kink length c2/c1 to observe the effect on K as the kinked crack grows. Three different values of α are illustrated in Figures 3.50 (a)-(c). It can be seen that as the kinked crack grows longer its Y value will be reduced. The reduction is large for a large kinked crack angle. The maximum kinked crack angle during the fatigue test is 30°. Figure 3.50 (a) shows that for a kink angle of 30°, the normalised K_I will be reduced from a value close to 1.12 to 0.919. It will maintain this value as the kinked crack grows longer. It is expected that the SIF will start to increase if the crack grows in a finite body because of the boundary effect on the crack tip plasticity as shown in Figure 3.48. This could introduce the U-shape as observed for all fatigue tensile tests results.

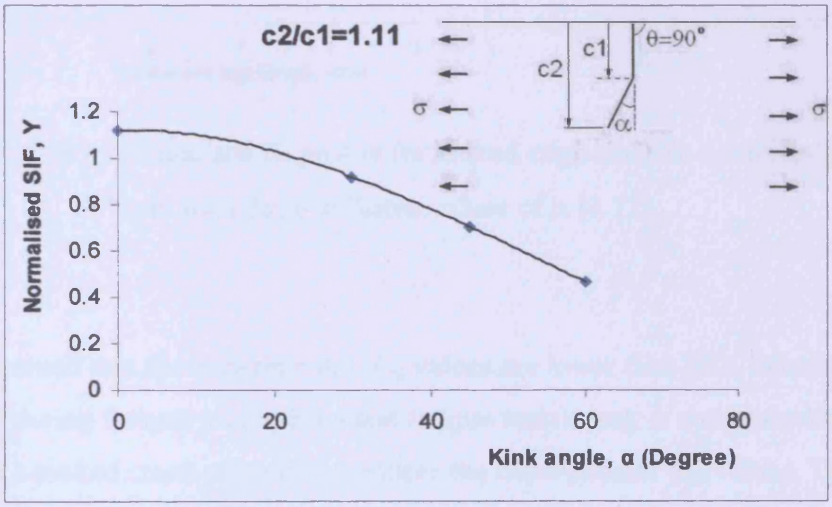

Figure 3.49: Normalised K_I profile with different kink angle, α [3.12].

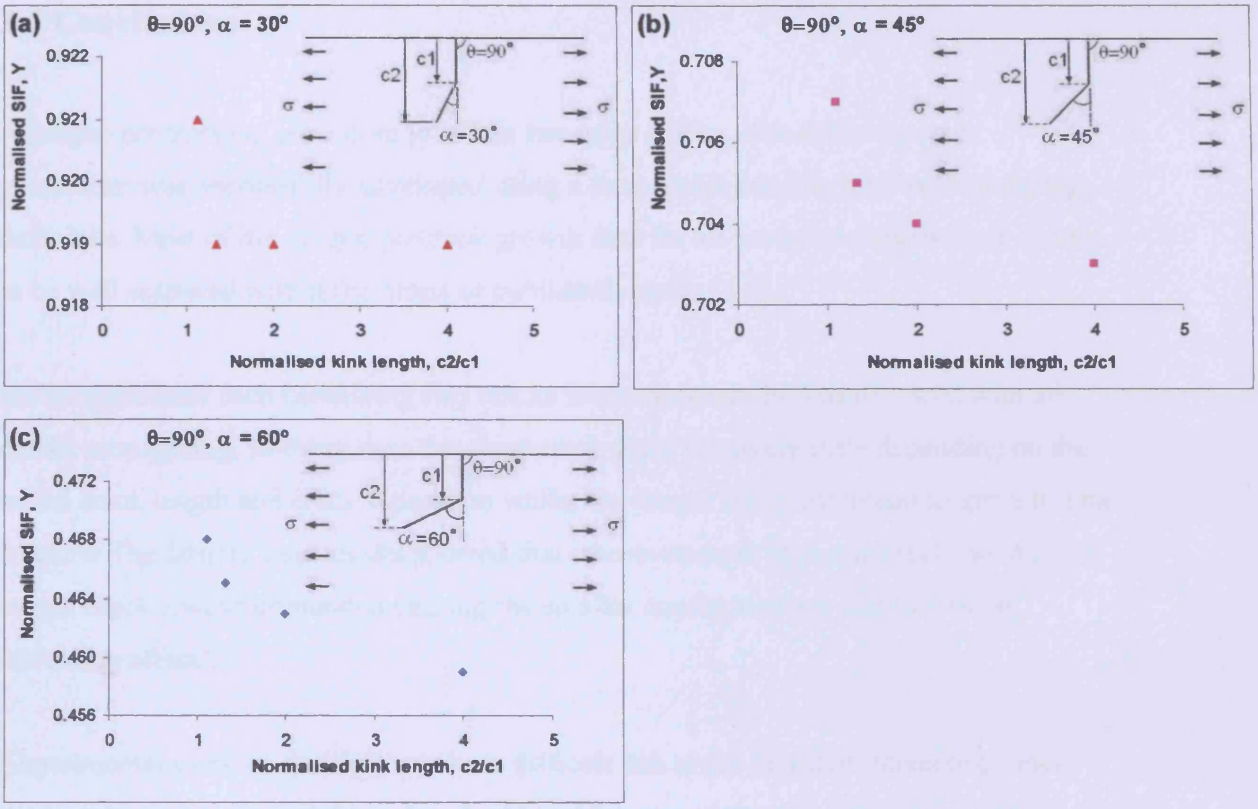

Figure 3.50 (a)-(c): Normalised K_I profile for kinked edge crack in a semi-infinite body with three different values of α [3.12].

It can be assumed that the experimental Y_{a2} values are lower than FEA because of their crack shape during fatigue precracking and fatigue tensile test. A combination of an oblique and a kinked crack effectively reduces the experimental Y_{a2} values. The U-shape of the experimental Y_{a2} values could be explained due to the start of a kinked crack during the fatigue tensile test and the boundary effect of a finite plate that forces the Y_{a2} value to increase. Since there is no Y solution available for a kinked edge crack in a finite plate, the experimental results for Y cannot be corrected and the assumptions can not be proved. The analysis of the U-shape is not simple as this could be affected by other factors such as the crack interaction effect. Since the main objective is to study crack interactions and not to study all these effects, further analysis on the U-shape would not be pursued.

3.6 Conclusions

A fatigue precracking procedure to obtain two edge cracks with differing crack geometries was successfully developed using a three-point bending and weld strapping technique. Most of the fatigue precrack growth data for all seven specimens were shown to be well scattered within the limits of published results [3.5].

Seven specimens each containing two cracks were successfully fatigue tested with all cracks propagating. In every case the short crack grew relatively little depending on the initial crack length and crack separation whilst the longer crack continued to grow to final fracture. The fatigue tests results showed that wherever more than one crack existed, the longer crack always dominated causing the smaller cracks to arrest due to a stress 'shielding effect'.

Experimental work on multiple cracks is difficult due to the fact that interacting cracks tend not to grow in a straight path and within this programme of work the necessity to precrack under bending. Both theory and experimental results show that cracks in close proximity to each other interact to varying degrees depending on relative crack lengths, crack separation and plate width.

Results of Y_{a2} show a U-shape in the crack depth-cycles graph during early crack growth. The most likely cause of this U-shape is thought to be due to the non linear crack 2 path during fatigue precracking and fatigue testing. The existence of a kinked crack during fatigue testing reduces the values of Y_{a2} while the boundary effect of a finite plate forces the Y_{a2} values to increase causing a U-shape. Numerical results for two edge cracks under tension appear conservative since most SIF values obtained experimentally were lower than the equivalent numerical models.

Reduction in Y_{a2} values at the start of the fatigue testing are not only due to the initial crack 2 shape but also due to an interaction effect between crack 1 and 2. This

combination of influences reduces the Y_{a2} values significantly compared to numerical results.

The experimental results concluded that the SIFs of interacting cracks for real engineering applications are much lower than the FEA results or other numerical solutions that assume the two cracks are perfectly parallel. The experimental results suggest that the interaction of kinked or oblique edge cracks produce lower SIFs than the equivalent theoretical results.

3.7 References

3.1 BS EN 10025, Hot rolled products of structural steels, Part 2, British Standard Institution (BSI), 2004.

3.2 Jiang, Z.D., Zeghloul, A., Bezine, G. and Petit, J., Stress intensity factors of parallel cracks in a finite width sheet. Engineering Fracture Mechanics, 1990, 35, pp.1073-1079.

3.3 ABAQUS, version 6.4. Hibbitt, Karlsson & Sorensen, Inc.

3.4 Engineering Science Data Unit, Fatigue threshold stress intensity factors and slow crack propagation rates in low and medium strength low alloy steel, 81012, Engineering Sciences Data Unit, 1981.

3.5 Engineering Science Data Unit, Fatigue crack propagation in low and medium strength low alloy steel plate, bar and forgings, 81011, Engineering Sciences Data Unit, 1981.

3.6 Brown, W.F. and Srawley, J.E., Plane strain crack toughness testing of high strength metallic materials. ASTM STP 410, 1966.

3.7 Murakami, Y., Stress Intensity Factors Handbook. Pergamon Press, 1st Edition, U.K., 1986, pp.13.

3.8 BS ISO 12108, Metallic materials – Fatigue testing – Fatigue crack growth method, British Standard Institution (BSI), 2002.

3.9 DIGITAL™ Visual Fortran, Profession Edition Version 5.0 for Windows NT and Windows 95, Digital Equipment Corporation (now COMPAQ), 1997.

3.10 Cotterell, B. and Rice, J.R., Slightly curved or kinked cracks. International Journal of Fracture, 1980, 16, pp.155-169.

3.11 Ma, C., Chang, Z. and Tsai, C., Weight functions of oblique edge and center cracks in finite bodies. Engineering Fracture Mechanics, 1990, 36, pp.267-285.

3.12 Murakami, Y., Stress Intensity Factors Handbook. Pergamon Press, 1st Edition, U.K., 1987, pp.120

3.13 Lo, K.K., Analysis of branched cracks. Journal of Applied Mechanics, 1978, 45, pp.797-802.

3.14 Murakami, Y., Stress Intensity Factors Handbook. Pergamon Press, 1st Edition, U.K., 1987, pp.352-361.

Chapter 4: Stress Intensity Factors for Multiple Cracks Using a Weight Function Method

4.0 Introduction

It is known that a powerful feature of a weight function approach is the ability to determine SIF solutions for an arbitrary applied stress. The weight function is a universal function of a cracked body for any given geometry. Weight function methods have been applied extensively to problems concerning a single crack. So far, no attempt has been made to use a weight function method to determine crack tip SIF of multiple cracks. In order to use the weight function method for multiple cracks, the interaction effect between cracks needs to be included. The crack interaction will enhance or shield the crack tip SIF depending on the crack separation, the applied stress and the crack geometry.

In this chapter the work is mainly to develop and to include this interaction effect into the weight function method. The non-uniform stress distributions due to the presence of an additional edge crack were used to establish the crack interaction in a general form. The work involved using a weight function for a single edge crack with non-uniform stress distribution caused by an additional crack. The stress distributions were obtained using FEA of a single edge crack in a finite strip. These were compared to SIFs obtained from FEA of a finite strip containing two edge cracks.

FEA analysis in this chapter will use two different types of models. As discussed in Chapter 2 one was used for non-uniform stress distribution studies and another used to solve the SIFs of two edge cracks. A full FE model was constructed to model a finite strip with length 10 times longer than its width. This ensured that there was no strip length effect on local stress distribution near the crack tip area. To model uniform tension, nodes at the end of the strip were constrained and nodes at the opposite end were applied with a

point load. The FE models used for non-uniform stress distribution studies contained a single edge crack while those used for solving SIFs contained two edge cracks.

4.1 A Weight Function Method for the Calculation of SIFs for Interacting Cracks

One possible method for developing the interaction effect between two edge cracks is by comparing the SIF solutions for a single edge crack and an edge crack in the presence of an additional crack. If these two solutions were known, a modification to a single edge crack weight function could be attempted to formulate a weight function for an edge crack in the presence of an additional edge crack. The solution for a single edge crack [4.1] in a finite strip under tension is available but the solution for two edge cracks in a finite strip is not available in published literature. Most of the solutions are for two cracks in semi-infinite and infinite bodies. There are solutions available for two cracks in a finite body but these either apply to edge cracks of the same length [4.2], central cracks of same length [4.3] and central coplanar cracks of same length [4.4]. SIF solutions for two cracks of differing lengths in finite bodies could be obtained using FEA. This however would require a considerable number of FE models to cover all different values of crack length and separation to compare with a single crack. Furthermore, if the interaction effect can be established using this comparison method, the way in which this effect is incorporated into the SIF weight function equation remains unclear.

Another method to develop the interaction effect of multiple cracks is by analysing the non-uniform stress distribution due to the presence of a single crack, along the crack plane of a potential second crack. The stress distribution used in conjunction with a weight function to calculate the SIF of the two edge cracks will be different to that used for a single edge crack. Under uniform applied stress, the stress distribution at the potential crack plane for a single edge crack will be uniform but for two edge cracks it will be non-uniform because of the crack interaction. Using this idea, the non-uniform stress distribution can be used as an interaction effect between cracks. Once established

the stress distribution can be used directly with the SIF weight function equation as the equation requires stress distribution at the potential crack plane. It is much more efficient to use this method as it requires fewer FE models to be solved than would be needed to model two cracks. The stress values can be taken at any nodes of the FE model for different crack geometries.

From Chapter 1 the SIF weight function equation for a single crack can be written as follows:

$$K = \int_0^a \sigma(x)m(a,x)dx \quad (MN/m^{3/2}) \tag{4.1}$$

where m(a,x) is a weight function for an edge crack with length *a* and σ(x) is stress distribution along the potential crack plane. In the absence of any geometric discontinuities the stress distribution in the potential crack plane is the same as the nominal stress distribution. For example Figure 4.1 (a) shows remotely applied uniform tension and therefore the stress distribution in the potential crack plane is also uniform. In order to calculate crack tip SIFs when two cracks are present the SIF weight function equation can be written as:

$$K_{a1} = \int_0^{a1} \sigma 1(x)m(a1,x)dx \quad (MN/m^{3/2}) \tag{4.2a}$$

and

$$K_{a2} = \int_0^{a2} \sigma 2(x)m(a2,x)dx \quad (MN/m^{3/2}) \tag{4.2b}$$

where weight function m(a1,x) and m(a2,x) are both single edge crack weight functions similar to m(a,x) in Eqn.(4.1). However, stress distribution σ1(x) and σ2(x) are not equal to nominal stress due to the geometric discontinuity arising from the presence of the other crack. These non-uniform stress distributions are used to include the interaction effect in solutions for K_{a1} and K_{a2}, the SIF of crack 1 and 2 respectively. The modification made is summarised in Figure 4.1.

Figure 4.2 shows an example of an FEA result used to determine σ2(x). It shows a contour plot of the y-component of stress in a plate with an edge crack under uniform

tension. The plane in which σ2(x) is required will depend on the location of the potential crack plane 2. The interaction effects exist as long as the potential crack plane 2 passes through the non-uniform stress region. If the potential crack plane 2 is completely in the region of uniform stress, σ2(x) will be equal to nominal stress, σ_0 and there will be no interaction effect between cracks. In this situation each crack can be treated as an individual edge crack. Therefore by analysing the non-uniform stress distribution profile the crack interaction can be established and hence the SIFs of both cracks can be predicted.

From Figure 4.1 (b) the only unknown information required to calculate the SIF of crack 2 is σ2(x) in the potential crack plane 2 in the presence of crack 1. The FE models as discussed in previous chapters were used to determine stress distributions in the potential crack plane 2 with differing crack 1 lengths and crack separations.

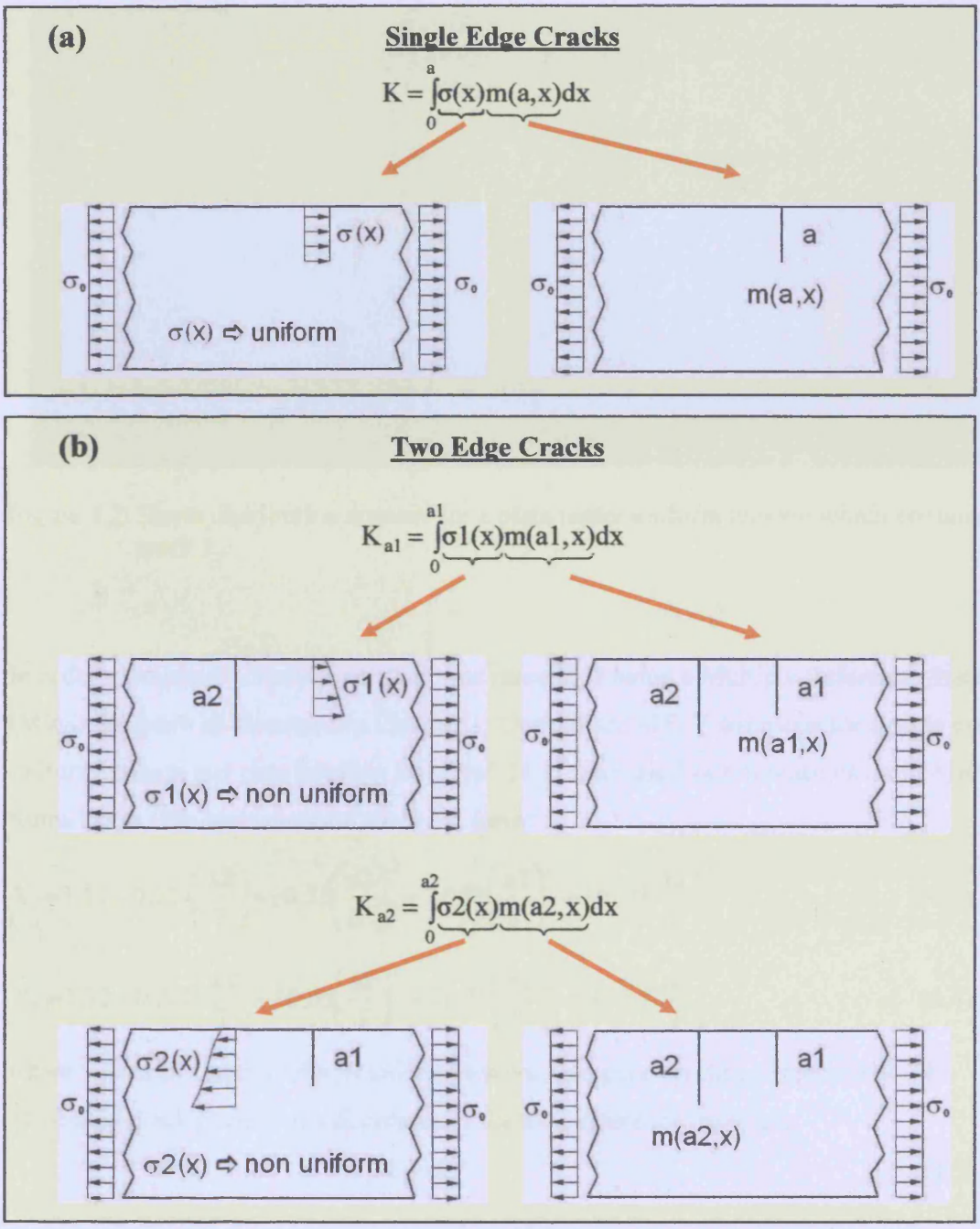

Figure 4.1: (a) SIF weight function equation used for a single edge crack, (b) Modifications made to predict SIF weight function of two edge cracks.

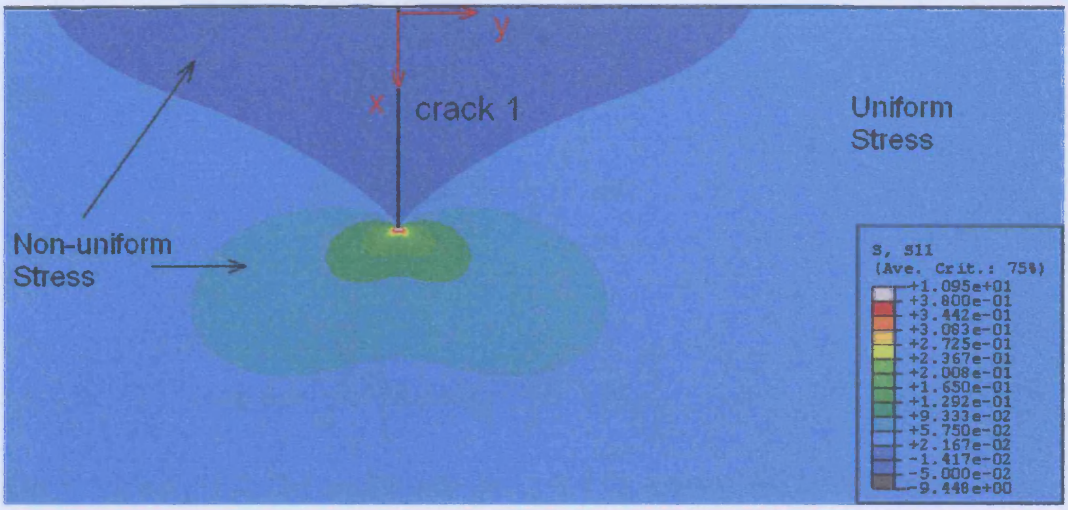

Figure 4.2: Stress distribution contour for a plate under uniform tension which contains crack 1.

In order to improve accuracy, m(a2,x) was calculated using a Multiple Reference State (MRS) approach as discussed in Chapter 1. Normalised SIF, Y solutions for a plate under uniform tension and pure bending from Ref. [4.1] were used as reference cases in MRS formulation. The two solutions are in the form:

$$Y_1 = 1.12 - 0.231\left(\frac{a2}{T}\right) + 10.55\left(\frac{a2}{T}\right)^2 - 21.72\left(\frac{a2}{T}\right)^3 + 30.39\left(\frac{a2}{T}\right)^4 \tag{4.3}$$

$$Y_2 = 1.12 - 0.231\left(\frac{a2}{T}\right) + 10.55\left(\frac{a2}{T}\right)^2 - 21.72\left(\frac{a2}{T}\right)^3 + 30.39\left(\frac{a2}{T}\right)^4 \tag{4.4}$$

where subscript 1 and 2 refer to uniform tension and pure bending respectively. The associated crack plane stress distributions for their reference cases are:

$$\sigma_1(x) = \sigma_0 \tag{4.5}$$

$$\sigma_2(x) = \sigma_0\left(1 - \frac{2x}{T}\right) \tag{4.6}$$

From Chapter 1, for two references cases the two coefficients that need to be solved are:

$$C_1 = \frac{q_1 W_{22} - q_2 W_{12}}{W_{11} W_{22} - W_{21} W_{12}} \tag{4.7}$$

$$C_2 = \frac{q_2 W_{11} - q_1 W_{21}}{W_{11} W_{22} - W_{21} W_{12}} \tag{4.8}$$

where

$$W_{ij} = \int_0^{a2} \sigma_i(x) \left(1 - \frac{x}{a2}\right)^{j-\frac{1}{2}} dx \tag{4.9}$$

and

$$q_i = \frac{Y_1\left(\frac{a2}{T}\right)}{2} \left[K_i(a2) \sqrt{\frac{\pi(a2)}{2}} - W_{i0} \right] \tag{4.10}$$

where i=1,2 and j=1,2. The coefficients for C_1 and C_2 were solved using programming code [4.5]. Knowing these two coefficients, the weight function is determined as:

$$m(a2,x) = 2\sqrt{2} \frac{\sigma_0}{K_1(a2)} \sum_{j=0}^{2} C_j \left(1 - \frac{x}{a2}\right)^{j-\frac{1}{2}} \tag{4.11}$$

Using this weight function, the SIF for crack 2 under remotely applied uniform tension is calculated using Eqn.(4.2b). It can be written as:

$$K_{a2} = \int_0^{a2} \sigma 2(x) (2\sqrt{2}) \frac{\sigma_0}{K_1(a2)} \sum_{j=0}^{2} C_j \left(1 - \frac{x}{a2}\right)^{j-\frac{1}{2}} dx \tag{4.12}$$

in which σ2(x) is the non-uniform stress distribution in a potential crack plane 2. As stated previously the stress distribution σ2(x) is non-uniform due to the presence of crack 1. The SIF, K_{a2} therefore incorporates the crack interaction effect.

The edge crack weight function coefficients C_1 and C_2 given by Eqn.(4.7) and Eqn.(4.8), and new SIF solutions K_{a2} given by Eqn.(4.12) were evaluated using a program coded in Visual Fortran [4.5]. Integrations in Eqn.(4.9) were solved using the intrinsic integration function that is available in the programming software [4.5]. The same intrinsic integration function was also used to calculate Eqn.(4.12) to generate the final K_{a2} values.

4.1.1 Verification of the Weight Function Method

Before establishing the interaction effect in parametric form for a wide range of geometric data, initial work was completed to assess the methodology of the modified SIF weight function method. The work used FE models containing a fixed length of crack 1 with three different crack separations to obtain stress distributions along the potential crack plane 2. These stress distributions were curve fitted and were used to calculate the SIFs of crack 2, K_{a2} using Eqn.(4.12). The geometric parameters of crack separation, d, distance along the potential crack plane 2, x and crack 1 length, a1 were normalised to strip width, T. The stress distribution along the potential crack plane 2, $\sigma 2(x)$ were normalised against the nominal stress, σ_0. Notations used are as shown in Figure 4.3. SIFs for crack 2 were compared to FEA results. The FE models used to obtain FEA results used a finite strip containing two edge cracks allowing K_{a2} to be evaluated directly.

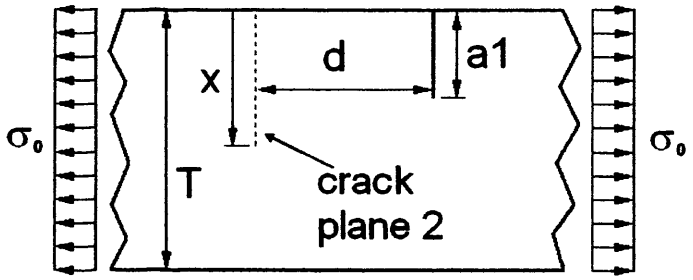

Figure 4.3: Notation used to determine stress distribution profile.

4.1.1.1 Calculation and Curve Fitting of Stress Distributions

An FE model with a1/T equal to 0.2 was used for this initial study. The y-component of stress was measured along x/T at d/T values equal to 0.2, 0.31 and 0.51. Stress measurements were taken from x/T equal to 0 until approximately 0.50. The value of x/T was limited to half of the strip width and therefore the weight function SIFs are only valid within this region. Details of the FE model used were as discussed in Chapter 2.

The stress values obtained were normalised against the stress remote from the crack plane, σ_0. The results of normalised stress distribution, $\sigma 2(x)/\sigma_0$ at three different locations are as shown in Figure 4.4. The distribution of $\sigma 2(x)/\sigma_0$ shows considerable variation and high stress gradients at d/T equal to 0.20. Both variation and gradients are reduced as the value of d/T increases. If the value of d/T is increased beyond this range the distribution $\sigma 2(x)/\sigma_0$ will tend towards 1.0 indicating a reduction of the interaction effect between cracks.

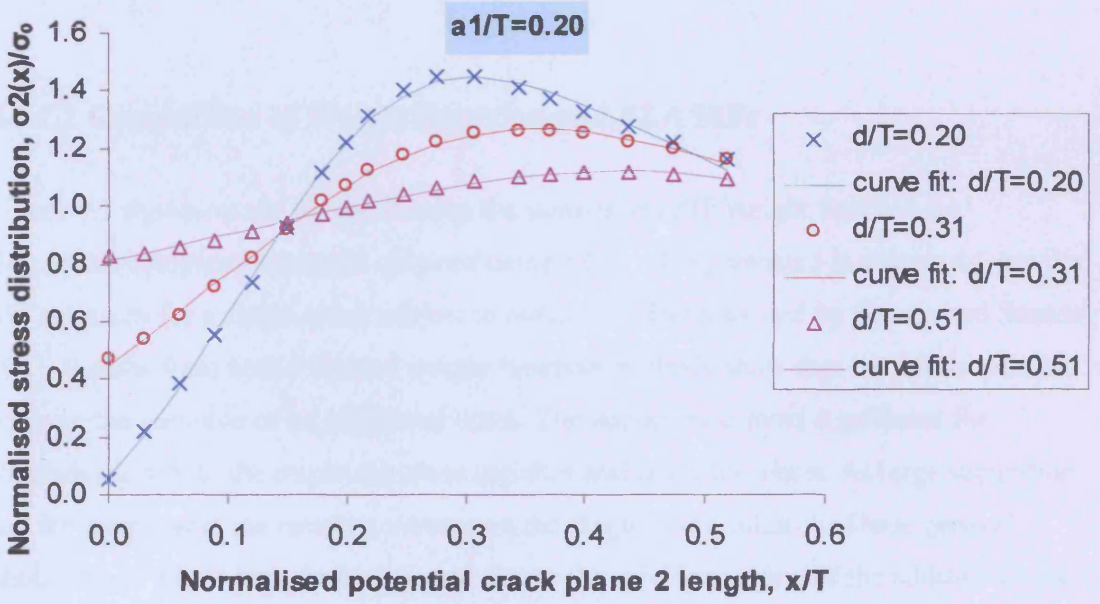

Figure 4.4: Results of normalised stress distribution $\sigma 2(x)/\sigma_0$ at d/T = 0.20, 0.31 and 0.51 together with their curve fit line.

The plotted points for three different d/T values were curved fitted using CurveExpert software [4.6]. Equations that were found to closely approximate finite element data at the three locations were as follows:

$$\frac{\sigma 2(x)}{\sigma_0} = \frac{0.05932 + 4.224(x/T)}{1 - 3.302(x/T) + 10.10(x/T)^2} \quad ; d/T = 0.20 \qquad (4.13)$$

$$\frac{\sigma 2(x)}{\sigma_0} = \frac{0.4501+1.985(x/T)}{1-2.014(x/T)+4.978(x/T)^2} \quad ; d/T=0.31 \tag{4.14}$$

$$\frac{\sigma 2(x)}{\sigma_0} = \frac{0.8088-0.5714(x/T)}{1-1.803(x/T)+1.507(x/T)^2} \quad ; d/T=0.51 \tag{4.15}$$

Using these stress distributions and Eqn.(4.12) in the weight function program the SIFs of crack 2 were calculated. SIF solutions presented in this thesis were normalised in the form below:

$$Y_{a2} = \frac{K_{a2}}{\sigma_0 \sqrt{\pi(a2)}} \tag{4.16}$$

where σ_0 is the remotely applied stress.

4.1.1.2 Comparison of Weight Function and FEA SIFs

Figure 4.5 shows results obtained using the normalised SIF weight function i.e. Eqn.(4.16) compared to results obtained using FEA. Also presented in Figure 4.5 are the SIF solutions for a single crack subject to remote tension provided by Brown and Srawley [4.1]. Results from both FEA and weight function methods show that the SIF is reduced when in the presence of an additional crack. The reduction is most significant for situations in which the cracks are close together and crack 2 is short. At large separation and for long cracks the results converge on the single crack solution. These general observations would have been expected due to the shielding effect of the additional crack.

Overall results obtained from the weight function approach are encouraging as they display the general trend expected and compare well to the FEA results. The correlation between weight function and FEA results are generally good except for results for small crack separation, d/T=0.20. At this separation error between weight function and FEA results are largest and occur when the two cracks are of the same length. A maximum relative error of 9.6% was measured when crack length a2 was the same as crack length a1 at a2/T equal to 0.2.

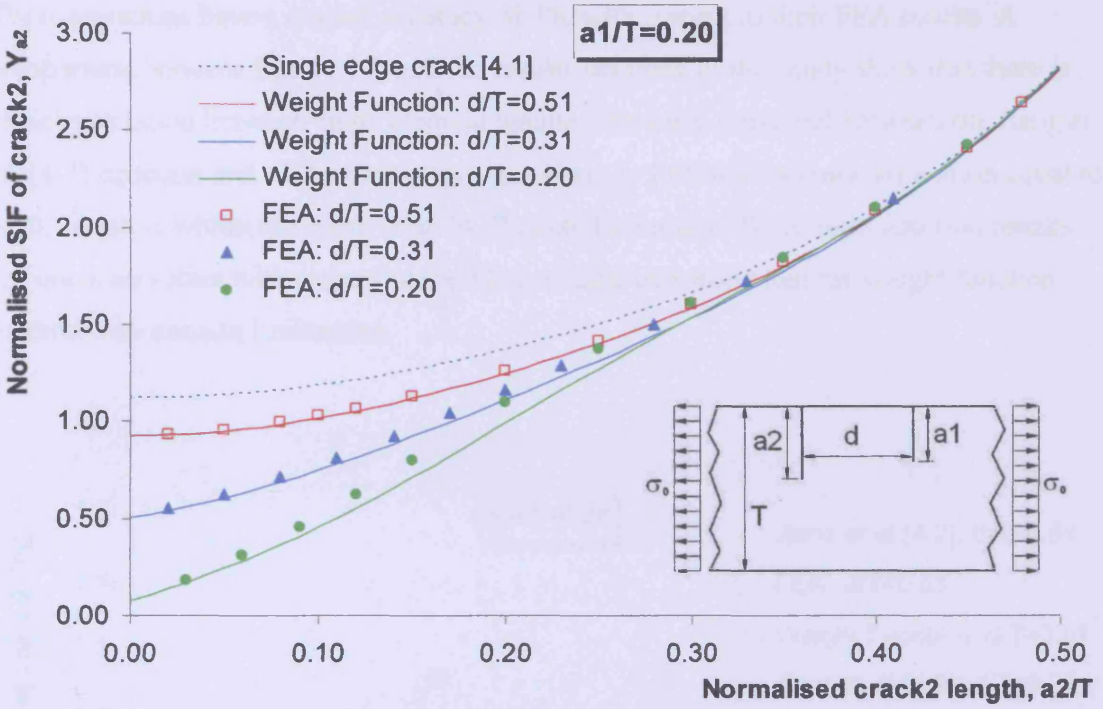

Figure 4.5: Comparison of Normalised SIF weight function obtained using the weight function with FEA results for a1/T=0.20 with d/T = 0.20, 0.31 and 0.51.

Figure 4.6 shows the FEA and weight function results in addition to results published by Jiang *et al.* [4.2] who investigated two edge cracks of equal length in a finite strip under remotely applied uniform tension. They used FEA to formulate an equation for their SIF results which are shown below:

$$Y = \frac{A_0 + A_1(a2/T)^{1.5} + A_2(a2/T)^4}{\sqrt{1-(a2/T)^2}} \tag{4.17}$$

$$A_0 = 0.79 + 0.07\left(\frac{d}{2(a2)}\right) + 0.04\left(\frac{d}{2(a2)}\right)^2 - 0.011\left(\frac{d}{2(a2)}\right)^3$$

$$A_1 = 1.74 + 0.07\left(\frac{d}{2(a2)}\right) - 1.44\left(\frac{d}{2(a2)}\right)^2 + 0.206\left(\frac{d}{2(a2)}\right)^3 \tag{4.18}$$

$$A_2 = 6.02 + 2.19\left(\frac{d}{2(a2)}\right) - 3.26\left(\frac{d}{2(a2)}\right)^2 + 0.828\left(\frac{d}{2(a2)}\right)^3$$

These equations have a quoted accuracy of 3% with respect to their FEA results. A comparison between Eqn.(4.17) and the results obtained in this study show that there is close correlation between finite element results. The error measured between the Jiang *et al.* [4.2] equation and FEA results from this study is 1.66% for a crack separation equal to 0.20, which is within the Jiang *et al.* [4.2] quoted accuracy. The weight function results are unconservative with respect to the FEA results, indicating that the weight function method may contain limitations.

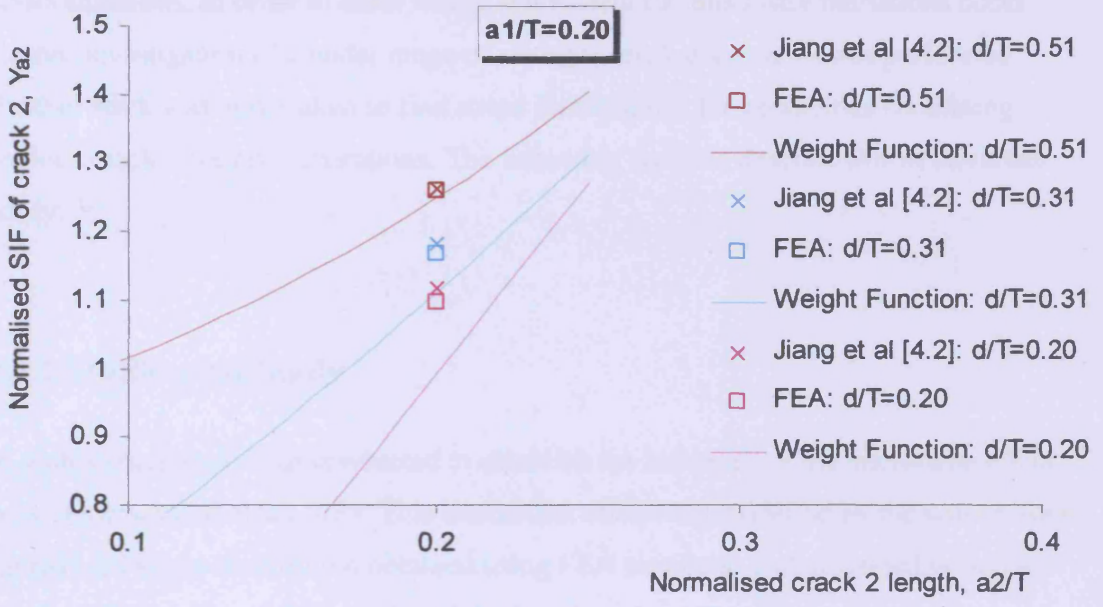

Figure 4.6: Comparison between FEA and weight function results, and solution of two edge cracks of equal length [4.2] for a1/T=0.20 with d/T=0.20, 0.31 and 0.51.

The limitations are expected to be greatest when cracks are close together. As crack separation is increased the performance of the weight function method is improved with respect to finite element data. At d/T equal to 0.31 the maximum relative error is reduced to 4.7%. The result for d/T equal to 0.51 shows a very good correlation with the FEA result. The maximum error is estimated at a negligible 0.8%.

The result shown in Figure 4.5 and Figure 4.6 demonstrate how the weight function method can be used to predict the SIFs of two edge cracks with good accuracy apart from cracks that are very close together. This initial study proves the validity of the proposed weight function method for problems containing interacting cracks. The study shows how new SIF solutions for multiple cracks problems can be predicted using weight functions and stress distributions only. This approach requires less work to implement than repeated finite element modelling of multiple cracks.

This initial study has shown that accuracy of the weight function solutions is degraded for some situations. In order to asses where and to help establish why limitations occur further investigation of a wider range of multiple crack geometries was performed. Further work was undertaken to find stress distributions for geometries containing various crack sizes and separations. The following sections describe this multivariate study.

4.1.2 Multivariate Study

A multivariate study was conducted to establish the influence of the interaction effect between cracks on crack SIFs. This interaction effect was modelled by the non-uniform normalised stress distribution obtained using FEA similar to that described in Section 4.1.1 together with an edge crack weight function. A multivariate study requires a general equation for the stress distribution which is a function of non-dimensional parameters a1/T, d/T and x/T. Use of this general equation approximating $\sigma 2(x)/\sigma_0$ can be applied to calculate SIFs of the two cracks using Eqn.(4.2) or Eqn.(4.16) for arbitrary crack lengths and separation.

4.1.2.1 Method of Multivariate Study

The first step of multivariate study was to calculate $\sigma 2(x)/\sigma_0$ at a number of positions in the potential crack plane 2 described by x/T with various a1/T and d/T values using FEA. Stress measurements were taken at x/T values between 0 and approximately 0.5 depending on the nodal position of the FE model used. Details of geometric parameters investigated are as shown in Table 4.1. A total of nine FE models with different a1/T values were used. For each model, measurements of $\sigma 2(x)/\sigma_0$ were taken for several d/T values. Values of d/T investigated are dependent upon the FE model used. Their values were limited to a maximum of 1.0 beyond which stress distributions were found to be uniform.

a1/T	d/T												
0.05	0.09	0.13	0.21	0.32	0.40	0.52	0.60	0.72	0.80	0.90	1.00		
0.10	0.06	0.10	0.14	0.18	0.22	0.29	0.41	0.49	0.61	0.69	0.84	0.92	1.00
0.15	0.07	0.11	0.14	0.22	0.30	0.42	0.50	0.61	0.69	0.81	0.93	1.00	
0.20	0.08	0.12	0.16	0.20	0.31	0.39	0.51	0.58	0.70	0.82	0.89	1.01	
0.25	0.08	0.12	0.16	0.20	0.23	0.31	0.39	0.51	0.62	0.70	0.82	0.89	1.01
0.30	0.08	0.11	0.15	0.19	0.23	0.30	0.42	0.50	0.58	0.69	0.81	0.89	1.01
0.35	0.09	0.13	0.17	0.20	0.28	0.40	0.51	0.59	0.71	0.82	0.90	1.02	
0.40	0.08	0.12	0.16	0.20	0.23	0.31	0.43	0.51	0.62	0.70	0.82	0.89	1.01
0.45	0.08	0.12	0.16	0.20	0.23	0.31	0.39	0.51	0.62	0.70	0.82	0.89	1.01

Table 4.1: Parameters used to obtain $\sigma 2(x)/\sigma_0$.

Detailed results of normalised stress distributions $\sigma 2(x)/\sigma_0$ for all a1/T and d/T values are shown in Figures 2.16 (a)-(i) in Chapter 2. For each graph, CurveExpert software [4.6] was employed to formulate a suitable general equation that can approximate the results of $\sigma 2(x)/\sigma_0$ for every d/T value. The recommended regression model is as given below:

$$\frac{\sigma 2(x)}{\sigma_0} = \frac{a + b(x/T)}{1 + c(x/T) + d(x/T)^2} \tag{4.19}$$

where *a, b, c* and *d* are coefficients that are dependent upon d/T. Eqn.(4.19) was found to be the most suitable regression model for stress distributions obtained for alternative a1/T values. Some distributions were more difficult to curve fit, especially for those of low d/T values. An R-squared value (R^2) is a statistical measure of how well the regression line approximates the real data points. Most regression analysis produced a curve fit with an R-squared value of more than 0.999 indicating a near perfect correlation. The minimum R-squared value recorded was 0.980. Knowledge of the coefficients of Eqn.(4.19) allows a continuous description of the stress distributions.

The next step was to obtain $\sigma 2(x)/\sigma_0$ as a function of d/T. The previous four coefficients from Eqn.(4.19) obtained for every a1/T with various d/T were plotted as a function of d/T as shown in Figure 4.7. For each coefficient the CurveExpert software [4.6] was used to find a common regression model to represent all a1/T values. The only regression model that can be used for curve fit is 6^{th} degree polynomial as:

$$\text{Coeff.}(a,b,c,d) = A + Bx + Cx^2 + Dx^3 + Ex^4 + Fx^5 + Gx^6 \qquad (4.20)$$

where *A,B,C,D,E,F,* and *G* are the coefficients that represent every a1/T value. The minimum R-squared value was 0.990. Other regression models produced relatively low values of R-squared.

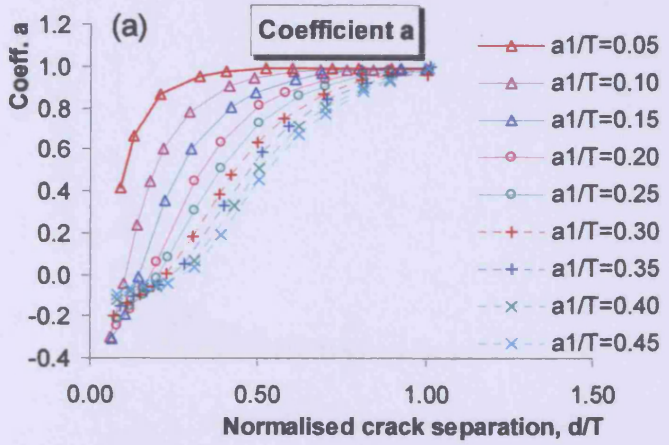

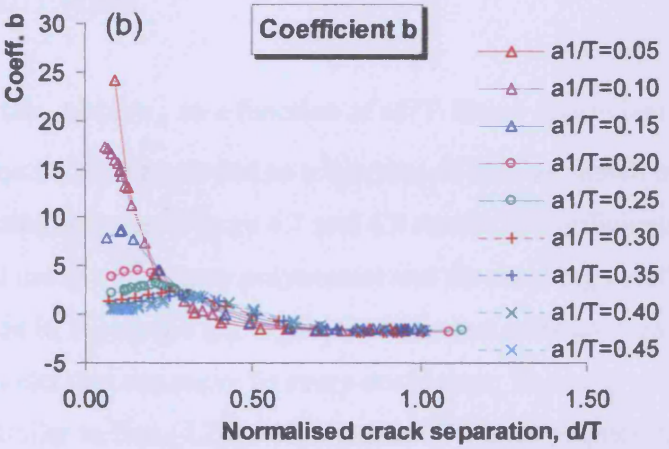

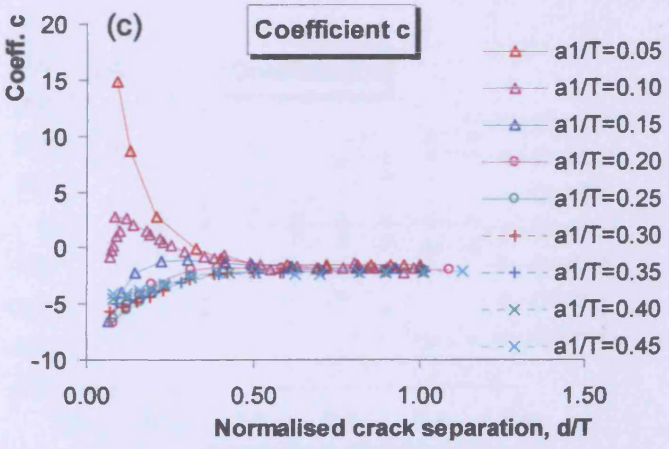

Figure 4.7 (a)-(c): Results of coefficient *a*, *b* and *c* from Eqn.(4.19) plotted as a function of d/T with various a1/T values.

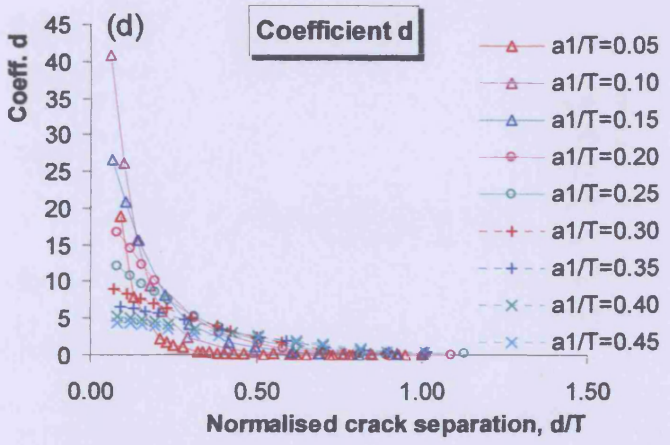

Figure 4.7 (d): Results of coefficient *d* from Eqn. (4.19) plotted as a function of d/T with various a1/T values.

The next step was to obtain $\sigma 2(x)/\sigma_0$ as a function of a1/T. Every coefficient i.e. coefficient *A-G* from Eqn.(4.20) was plotted as a function of a1/T as shown in Figure 4.8. To illustrate the relationship between Figure 4.7 and 4.8 results of coefficients *a* in Figure 4.7 (a) were curve fitted using a 6^{th} degree polynomial and the resulting coefficients of this curve fit were plotted in Figure 4.8 (a). Again CurveExpert software was used to find a common regression model that can curve fit every coefficient. The most suitable regression model was similar to Eqn.(4.20) which uses a 6^{th} degree polynomial. The minimum value of R-squared was 0.980.

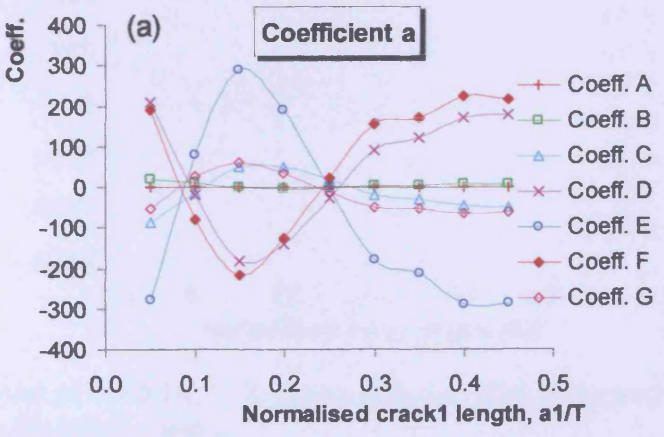

Figure 4.8 (a): A plot of coefficients A-G as a function of a1/T derived from coefficient *a*.

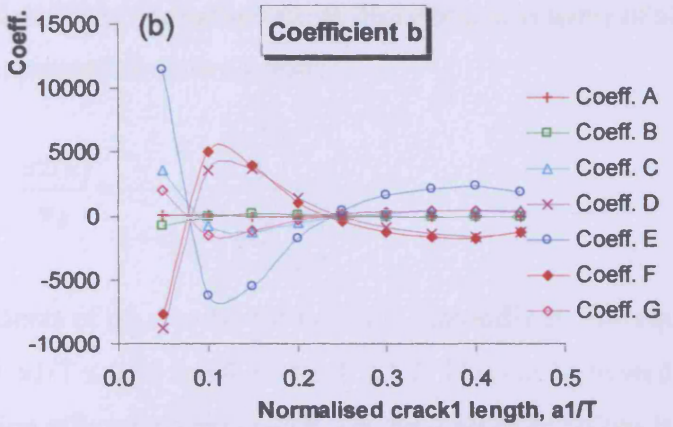

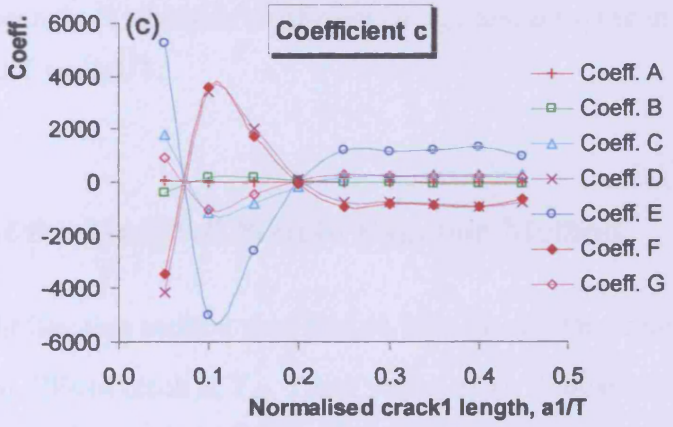

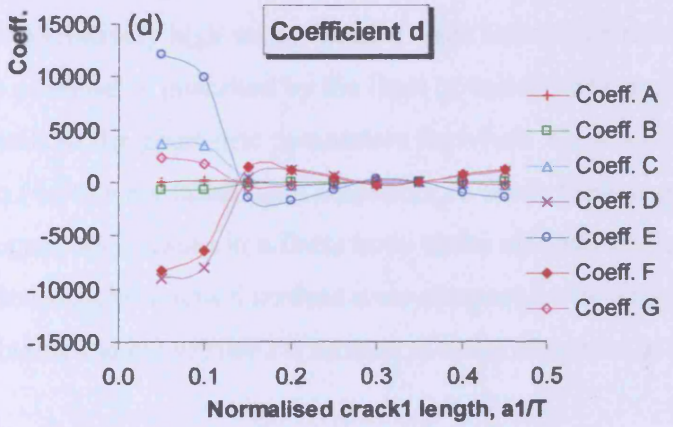

Figure 4.8 (b)-(d): A plot of coefficients A-G as a function of a1/T derived from coefficient *b*, *c* and *d*.

The final equation describing normalised stress distributions in terms of all geometric parameters can be expressed as shown below:

$$\frac{\sigma 2(x)}{\sigma_0} = \frac{a + b\left(\frac{x}{T}\right)}{1 + c\left(\frac{x}{T}\right) + d\left(\frac{x}{T}\right)^2} \tag{4.21}$$

where detail coefficients of a,b,c and d are shown in Appendix B. The equation is only valid for $x/T \leq 0.50$, $a1/T \leq 0.50$ and $0.10 < d/T \leq 1.0$. This can be treated as a general form of the interaction effect between cracks. The final set of equations is numerous due to the usage of 6^{th} degree polynomials as a regression model during the curve fitting of the coefficients. Appendix B tabulates coefficients *a*, *b*, *c* and *d* for use in Eqn.(4.21) with different values of d/T and a1/T.

4.2 Validation of the Modified Weight Function Method

The modified weight function method used Eqn.(4.16) and $\sigma 2(x)/\sigma_0$ from Eqn.(4.21) to calculate normalised SIFs of crack 2, Y_{a2}. Three values of a1/T equal to 0.125, 0.25 and 0.375 were investigated. For each crack length a1/T a number of d/T values were investigated to show the full range of interaction from a low d/T value where strong interaction occurs to a relatively high value where a weak interaction occurs. The minimum d/T value possible, is governed by the limit of validity of Eqn.(4.21) at 0.10. Table 4.2 shows details of the geometric parameters for which Y_{a2} was calculated. Coefficients for Eqn.(4.21) were taken from Appendix A. Since there is no published solution for two unequal edge cracks in a finite body under uniform tension available, results of the modified weight function method were compared with FEA results. The FEA results were obtained using similar FE models to those discussed in the previous chapter.

a1/T	d/T			
0.125	0.10	0.28	0.45	-
0.25	0.10	0.30	0.50	0.75
0.375	0.15	0.45	0.85	-

Table 4.2: Detailed parameter used to obtain Y_{a2}.

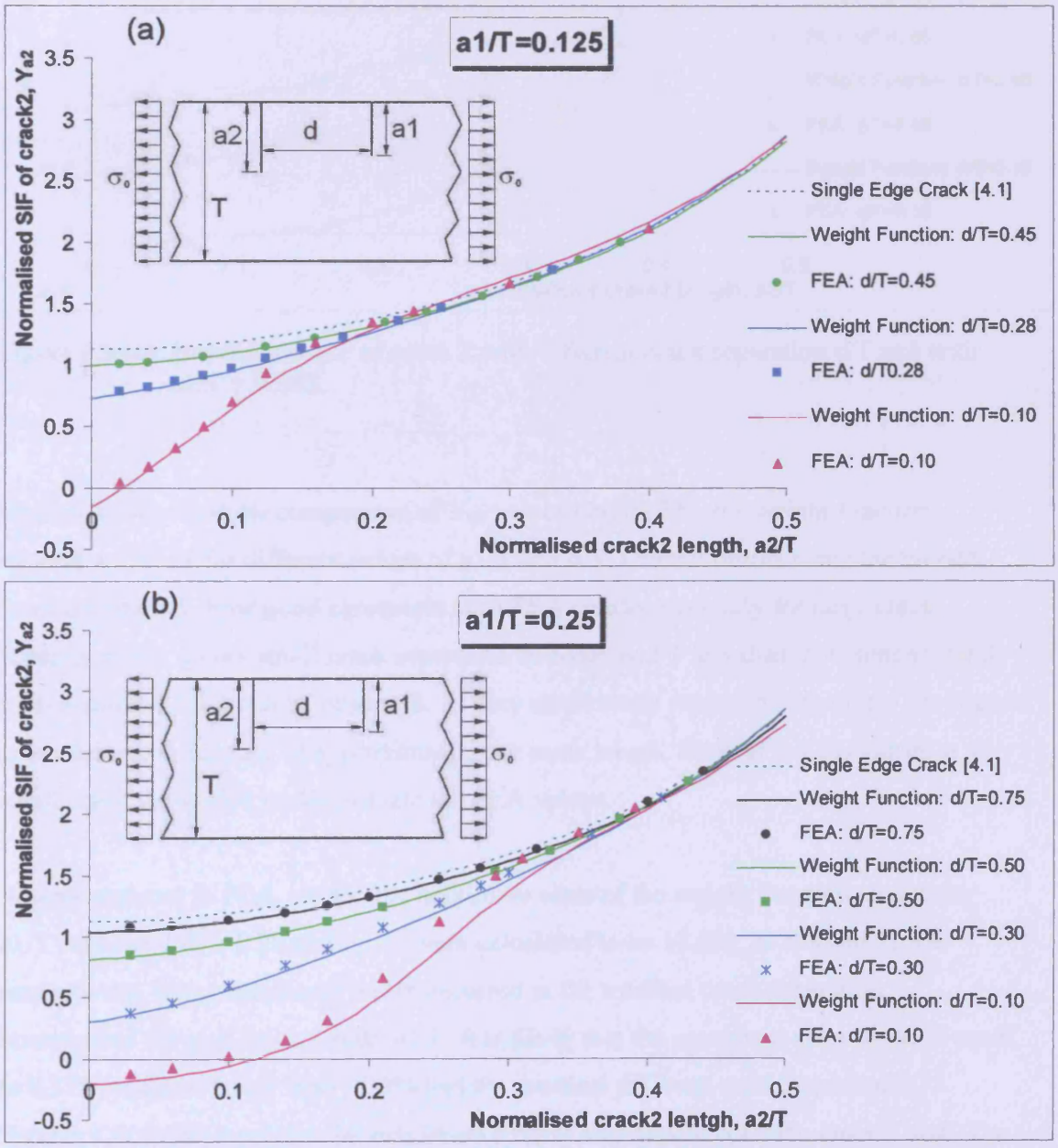

Figure 4.9 (a)-(b): Normalised SIF of crack 2 with different crack separation d/T and with a1/T = 0.125 and 0.25.

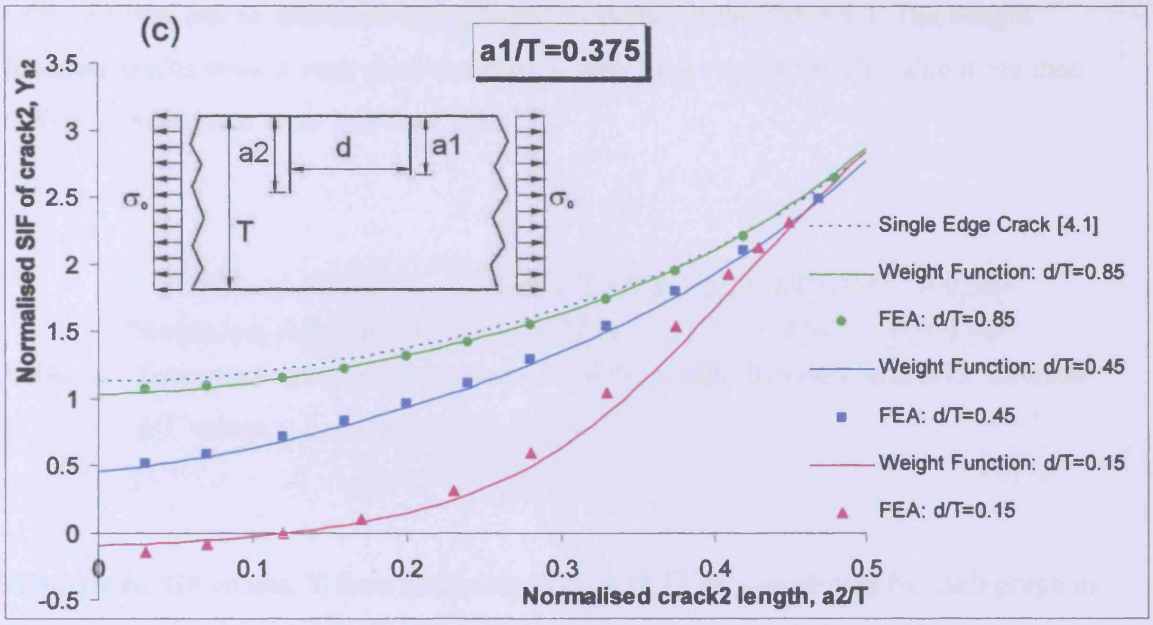

Figure 4.9 (c): Normalised SIF of crack 2 with different crack separation d/T and with a1/T = 0.375.

Figures 4.9(a)-(c) show comparison of Y_{a2} values obtained by the weight function method and FEA for different values of a1/T and d/T. Overall results using the weight function method show good agreement with FEA results especially for large crack separation. For a very small crack separation or roughly d/T less than 0.30 similar trends as in Section 4.1.1.2 can be observed. At very small crack separation the errors are largest when the two cracks are of approximately the same length. Most of the Y_{a2} values at very small crack separation underestimate the FEA values.

When compared to FEA results, the maximum error of the weight function results for a1/T equal to 0.125, 0.25 and 0.375 were calculated to be 10.6%, 20.4% and 11.3% respectively. These maximum errors occurred at the smallest crack separation investigated for each crack length a1/T. It is likely that the maximum error for a1/T equal to 0.375 would be larger than 11.3% had the smallest d/T been used instead of 0.15. Figures 4.9(a)-(b) show that the maximum error is also dependent upon crack 1 size. The error increases as a1/T increases. Based on results shown in Figure 4.9, the maximum

relative errors can be estimated and grouped as shown in the Table 4.3. The weight function results show a very good correlation with FEA results for d/T value more than 0.50 with maximum error less than 1%.

Group of d/T	0.1< d/T ≤0.3	0.3< d/T ≤ 0.5	> 0.50
Maximum relative error	< 21 %	< 5 %	< 1 %

Table 4.3: Estimated maximum relative error of the weight function results for different d/T values.

Normalised SIF values, Y for a single edge crack [4.1] are also plotted for each graph in Figure 4.9 as a comparison with Y_{a2} values. Values of Y_{a2} are similar to Y for cases where there is little interaction between cracks. These correspond to situations where the potential crack plane stress distributions $\sigma 2(x)/\sigma_0$ are more uniform and approximately equal to 1.0. For cases where there is no interaction between cracks both FEA and weight function results would be equal to the single crack results. For situations where an interaction between cracks exists, the results would be expected to be lower than the single crack solution due to a shielding effect. As crack 2 increases in length the shielding due to crack 1 is reduced, thereby reducing the interaction, and the SIF solution would be expected to converge upon the single crack solution. However Figure 4.9(a) shows that for d/T equal to 0.10 and a2/T values greater than approximately 0.25, Y_{a2} solutions obtained using the weight function approach are slightly greater than Y for a single edge crack. Figure 4.9(b) shows Y_{a2} solutions obtained using the weight function approach for d/T equal to 0.10 and 0.75 diverge slightly from the single edge crack solution as a2/T increases beyond 0.41.

Despite some discrepancy between weight function and FEA results, it can be observed that general results of weight function method predictions are very good. It demonstrates that, the methodology that uses non-uniform stress distribution of the potential crack

plane in conjunction with a weight function is a valid method for the calculation of SIFs for interacting cracks.

4.3 Discussion

This chapter has sought to develop a methodology to allow determination of SIFs for interacting cracks. Few published solutions exist relevant to this situation. A methodology utilising an edge crack weight function and a complex potential crack plane stress distribution due to the presence of additional cracks was suggested as a possible tool for the analysis of problems of this type. The work contained in this chapter has firstly validated the general approach by application to two edge cracks in a finite strip under remote tension. Subsequently a multivariate study was undertaken to assess more rigorously the performance of the methodology for a variety of geometric parameters. This was achieved by the development of a general equation for stress distributions in the vicinity of a crack. This general equation allows the calculation of SIFs for arbitrary crack lengths and separation when used in conjunction with a single edge crack weight function. Calculation of SIFs using this novel approach provides engineers with a methodology that is more readily implemented than successive FE modelling of multiple cracks. FE modelling of two cracks was carried out in this study to develop SIFs against which the performance of the weight function method could be assessed. Comparisons of results achieved by these two methods were presented for a wide range of crack sizes and separations.

Comparisons between FE and weight function results showed, in all cases a high degree of correlation. The general trends expected and observed in the FE results were present in the weight function results. For some cases especially in situations where cracks are close together the interaction effect has a considerable influence on SIFs with respect to single edge crack solutions. This is primarily due to a shielding effect that prevents the full remote stress being applied to each crack. Resulting SIFs are therefore reduced with respect to single edge crack which are exposed to the full remote stress.

The weight function methodology has been shown to be capable of modelling the shielding effect over the range of geometric parameters investigated and has provided SIF solutions that compare well to the FEA results. With reference to Figures 4.9(a)-(c) it can be seen that absolute errors between weight function and FEA results are generally small compared to the large influence of the shielding effect indicated by the difference between single and multiple crack solutions. Errors between weight function and FEA results as described in the preceding section and were noted to be greatest for geometries in which crack separation is small and where cracks are approximately of equal length.

There are several possible reasons for the disparity between FEA results and weight function predictions for very low values of d/T and roughly equal crack lengths. Generally FEA results are not exact due to numerical processes involve in calculation of SIFs for the two cracks. Errors in FEA results are largely dependent on the density of the mesh used for the analysis. However the errors due to mesh density are suspected to be very small since a close correlation between results obtained from models used in this study and results achieved by Jiang *et al.* [4.7] was described in Chapter 2. Furthermore, FE modelling practises used in this study are consistent with those employed by Teh *et al.* [4.8] who conducted extensive validation of SIFs for a single edge crack by comparison with published solutions.

Another possible source of error in the weight function solution is due to errors introduced during the curve fitting of the stress distributions. The value of R-squared obtained to curve fit the stress distribution for smaller d/T values are lower than those obtained for larger values. This means that the curve fitted expression have less correlation with FEA data points as the d/T value is reduced. Table 4.4 summarises values of R-squared obtained for each d/T value. The R-squared values approach unity for d/T values greater than 0.31 but for d/T values less than 0.31, the R-squared value is reduced. Additionally, since the curve fitting process was conducted by considering each geometric parameter individually, overall prediction of stress is degraded as the number of dependent geometric parameters is increased. Although R-squared values for each individual curve fitting process were generally close to unity, when resulting equations

are compounded errors present are increased. Errors present in the stress distribution will directly influence the quality of SIFs obtained when integrated with the weight function over the crack length.

d/T	R-squared (R^2)
0.08	0.98995
0.12	0.99695
0.16	0.99868
0.2	0.99926
0.23	0.99965
0.31	0.99999
0.39	0.99999
0.51	0.99999
0.62	0.99999
0.7	0.99999
0.82	0.99999
0.89	0.99999
1.01	0.99999

Table 4.4: R-squared values obtained during curve fitting $\sigma 2(x)/\sigma_0$ for a1/T = 0.25 with various d/T values.

Assuming that the stress distribution is accurate, errors could be introduced due to the influence of high stress gradients used in the SIF weight function calculation. Weight functions are generally calculated as an approximation to the exact weight function. Even though the accuracy of weight function calculation has been improved by using an MRS approach the accuracy is still dependent upon the number and quality of reference solutions. If the reference solutions are exact, weight function accuracy is improved with increasing number of references solutions. In most cases use of two reference solutions, typically tension and bending as used in this study, is judged satisfactory for usage with smoothly varying stress distributions. It is known however that usage of this weight function with more variable stress distribution containing high stress gradients can introduce errors into calculated SIF values.

In this study high stress gradients occur where cracks are approximately of the same length. This could possibly explain why the maximum error can be observed to occur approximately for cracks of the same length. Consider Figures 2.16 (a)-(i) in Chapter 2 which show stress distributions for different a1/T and d/T values. The figures indicate the strong dependence of stress gradient on d/T. The gradient of $\sigma 2(x)/\sigma_0$ is high for smaller d/T values which are the situations where maximum errors in weight function SIF solutions have been observed. The magnitude of stress gradient will be increased for larger a1/T values because the range of $\sigma 2(x)/\sigma_0$ is larger compared to smaller a1/T. Figure 4.10 shows the increased stress gradients obtained for higher a1/T values. Errors in weight function SIF predictions in Figures 4.9(a)-(c) are increased with increasing a1/T. Therefore geometries for which weight function solutions display highest errors correspond to those having highest stress gradients.

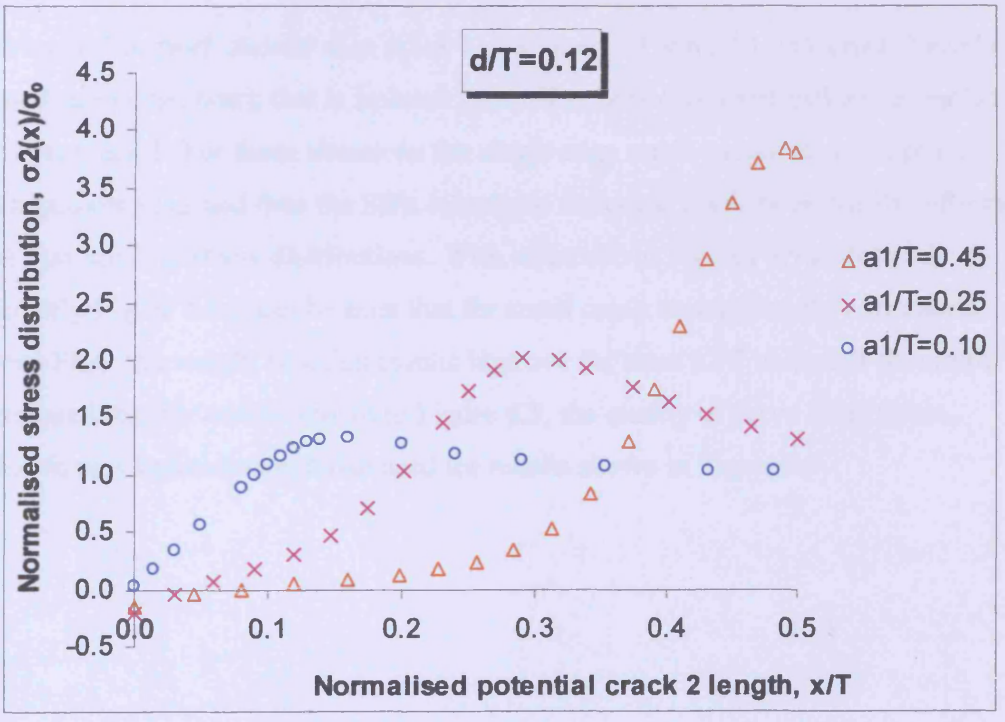

Figure 4.10: Stress gradient comparison for d/T=0.12 with a1/T = 0.10, 0.25 and 0.45.

As discussed in Section 4.1 the weight function equation (Eqn.4.2) is formulated using a weight function for a single edge crack used in conjunction with a non-uniform stress distribution in order to calculate SIFs for two edge cracks. The weight function is uniquely a property of crack and component geometry. A single edge crack weight function does not incorporate the geometric influence of an additional crack. This additional geometric influence will affect the SIFs of two edge cracks for situations where the crack separation is small. When the crack separation is large the crack geometry is governed by an individual edge crack weight function but at small crack separations the crack geometry is governed by a combination of two edge cracks. Since the weight function is formulated using a single edge crack weight function errors could be introduced at small crack separations. However, at small separations the single edge crack weight function is thought to provide a good approximation for cases where crack 2 is much shorter or much longer than crack 1. Figures 4.11(a) and (b) shows these two cases where crack 2 is relatively shorter and longer than crack 1.

When crack 2 is much shorter than crack 1 as shown in Figure 4.11(a), crack 2 can be assumed as an edge crack that is isolated from all remote geometric influences including the longer crack 1. For these situations the single edge crack weight function provides a good approximation and thus the SIFs calculated for crack 2 will be primarily influenced by the non-uniform stress distributions. With reference to Figures 4.9(a)-(c) and particularly Figure 4.5 it can be seen that for small crack separations the correlation between FEA and weight function results improve for short a2/T values. It should be remembered that for results shown in Figure 4.5, the quality of curve fitted stress distributions is superior than those used for results shown in Figure 4.9.

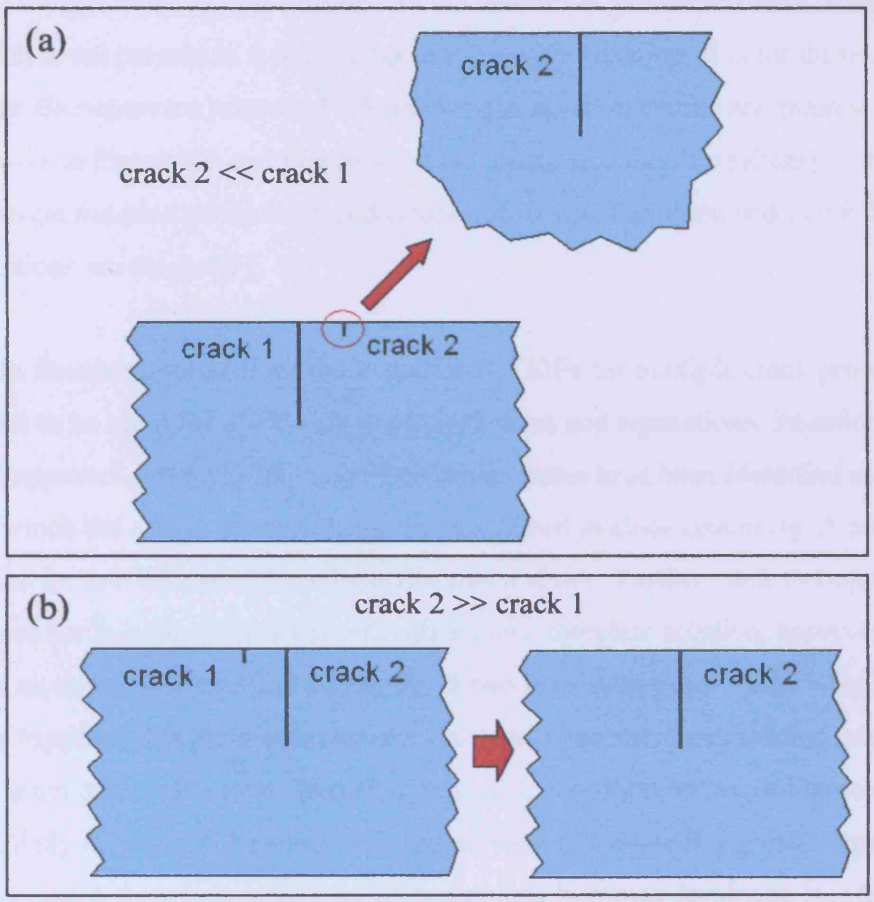

Figure 4.11: Two different cases for small crack separation where crack 2 is much (a) shorter than crack 1, and (b) longer than crack 1.

Considering Figure 4.11(b) in which crack 1, although very close to crack 2, is much smaller than crack 2. For this situation the additional geometric influence on crack 2 is small due to the small size of crack 1 and hence the single edge crack weight function provides a good approximation. Weight function results would therefore be expected to improve for this situation. As shown in Figure 4.9 and Figure 4.5, at small d/T values weight function results agree well with FEA results for large a2/T values.

The two conditions shown in Figure 4.11 can be considered as two extreme cases. For other geometric arrangements, where the cracks are close and are both of significant

length, the weight function is influenced by the additional geometric effect of the other crack which is not present in a single edge crack weight function. It is for these cases that the greatest discrepancies between FEA and weight function results are greatest. From results shown in Figure 4.9 and Figure 4.5 it is thought that this is a primary source of error in weight function predictions and errors due to stress gradient and curve fitting approximations are secondary.

The weight function approach for the evaluation of SIFs for multiple crack problems has been shown to be valid for a wide range of crack sizes and separations. Situations for which the approach gives slightly unconservative results have been identified as being those for which the cracks are both long and positioned in close proximity. A number of possibilities for this limitation have been discussed above. Further work to improve performance for this situation would provide a more complete solution, however it represents an unrealistic practical condition. If two very short edge cracks were to initiate very close together, it is inevitable that one crack will become dominant and continue to grow while the other will arrest. Therefore the crack condition shown in Figure 4.12a is highly unlikely to occur. If however, two cracks were to initiate at a greater separation the two cracks would grow to a greater length before one becomes dominant. It is this situation shown in Figure 4.12b that has the greater practical application. The weight function approach has been shown to incorporate interaction effects successfully for cracks at greater separations. The approach described permits accurate SIFs to be calculated allowing crack growth rates to be determined.

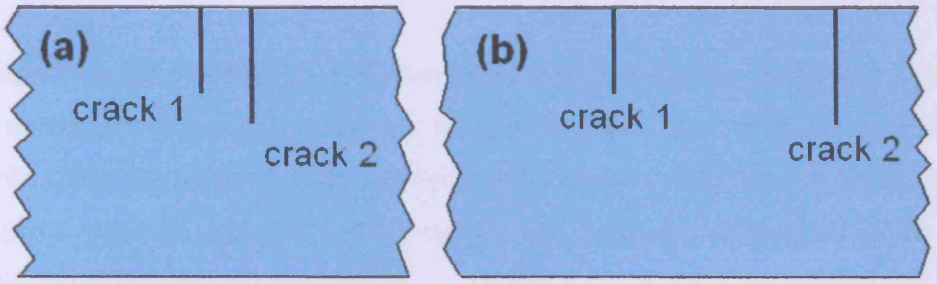

Figure 4.12: Two cracks of significant length with (a) small separation, and (b) large separation.

4.4 Conclusions

The non-uniform stress distributions due to the presence of an additional edge crack in a finite body under uniform tension can be used to establish the crack interaction in a general form. With this crack interaction the traditional weight function method can be applied to predict the SIFs of two edge cracks in a finite body under uniform tension. The weight function method has been proven to give reliable solutions for a wide range of geometric parameters.

Generally the accuracy of the modified weight function method is very good compared to FEA results. For small crack separations generally for d/T, less than 0.30, small disparities between weight function calculations and FEA results can be observed especially where cracks are of the same length. Most likely sources of error are due to usage of a single crack weight function and high stress gradients used to calculate SIFs. Errors were observed to be small for realistic crack situations. The procedure therefore provides a valid method for the calculation of SIFs of high accuracy for problems concerning multiple cracks without the need of extensive finite elements computations.

A general equation for the stress distribution in the potential plane of a crack due to the presence of an existing crack was produced using a multivariate study. This equation allows new SIF solutions for two cracks in a finite strip under tension to be rapidly generated with little computational effort.

Although the work contained in this chapter is based on two edge cracks in a finite body under uniform tension, the results prove that the weight function method can be used to determine SIFs for multiple cracks provided that the stress distribution at the potential crack plane is known. This will further improve the versatility of weight function methods beyond single crack problems.

4.5 References

4.1 Brown, W.F. and Srawley, J.E., Plane strain crack toughness testing of high strength metallic materials. ASTM STP 410, 1966.

4.2 Jiang, Z.D., Zeghloul, A., Bezine, G. and Petit, J., Stress intensity factors of parallel cracks in a finite width sheet. Engineering Fracture Mechanics, 1990, 35, pp.1073-1079.

4.3 Chen, Y.Z., Multiple crack problems for finite plate with arbitrary contour configuration. Engineering Fracture Mechanics, 1988, 31, pp.289-295.

4.4 Chen, W.H. and Chen, T.C., An efficient dual boundary element technique for a two-dimensional fracture problem with multiple cracks. International Journal For Numerical Methods In Engineering, 1995, 38, pp.1739-1756.

4.5 DIGITAL™ Visual Fortran, Profession Edition Version 5.0 for Windows NT and Windows 95, Digital Equipment Corporation (now COMPAQ), 1997.

4.6 CurveExpert, version 1.34. Daniel Hyams. 1995

4.7 Jiang, Z.D., Petit, J. and Bezine, G., An investigation of stress intensity factors for two unequal parallel cracks in a finite width plate. Engineering Fracture Mechanics, 1992, 42, pp. 129-138.

4.8 Teh, L.S., Love, A.J. and Brennan, F.P., Mode I stress intensity factors for edge cracks emanating from 2-D U-notches using composition of SIF weight functions. International Journal of Fatigue, 2006, 28, pp. 355-365.

Chapter 5: Conclusions and Recommendations for Future Work

5.0 Introduction

The main objective of the thesis is to study the crack behaviour of interacting cracks and to develop a weight function method as a means to determine SIFs of these interacting cracks. The preceding chapters of this thesis report the findings of the experimental results of fatigue tension loading for a specimen containing two edge cracks. A new weight function based method to predict the SIFs of two edge cracks in a strip under uniform tension was also detailed. This chapter draws the main conclusions from the work undertaken to highlight the significant achievements. The chapter also proposes work in order to further explore the wide range of multiple cracks that can be modelled using the new SIF weight function method.

5.1 Fatigue Testing for Multiple Cracks

Fatigue tests were conducted to study the interaction effect between two edge cracks. The material used for the experiment was a Mild Steel which has minimum yield strength of 275MPa. A total of seven specimens with different geometries were completed for the tests. Specimens containing two edge cracks were prepared successfully using three-point bending and a weld strapping technique. The cracks grown using three-point bending were not straight causing a kinked cracks. Using fatigue tension loading to precrack would improve the results of the early fatigue crack growth data.

During the fatigue tests, the two crack lengths were measured using two travelling microscopes. The crack length was measured until approximately half of the plate width beyond which severe crack branches were observed.

Results of Y_{a2} show a U-shape at the early crack growth. Most likely the U-shape occurred due to the crack 2 path during fatigue precracking and fatigue testing. The start of a kinked crack during fatigue testing reduces the values of Y_{a2} while the boundary effect of a finite plate forces the Y_{a2} values to increase causing a U-shape. Another possibility is due to crack 1 arrest that allows the crack 2 growth rate to increase. The combinations of the crack 2 path and the crack 1 arrest also could possibly cause the U-shape.

The experimental results concluded that the SIFs of interacting cracks for real engineering applications are much lower than the FEA results. It is almost impossible to have very straight parallel edge cracks. The interaction of kinked or oblique edge cracks produces lower SIFs than the equivalent theoretical results.

The experimental results could be further improved by precracking using fatigue tension loading and by using two sets of pin and clevis assemblies in order to allow rotation in all directions. Because of the limitation on a specimen dimensions and the test machine capability, the specimen was precracked using bending loading. During the fatigue loading the specimen was assembled with one set of pin and clevis which allowed rotation in only one direction. This possibly introduced a bending moment to the specimen and affected the applied axial load. However, using two sets of pin and clevis for a specimen with 450mm length was unachievable as there was limited gap between the two test machine grips.

5.2 Development of Weight Function Method for Multiple Cracks

A novel weight function approach to determine SIFs of multiple cracks was successfully developed by including the interaction effect between cracks into the weight function equation. The interaction effect was established into a general equation by analysing the non-uniform stress distribution due to the presence of a single crack, along the crack

plane of a potential second crack. This general equation allows the calculation of SIFs for arbitrary crack lengths and separation when used in conjunction with the traditional weight function approach. Calculation of SIFs using this novel approach provides engineers with a methodology that is more readily implemented than successive FE modelling of multiple cracks.

Generally the SIF results of multiple cracks obtained using the weight function approach show very good correlation with FEA results. The general trends expected and observed in the FEA results were present in the weight function results. For small crack separations generally for d/T, less than 0.30, small disparities between weight function calculations and FEA results can be observed especially where cracks are of the same length. Most likely sources of error are due to usage of a single crack weight function and high stress gradients used to calculate SIFs.

The weight function approach for multiple cracks is based on a weight function for a single edge crack used in conjunction with a non-uniform stress distribution. The weight function is uniquely a property of crack and component geometry. A single edge crack weight function does not incorporate the geometric influence of an additional crack. This additional geometric influence will affect the SIFs of two edge cracks for situation where the crack separation is small. High stress gradients also could influence the SIF weight function calculation. The high stress gradients occur where cracks are approximately of the same length which possibly explains why the maximum error can be observed to occur at this situation. The use of the weight function with a more variable stress distribution containing high stress gradients can introduce errors into calculated SIF values.

Although the novel weight function approach to determine SIFs of multiple cracks was developed based on two edge cracks in a finite body under uniform tension, the results prove that the weight function method can be used to determine SIFs for multiple cracks provided that the stress distribution at the potential crack plane is known. This permits

more complex or two-dimensional multiple crack geometry problems to be solved such as a structure containing multiple surface cracks.

5.3 Conclusions

Based on the research work, the main conclusions can be summarised as below:

- Experimental work on multiple cracks is difficult due to the fact that interacting cracks tend not to grow in a straight path and within this programme of work the necessity to precrack under bending.

- Both theory and experimental results show that cracks in close proximity to each other interact to varying degrees depending on relative crack lengths, crack separation and plate width.

- The interaction of kinked or oblique edge cracks produces lower SIFs than the equivalent theoretical results.

- Numerical results for two edge cracks under tension appear conservative since most SIF values obtained experimentally were lower than the numerical equivalent models.

- The study shows that wherever more than one crack exists, the longer crack will always dominate causing the smaller cracks to arrest due to the stress 'shielding effect'.

- The unique feature of the non-uniform stress distribution along the uncracked plane with the presence of another crack was used as a basis to model the shielding effect using a weight function approach.

- A novel weight function approach modelling the shielding effect on the through wall stress distribution in the crack plane gave good results compared to finite element analysis for cracks where the ratio of crack separation to strip width, d/T is greater than 0.30.

- This weight function approach allows the rapid calculation of crack interaction effects knowing the stress distribution in the uncracked plane.

5.4 Future Development Work of Weight Function Method

It is known that an immense advantage of the weight function is it can be isolated, combined and composed to allow evaluation of SIFs for real engineering application. For example Brennan and Teh [5.1] used a composition model as shown in Figure 5.1 to determine SIF of a single crack emanating from a two-dimensional semicircular notch in a finite body. With the capability of the weight function method to calculate the SIFs of multiple cracks, more complex geometries could be determined using this composition method.

Consider two cracks with differing length emanating from two semicircular notches in a finite body as shown in Figure 5.2(a). With the interaction effect incorporated into the weight function equation, the SIFs for the two cracks can be determined using a similar composition model to the single crack. Figure 5.2(b) illustrates a composition model that could be used to determine the SIF of the longer crack. If this composition model proves successful it will be great advantage as very complex multiple crack problems would be relatively easily solved.

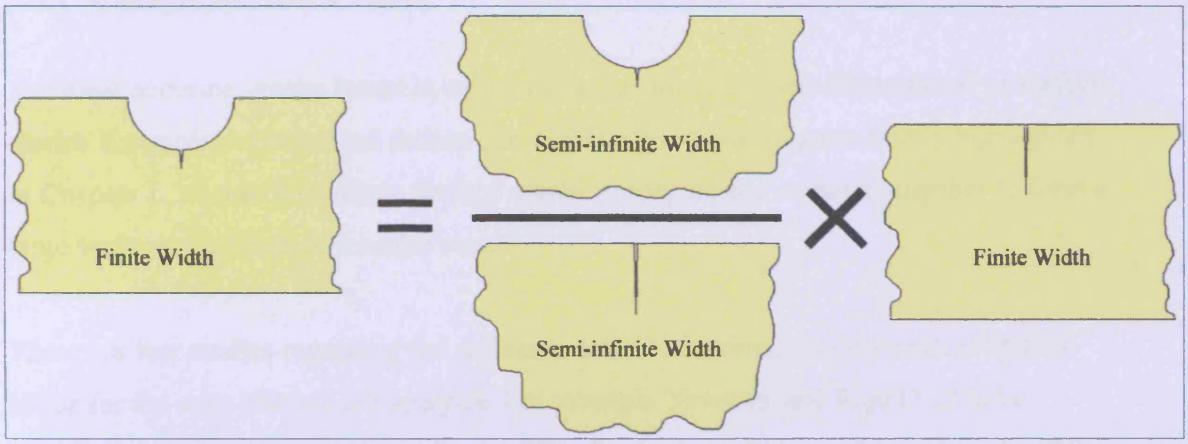

Figure 5.1: Composition model used in Ref.[5.1] to determine SIF for an edge crack emanating from a two-dimensional semicircular notch in a finite body.

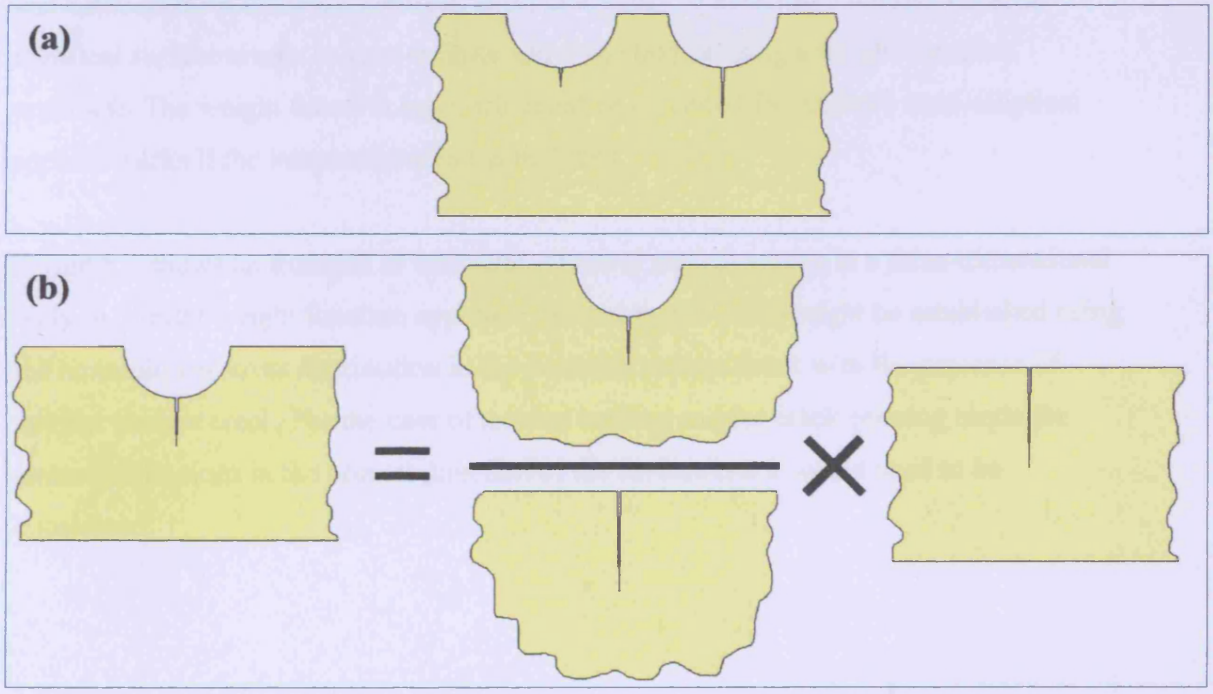

Figure 5.2: (a) Two cracks with differing length emanating from two semicircular notches, (b) Equivalent composition model that could be used to determine the SIF of longer crack.

5.4.1 Multiple Surface Cracks

The most common cracks found in structural components are two-dimensional or surface cracks. Examples of structural failure due to this type of cracking are briefly highlighted in Chapter 1. Normally multiple surface cracks propagate and coalesce together to form a large surface crack before fracture occurs.

There are few studies regarding the surface crack which commonly use semi elliptical shape for the simplicity of the analysis. For example Newman and Raju [5.2] have established an empirical equation for the SIF of a single surface crack based on the SIFs obtained from three-dimensional, finite element analysis of semi elliptical surface cracks in finite elastic plates subjected to tension or bending loads. Soboyejo *et al.* [5.3] studied the interaction and coalescence of two surface cracks under bending using experiment and finite element analysis. Orynyak *et al.* [5.4]and[5.5] establish solutions for semi-elliptical surface cracks in semi-infinite and finite bodies using a weight function approach. The weight function approach could be extended for multiple semi-elliptical surface cracks if the interaction effect is included.

Figure 5.2 shows an example of two semi-elliptical surface cracks in a three-dimensional body. A similar weight function approach as used in this thesis might be established using the non-uniform stress distribution in the potential surface crack with the presence of another surface crack. For the case of tension loading and for crack opening mode the stress distributions in the normal direction of the surface crack would need to be considered.

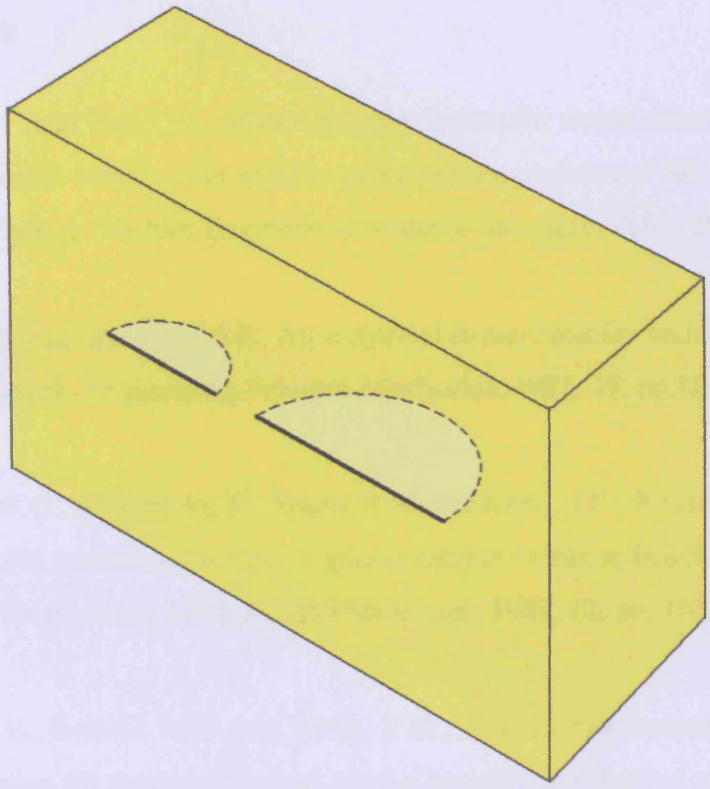

Figure 5.3: Two different sizes of surface cracks in three-dimensional body.

5.5 References

5.1 Brennan, F.P. and Teh, L.S., Stress intensity factors for cracks emanating from two-dimensional semicircular notches using the composition of SIF weight functions. Fatigue Fracture Engineering Material Structure, 2005, 28, pp.423-435.

5.2 Newman, J.C.Jnr. and Raju, I.S., An empirical stress-intensity factor equation for the surface crack. Engineering Fracture Mechanics, 1981, 15, pp.185-192.

5.3 Soboyejo, W.O., Kishimoto, K., Smith, R.A. and Knott, J.F., A study of the interaction and coalescence of two coplanar fatigue cracks in bending. Fatigue and Fracture of Engineering Materials and Structures, 1989, 12, pp. 167-174.

5.4 Orynyak, I.V., Borodii, M.V. and Torop, V.M., Approximate construction of a weight function for quarter-elliptical, semi-elliptical and elliptical cracks subjected to normal stresses. Engineering Fracture Mechanics, 1994, 49, pp.143-151.

5.5 Orynyak, I.V. and Borodii, M.V., Point weight function method application for semi-elliptical mode I cracks. International Journal of Fracture, 1995, 70, pp.117-124.

Appendix A: Fatigue Test Stress Calculations

Shearing/tearing stress.

Shearing stress is calculated as below:

Tensile Load, P = 50kN

Thickness, t = 0.01m

Length from hole centre as shown in Figure A.1, b = 0.05m

Area, $A = b \times t$

$= 5 \times 10^{-4}\ m^2$

Stress, $\sigma = P/A$

$= 100MPa$

Shear stress, $\tau = \sigma/2$

$= 50MPa$

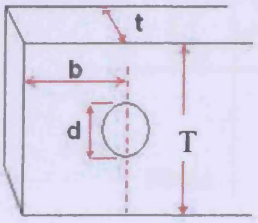

Figure A.1: Notation used for stress calculation.

Bearing Stress.

Bearing stress is calculated as below:

Tensile Load, P = 50kN

Diameter of hole, d = 0.03m

Thickness, t = 0.01m

Area, $A = d \times t$

$= 3 \times 10^{-4}\ m^2$

Bearing Stress, $\sigma = P/A$

$= 167MPa$

Stress on ligament width.

Stress on ligament width of the plate after drilling a hole is calculated as below:

Tensile Load, P = 50kN

Thickness, t = 0.01m

Diameter of hole, d = 0.03m

Plate width, T = 0.1m

Area, A = (T-d) x t

$= 7 \times 10^{-4}\ m^2$

Stress Concentration Factor for circular shape, $K_t = 3.0$

Stress on ligament width, $\sigma = K_t P/A$

$= 214MPa$

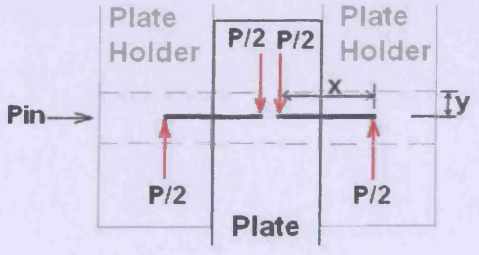

Figure A.2: Reaction forces acting on the pin that hold the plate.

Bending Stress.

Bending stress is calculated as below:

Tensile Load, P = 50kN

Reaction forces, F = P/2

= 25kN

Distance between two reaction forces as shown in Figure A.2, x = 0.016m

Moment, M = Fx

= 400Nm

Pin diameter, d = 0.029m

Second moment, $I = \pi d^4/64$

$= 3.47 \times 10^{-8} m^4$

Radius of pin, $y = 0.0145m$

Bending stress, $\sigma = My/ I$

$= 167MPa$

Appendix B.

Detail coefficients a,b,c and d for Eqn.(4.21).

$$a = A_1 + B_1\left(\frac{d}{T}\right) + C_1\left(\frac{d}{T}\right)^2 + D_1\left(\frac{d}{T}\right)^3 + E_1\left(\frac{d}{T}\right)^4 + F_1\left(\frac{d}{T}\right)^5 + G_1\left(\frac{d}{T}\right)^6 \quad \text{(B.1)}$$

$$A_1 = 3.08 - 1.41\times10^{2}\left(\frac{al}{T}\right) + 1.78\times10^{3}\left(\frac{al}{T}\right)^2 - 1.02\times10^{4}\left(\frac{al}{T}\right)^3 + 2.97\times10^{4}\left(\frac{al}{T}\right)^4 - 4.29\times10^{4}\left(\frac{al}{T}\right)^5 + 2.47\times10^{4}\left(\frac{al}{T}\right)^6$$

$$B_1 = -25.5 + 1.98\times10^{3}\left(\frac{al}{T}\right) - 3.04\times10^{4}\left(\frac{al}{T}\right)^2 + 1.93\times10^{5}\left(\frac{al}{T}\right)^3 - 6.05\times10^{5}\left(\frac{al}{T}\right)^4 + 9.28\times10^{5}\left(\frac{al}{T}\right)^5 - 5.60\times10^{5}\left(\frac{al}{T}\right)^6$$

$$C_1 = 112 - 1.02\times10^{4}\left(\frac{al}{T}\right) + 1.75\times10^{5}\left(\frac{al}{T}\right)^2 - 1.19\times10^{6}\left(\frac{al}{T}\right)^3 + 3.88\times10^{6}\left(\frac{al}{T}\right)^4 - 6.14\times10^{6}\left(\frac{al}{T}\right)^5 + 3.80\times10^{6}\left(\frac{al}{T}\right)^6$$

$$D_1 = -240 + 2.57\times10^{4}\left(\frac{al}{T}\right) - 4.78\times10^{5}\left(\frac{al}{T}\right)^2 + 3.40\times10^{6}\left(\frac{al}{T}\right)^3 - 1.14\times10^{7}\left(\frac{al}{T}\right)^4 + 1.84\times10^{7}\left(\frac{al}{T}\right)^5 - 1.16\times10^{7}\left(\frac{al}{T}\right)^6 \quad \text{(B.2)}$$

$$E_1 = 269 - 3.43\times10^{4}\left(\frac{al}{T}\right) + 6.77\times10^{5}\left(\frac{al}{T}\right)^2 - 4.97\times10^{6}\left(\frac{al}{T}\right)^3 + 1.71\times10^{7}\left(\frac{al}{T}\right)^4 - 2.79\times10^{7}\left(\frac{al}{T}\right)^5 + 1.77\times10^{7}\left(\frac{al}{T}\right)^6$$

$$F_1 = -150 + 2.32\times10^{4}\left(\frac{al}{T}\right) - 4.80\times10^{5}\left(\frac{al}{T}\right)^2 + 3.61\times10^{6}\left(\frac{al}{T}\right)^3 - 1.26\times10^{7}\left(\frac{al}{T}\right)^4 + 2.08\times10^{7}\left(\frac{al}{T}\right)^5 - 1.33\times10^{7}\left(\frac{al}{T}\right)^6$$

$$G_1 = 33.0 - 6.25\times10^{3}\left(\frac{al}{T}\right) + 1.34\times10^{5}\left(\frac{al}{T}\right)^2 - 1.03\times10^{6}\left(\frac{al}{T}\right)^3 + 3.63\times10^{6}\left(\frac{al}{T}\right)^4 - 6.07\times10^{6}\left(\frac{al}{T}\right)^5 + 3.90\times10^{6}\left(\frac{al}{T}\right)^6$$

$$b = A_2 + B_2\left(\frac{d}{T}\right) + C_2\left(\frac{d}{T}\right)^2 + D_2\left(\frac{d}{T}\right)^3 + E_2\left(\frac{d}{T}\right)^4 + F_2\left(\frac{d}{T}\right)^5 + G_2\left(\frac{d}{T}\right)^6 \quad \text{(B.3)}$$

$$A_2 = 180 - 3.04\times10^{3}\left(\frac{al}{T}\right) + 1.99\times10^{4}\left(\frac{al}{T}\right)^2 - 6.42\times10^{4}\left(\frac{al}{T}\right)^3 + 1.06\times10^{5}\left(\frac{al}{T}\right)^4 - 7.70\times10^{4}\left(\frac{al}{T}\right)^5 + 1.30\times10^{4}\left(\frac{al}{T}\right)^6$$

$$B_2 = -3.02\times10^{3} + 6.72\times10^{4}\left(\frac{al}{T}\right) - 5.53\times10^{5}\left(\frac{al}{T}\right)^2 + 2.28\times10^{6}\left(\frac{al}{T}\right)^3 - 5.07\times10^{6}\left(\frac{al}{T}\right)^4 + 5.81\times10^{6}\left(\frac{al}{T}\right)^5 - 2.68\times10^{6}\left(\frac{al}{T}\right)^6$$

$$C_2 = 1.85\times10^{4} - 4.66\times10^{5}\left(\frac{al}{T}\right) + 4.21\times10^{6}\left(\frac{al}{T}\right)^2 - 1.88\times10^{7}\left(\frac{al}{T}\right)^3 + 4.52\times10^{7}\left(\frac{al}{T}\right)^4 - 5.62\times10^{7}\left(\frac{al}{T}\right)^5 + 2.82\times10^{7}\left(\frac{al}{T}\right)^6$$

$$D_2 = -5.44\times10^{4} + 1.47\times10^{6}\left(\frac{al}{T}\right) - 1.40\times10^{7}\left(\frac{al}{T}\right)^2 + 6.55\times10^{7}\left(\frac{al}{T}\right)^3 - 1.64\times10^{8}\left(\frac{al}{T}\right)^4 + 2.12\times10^{8}\left(\frac{al}{T}\right)^5 - 1.11\times10^{8}\left(\frac{al}{T}\right)^6 \quad \text{(B.4)}$$

$$E_2 = 8.22\times10^{4} - 2.32\times10^{6}\left(\frac{al}{T}\right) + 2.29\times10^{7}\left(\frac{al}{T}\right)^2 - 1.11\times10^{8}\left(\frac{al}{T}\right)^3 + 2.86\times10^{8}\left(\frac{al}{T}\right)^4 - 3.80\times10^{8}\left(\frac{al}{T}\right)^5 + 2.04\times10^{8}\left(\frac{al}{T}\right)^6$$

$$F_2 = -6.16\times10^{4} + 1.79\times10^{6}\left(\frac{al}{T}\right) - 1.81\times10^{7}\left(\frac{al}{T}\right)^2 + 8.98\times10^{7}\left(\frac{al}{T}\right)^3 - 2.37\times10^{8}\left(\frac{al}{T}\right)^4 + 3.21\times10^{8}\left(\frac{al}{T}\right)^5 - 1.75\times10^{8}\left(\frac{al}{T}\right)^6$$

$$G_2 = 1.81\times10^{4} - 5.37\times10^{5}\left(\frac{al}{T}\right) + 5.56\times10^{6}\left(\frac{al}{T}\right)^2 - 2.80\times10^{7}\left(\frac{al}{T}\right)^3 + 7.50\times10^{7}\left(\frac{al}{T}\right)^4 - 1.03\times10^{5}\left(\frac{al}{T}\right)^5 + 5.70\times10^{7}\left(\frac{al}{T}\right)^6$$

$$c = A_3 + B_3\left(\frac{d}{T}\right) + C_3\left(\frac{d}{T}\right)^2 + D_3\left(\frac{d}{T}\right)^3 + E_3\left(\frac{d}{T}\right)^4 + F_3\left(\frac{d}{T}\right)^5 + G_3\left(\frac{d}{T}\right)^6 \quad \text{(B.5)}$$

$$A_3 = 1.91\times10^2 - 4.72\times10^3\left(\frac{al}{T}\right) + 4.22\times10^4\left(\frac{al}{T}\right)^2 - 1.90\times10^5\left(\frac{al}{T}\right)^3 + 4.64\times10^5\left(\frac{al}{T}\right)^4 - 5.87\times10^5\left(\frac{al}{T}\right)^5 + 3.02\times10^5\left(\frac{al}{T}\right)^6$$

$$B_3 = -2.76\times10^3 + 7.65\times10^4\left(\frac{al}{T}\right) - 7.53\times10^5\left(\frac{al}{T}\right)^2 + 3.64\times10^6\left(\frac{al}{T}\right)^3 - 9.38\times10^6\left(\frac{al}{T}\right)^4 + 1.24\times10^7\left(\frac{al}{T}\right)^5 - 6.63\times10^6\left(\frac{al}{T}\right)^6$$

$$C_3 = 1.51\times10^4 - 4.44\times10^5\left(\frac{al}{T}\right) + 4.57\times10^6\left(\frac{al}{T}\right)^2 - 2.28\times10^7\left(\frac{al}{T}\right)^3 + 6.03\times10^7\left(\frac{al}{T}\right)^4 - 8.15\times10^7\left(\frac{al}{T}\right)^5 + 4.43\times10^7\left(\frac{al}{T}\right)^6$$

$$D_3 = -4.04\times10^4 + 1.23\times10^6\left(\frac{al}{T}\right) - 1.30\times10^7\left(\frac{al}{T}\right)^2 + 6.59\times10^7\left(\frac{al}{T}\right)^3 - 1.77\times10^8\left(\frac{al}{T}\right)^4 + 2.41\times10^8\left(\frac{al}{T}\right)^5 - 1.32\times10^8\left(\frac{al}{T}\right)^6 \quad \text{(B.6)}$$

$$E_3 = 5.69\times10^4 - 1.76\times10^6\left(\frac{al}{T}\right) + 1.89\times10^7\left(\frac{al}{T}\right)^2 - 9.69\times10^7\left(\frac{al}{T}\right)^3 + 2.62\times10^8\left(\frac{al}{T}\right)^4 - 3.61\times10^8\left(\frac{al}{T}\right)^5 + 1.99\times10^8\left(\frac{al}{T}\right)^6$$

$$F_3 = -4.02\times10^4 + 1.26\times10^6\left(\frac{al}{T}\right) - 1.36\times10^7\left(\frac{al}{T}\right)^2 + 7.05\times10^7\left(\frac{al}{T}\right)^3 - 1.92\times10^8\left(\frac{al}{T}\right)^4 + 2.65\times10^8\left(\frac{al}{T}\right)^5 - 1.47\times10^8\left(\frac{al}{T}\right)^6$$

$$G_3 = 1.12\times10^4 - 3.56\times10^5\left(\frac{al}{T}\right) + 3.87\times10^6\left(\frac{al}{T}\right)^2 - 2.02\times10^7\left(\frac{al}{T}\right)^3 + 5.51\times10^7\left(\frac{al}{T}\right)^4 - 7.65\times10^7\left(\frac{al}{T}\right)^5 + 4.25\times10^7\left(\frac{al}{T}\right)^6$$

$$d = A_4 + B_4\left(\frac{d}{T}\right) + C_4\left(\frac{d}{T}\right)^2 + D_4\left(\frac{d}{T}\right)^3 + E_4\left(\frac{d}{T}\right)^4 + F_4\left(\frac{d}{T}\right)^5 + G_4\left(\frac{d}{T}\right)^6 \quad \text{(B.7)}$$

$$A_4 = -2.17\times10^2 + 1.06\times10^4\left(\frac{al}{T}\right) - 1.35\times10^5\left(\frac{al}{T}\right)^2 + 7.88\times10^5\left(\frac{al}{T}\right)^3 - 2.37\times10^6\left(\frac{al}{T}\right)^4 + 3.57\times10^6\left(\frac{al}{T}\right)^5 - 2.14\times10^6\left(\frac{al}{T}\right)^6$$

$$B_4 = 2.97\times10^3 - 1.48\times10^5\left(\frac{al}{T}\right) + 1.99\times10^6\left(\frac{al}{T}\right)^2 - 1.20\times10^7\left(\frac{al}{T}\right)^3 + 3.71\times10^7\left(\frac{al}{T}\right)^4 - 5.69\times10^7\left(\frac{al}{T}\right)^5 + 3.45\times10^7\left(\frac{al}{T}\right)^6$$

$$C_4 = -1.54\times10^4 + 7.76\times10^5\left(\frac{al}{T}\right) - 1.08\times10^7\left(\frac{al}{T}\right)^2 + 6.67\times10^7\left(\frac{al}{T}\right)^3 - 2.09\times10^8\left(\frac{al}{T}\right)^4 + 3.24\times10^8\left(\frac{al}{T}\right)^5 - 1.98\times10^8\left(\frac{al}{T}\right)^6$$

$$D_4 = 3.93\times10^4 - 2.01\times10^6\left(\frac{al}{T}\right) + 2.84\times10^7\left(\frac{al}{T}\right)^2 - 1.79\times10^8\left(\frac{al}{T}\right)^3 + 5.66\times10^8\left(\frac{al}{T}\right)^4 - 8.86\times10^8\left(\frac{al}{T}\right)^5 + 5.45\times10^8\left(\frac{al}{T}\right)^6 \quad \text{(B.8)}$$

$$E_4 = -5.29\times10^4 + 2.73\times10^6\left(\frac{al}{T}\right) - 3.92\times10^7\left(\frac{al}{T}\right)^2 + 2.50\times10^8\left(\frac{al}{T}\right)^3 - 7.97\times10^8\left(\frac{al}{T}\right)^4 + 1.25\times10^9\left(\frac{al}{T}\right)^5 - 7.75\times10^8\left(\frac{al}{T}\right)^6$$

$$F_4 = 3.60\times10^4 - 1.88\times10^6\left(\frac{al}{T}\right) + 2.72\times10^7\left(\frac{al}{T}\right)^2 - 1.75\times10^8\left(\frac{al}{T}\right)^3 + 5.62\times10^8\left(\frac{al}{T}\right)^4 - 8.89\times10^8\left(\frac{al}{T}\right)^5 + 5.51\times10^8\left(\frac{al}{T}\right)^6$$

$$G_4 = -9.76\times10^3 + 5.13\times10^5\left(\frac{al}{T}\right) - 7.51\times10^6\left(\frac{al}{T}\right)^2 + 4.85\times10^7\left(\frac{al}{T}\right)^3 - 1.57\times10^8\left(\frac{al}{T}\right)^4 + 2.49\times10^8\left(\frac{al}{T}\right)^5 - 1.54\times10^8\left(\frac{al}{T}\right)^6$$

Table B.1: Coefficients a,b,c and d values for Eqn.(4.21) with different d/T and a1/T values.

d/T	a1/T	a	b	c	d	d/T	a1/T	a	b	c	d
0.1	0.05	0.5070	20.2108	12.7010	14.9214	0.5	0.05	0.9850	-1.1876	-1.3396	0.1491
	0.1	-0.0047	14.7951	1.3848	25.2772		0.1	0.9405	-0.8344	-1.4917	0.5396
	0.15	-0.1974	8.5043	-4.1398	21.2809		0.15	0.8791	-0.7790	-1.5549	0.9836
	0.2	-0.2175	4.3231	-5.9380	15.4994		0.2	0.8055	-0.5933	-1.7875	1.5284
	0.25	-0.1845	2.3009	-5.9370	11.3394		0.25	0.7233	-0.2904	-2.0590	2.0555
	0.3	-0.1568	1.4637	-5.4302	8.5530		0.3	0.6383	0.0106	-2.2194	2.4340
	0.35	-0.1338	0.9873	-4.9484	6.5171		0.35	0.5588	0.2587	-2.2629	2.6057
	0.4	-0.0951	0.6334	-4.4979	5.2845		0.4	0.4918	0.4826	-2.2839	2.5997
	0.45	-0.0774	0.4472	-4.1644	4.4082		0.45	0.4360	0.6420	-2.2268	2.4786
0.2	0.05	0.8644	4.1531	2.9778	2.2825	0.6	0.05	0.9974	-1.6970	-1.6081	-0.2204
	0.1	0.5305	6.4830	1.3783	7.0794		0.1	0.9609	-1.0182	-1.5092	0.1192
	0.15	0.2433	5.6736	-1.3699	9.9522		0.15	0.9244	-1.0541	-1.6286	0.5994
	0.2	0.0778	4.1429	-3.2508	9.9168		0.2	0.8867	-1.1936	-1.8887	0.9386
	0.25	0.0026	2.9032	-4.0285	8.3899		0.25	0.8422	-1.1681	-2.1025	1.2171
	0.3	-0.0325	2.1409	-4.1349	6.8247		0.3	0.7899	-0.9698	-2.1923	1.5330
	0.35	-0.0526	1.6781	-3.9906	5.6473		0.35	0.7349	-0.7304	-2.2356	1.8530
	0.4	-0.0557	1.3136	-3.7619	4.4954		0.4	0.6847	-0.5620	-2.3403	2.0600
	0.45	-0.0521	1.0451	-3.5510	3.7590		0.45	0.6380	-0.3608	-2.3480	2.1972
0.3	0.05	0.9446	0.4398	0.0786	0.5370	0.7	0.05	0.9944	-1.5966	-1.5688	-0.0372
	0.1	0.8005	1.2450	-0.3513	2.1813		0.1	0.9831	-1.6202	-1.7289	0.0686
	0.15	0.5985	2.0003	-1.1792	4.2124		0.15	0.9656	-1.4422	-1.7547	0.2517
	0.2	0.4126	2.2981	-2.0624	5.3966		0.2	0.9376	-1.4934	-1.9275	0.4962
	0.25	0.2703	2.2451	-2.7063	5.6244		0.25	0.9046	-1.5690	-2.0947	0.7431
	0.3	0.1702	2.0871	-2.9861	5.2168		0.3	0.8716	-1.4763	-2.1440	0.9684
	0.35	0.0994	1.9773	-2.9692	4.5081		0.35	0.8385	-1.2915	-2.1694	1.1995
	0.4	0.0480	1.8904	-2.8366	3.7040		0.4	0.8035	-1.2268	-2.3276	1.4713
	0.45	0.0217	1.6823	-2.7059	3.0160		0.45	0.7728	-1.1065	-2.3859	1.7193
0.4	0.05	0.9656	-0.4413	-0.8333	0.5583	0.8	0.05	0.9879	-1.2859	-1.4263	0.2660
	0.1	0.9063	-0.6177	-1.3238	1.0906		0.1	0.9930	-1.9861	-1.9261	0.2191
	0.15	0.7940	-0.0760	-1.4277	1.8187		0.15	0.9931	-1.7663	-1.8479	0.0224
	0.2	0.6591	0.5451	-1.7417	2.7573		0.2	0.9722	-1.6502	-1.9290	0.1647
	0.25	0.5283	0.9762	-2.1452	3.4822		0.25	0.9442	-1.6581	-2.0637	0.4317
	0.3	0.4165	1.2092	-2.3932	3.7004		0.3	0.9210	-1.6101	-2.0832	0.5955
	0.35	0.3262	1.3607	-2.4210	3.4753		0.35	0.9008	-1.5104	-2.0735	0.7037
	0.4	0.2539	1.5073	-2.3596	3.1046		0.4	0.8754	-1.5150	-2.2308	0.9669
	0.45	0.2045	1.4927	-2.2630	2.6523		0.45	0.8570	-1.4824	-2.2549	1.2457

d/T	a1/T	a	b	c	d
0.9	0.05	0.9961	-1.4930	-1.5088	-0.0413
	0.1	0.9793	-1.5149	-1.7518	0.0927
	0.15	0.9864	-1.6346	-1.7648	0.0827
	0.2	0.9863	-1.6962	-1.9537	0.1307
	0.25	0.9793	-1.6890	-2.1129	0.2175
	0.3	0.9710	-1.6611	-2.0971	0.3135
	0.35	0.9611	-1.6555	-2.0467	0.4638
	0.4	0.9450	-1.6677	-2.1668	0.7473
	0.45	0.9297	-1.6249	-2.0590	1.1107
1.0	0.05	0.9923	-1.3457	-1.4523	0.2973
	0.1	0.9854	-1.9198	-1.9129	0.1556
	0.15	0.9946	-1.7554	-1.7976	0.0747
	0.2	0.9846	-1.6903	-1.9359	0.1662
	0.25	0.9725	-1.7218	-2.1087	0.2820
	0.3	0.9756	-1.6952	-2.0850	0.3534
	0.35	0.9887	-1.6260	-2.0119	0.4970
	0.4	0.9901	-1.6531	-2.1580	0.8861
	0.45	0.9776	-1.6250	-2.0102	1.3896